

## **General Disclaimer**

### **One or more of the Following Statements may affect this Document**

- This document has been reproduced from the best copy furnished by the organizational source. It is being released in the interest of making available as much information as possible.
- This document may contain data, which exceeds the sheet parameters. It was furnished in this condition by the organizational source and is the best copy available.
- This document may contain tone-on-tone or color graphs, charts and/or pictures, which have been reproduced in black and white.
- This document is paginated as submitted by the original source.
- Portions of this document are not fully legible due to the historical nature of some of the material. However, it is the best reproduction available from the original submission.

9950-961

# FEASIBILITY STUDY FOR A 34 GHz (Ka Band) GYROAMPLIFIER

(NASA-CR-174439) FEASIBILITY STUDY FOR A 34  
GHz (Ka BAND) GYROAMPLIFIER Final Report  
(Varian Associates) 160 P HC A08/MF A01  
CSCI 09A

N85-19325

Unclas

G3/33 14294

## FINAL REPORT

By

D.S. Stone, R.E. Bier, M. Caplan, H.E. Huey,  
D.R. Pirkle, J.D. Robinson and L. Thompson

SEPTEMBER 1984

JPL CONTRACT NO. SC 956813



Prepared for:  
CALIFORNIA INSTITUTE OF TECHNOLOGY  
JET PROPULSION LABORATORY  
4800 OAK GROVE DRIVE  
PASADENA, CALIFORNIA 91103

Prepared by:  
VARIAN ASSOCIATES, INC.  
MICROWAVE TUBE DIVISION  
611 HANSEN WAY  
PALO ALTO, CALIFORNIA 94303



## ABSTRACT

The purpose of this study was to investigate the feasibility of using a gyrokystron power tube as the final amplifier in a 400 kW CW 34-GHz transmitter on the Goldstone Antenna.

Project goals were to:

- work out a conceptual design of the gyrokystron and the transmission line connecting it with the antenna feed horn,
- compare the performance characteristics of the tube and transmission line to the transmitter requirements for a deep space radar system,
- identify areas of technical risk for a follow-on hardware development program for the gyrokystron amplifier and overmoded transmission line components.

Conclusions of the study are as follows:

- A gyrokystron amplifier and overmoded transmission components are feasible for this application,
- technical risks, in descending order of importance, are:
  - problems with unwanted oscillations in the gyrokystron circuit which could adversely affect power output (400 kW goal), efficiency (40% goal), and gain (50 dB goal).
  - poor electron beam quality which could reduce device efficiency to 20-25%,
  - difficulties in maintaining the required (-30 dBc) spurious mode level of the  $TE_{11}^0$  right circularly polarized waveguide mode at the antenna feed,

- difficulty in demonstrating a microwave output window for the gyrokystron capable of handling the full 400 kW CW.

Sound approaches to overcoming the anticipated problems are to:

- design the gyrokystron circuit with several  $TE_{11}^0$  buncher resonators and conduct extensive hardware tests with prototype tubes,
- optimize the circuit design for insensitivity to poor beam quality and develop a magnetron injection gun as a back-up for the proposed Pierce gun/wiggler,
- conduct extensive microwave tests of a  $TE_{11}^0$  mode filter and quasi-optical transmission system, or alternatively, reduce the spurious mode requirement to a value ( $\sim 12$  dBc) which could be achieved at the tube output, obviating development of a mode filter.
- utilize double-disc gyrotron window technology which has already been demonstrated for 340 kW, CW at 28 GHz.

The probability of a timely and successful development effort for the 34 GHz transmitter is high if the hardware development phase is properly staffed and supported.

## TABLE OF CONTENTS

<u>Section</u>	<u>Page</u>
I. INTRODUCTION AND TECHNICAL OVERVIEW .....	1
A. Objectives and Scope .....	1
B. Transmitter Requirements .....	1
C. Choice of Transmitter Tube: Gyroklystrons vs Conventional Tubes .....	4
D. Transmitter Layout .....	6
E. Gyroklystron Design .....	6
F. Organization of Report Contents .....	10
II. ELECTRON BEAM OPTICS .....	11
A. Pierce Gun/Wiggler Configuration .....	11
B. Velocity Spread Effects .....	14
C. Magnetron Injection Gun .....	23
D. Feasibility Summary - Beam Optics .....	25
III. SOLENOID AND DEWAR .....	26
A. Conceptual Design .....	26
B. Feasibility Summary - Solenoid and Dewar .....	29
IV. GYROKLYSTRON CIRCUIT .....	30
A. Choice of Resonator Modes .....	30
B. Stability Criteria .....	34
C. Circuit Design Details .....	35
D. Calculated Circuit Performance .....	40
E. Velocity Spread Effects .....	47
F. Polarization .....	53
G. Noise Figure .....	54
H. Harmonic Output .....	56
I. Feasibility Summary - Gyroklystron Circuit ...	57
V. MODE CONVERTER .....	59
A. Design Approach .....	59
B. Conceptual Design .....	59
C. Feasibility Summary - Mode Converter .....	65
VI. COLLECTOR-TAPERS .....	66
A. Taper Design Approach for Minimal Mode Conversion .....	66
B. Collector Beam Power Density Calculations ....	68
C. Feasibility Summary - Collectors and Tapers ..	70

TABLE OF CONTENTS (Cont'd)

VII.	CW OUTPUT WINDOW .....	73
	A. Design Approach .....	73
	B. Feasibility Summary - CW Output Window .....	78
VIII.	DIRECTIONAL COUPLER .....	82
	A. Coupler Geometry .....	82
	B. Coupling Coefficient .....	84
	C. Directivity and Selectivity .....	85
	D. Uniform Coupling .....	85
	E. Linearly Tapered Coupling .....	86
	F. Conceptual Design .....	87
	G. Feasibility Summary - Directional Coupler ....	92
IX.	MODE FILTER .....	93
	A. Theory .....	93
	B. Calculation of Attenuation Constants .....	96
	C. Sensitivity to Pitch and Frequency .....	101
	D. Realization of the Helix Waveguide .....	102
	E. Feasibility Summary - Mode Filter .....	105
X.	SENSITIVITY ANALYSIS .....	107
XI.	CRITICAL TECHNICAL ISSUES AND SUMMARY .....	114
XII.	REFERENCES .....	116
	Appendix A - Injection Locked Gyrotron Oscillator .	
	Appendix B - Directional Coupler Computer Program .	
	Appendix C - Details of Sensitivity Calculations ..	

## LIST OF ILLUSTRATIONS

<u>Figure</u>		<u>Page</u>
1.	Milestone Chart .....	2
2.	Goldstone Antenna .....	3
3.	Power vs Frequency for CW Microwave Amplifiers .....	5
4.	Layout Gyroklystron Transmitter (To Scale) .....	7
5.	Schematic of Proposed JPL Gyroklystron .....	8
6.	Schematic for Pierce/Wiggler Configuration .....	12
7.	Wiggler Configuration .....	13
8.	Velocity Spread and Alpha ( $v_{\perp}/v_z$ ) vs Distance .....	15
9.	Criteria for Optimal Design of Pierce/Wiggler System .....	17
10.	Beam Optics for 80 KV Pierce Gun .....	18
11.	Electrostatic Fields in Gun .....	19
12.	Magnetic Profile Shaping to Reduce Beam Ripple .....	20
13.	Pole Piece Configuration for Optimized Magnetic Field Profile .....	21
14.	Realization of Pierce/Wiggler Design .....	22
15.	Beam Optics for 80 KV MIG Gun .....	24
16.	Axial Magnetic Field Profile, $B_z$ .....	27
17.	Solenoid and Dewar .....	28
18.	Schematic of Proposed Gyroklystron Configuration ...	32
19.	Beam Loaded $Q_B$ and "Transadmittance" $Y^{5,4}$ , $Y^{5,1}$ vs Frequency .....	36
20.	Electric Field Profile for $TE_{12}$ Output Cavity .....	38
21.	Gyroklystron Circuit .....	39
22.	Linear Gain and Phase vs Frequency .....	41
23.	Power Out vs Frequency and Drive Level .....	42
24.	Power Out vs Power In (Different Frequencies) .....	43

LIST OF ILLUSTRATIONS (Cont'd)

25.	Power Out and Phase vs Voltage .....	44
26.	Power Out and Phase vs Beam Current .....	45
27.	Power Out and Phase vs Circuit Magnetic Field .....	46
28.	Power Out and Phase vs Alpha (Wiggler Fields) .....	48
29.	Effect of Load Mismatch .....	49
30.	Power Out and Phase vs Cavity Heating (Shift of Resonant Cavity Frequencies) .....	50
31.	Tuning Penultimate Cavity for Efficiency .....	51
32.	Effect of Velocity Spread .....	52
33.	Hard and Soft Excitation of Gyrotron Oscillator ....	58
34.	Mode Converter .....	60
35.	Mode Converter $TE_{12} \rightarrow TE_{11}$ (34 GHz) .....	62
36.	$TE_{12} \rightarrow TE_{11}$ Mode Converter Passband .....	64
37.	Collector and Tapers .....	67
38.	Mode Conversion in Collector Tapers .....	69
39.	Typical Simulation of Particle Trajectories from Output Cavity to Collector .....	71
40.	Wall Power Density Profile in the Collector Region .	72
41.	Output Window .....	74
42.	VSWR for 34 GHz Double-Disc Window .....	75
43.	Finite Element Mesh for One Disc of 34 GHz Window ..	76
44.	34 GHz Double-Disc Window Coolant-Side Deflection ..	77
45.	34 GHz Double-Disc Window Temperatures .....	79
46.	34 GHz Double-Disc Window Vacuum-Side Stresses .....	80
47.	34 GHz Double-Disc Window Coolant-Side Stresses ....	81
48.	Directional Coupler .....	83

LIST OF ILLUSTRATIONS (Cont'd)

49.	Directivity vs Frequency .....	90
50.	Selectivities vs Frequency .....	91
51.	Mode Filter .....	94
52.	Mechanical Configuration/Fabrication Scheme .....	103

LIST OF TABLES

<u>Table</u>	<u>Page</u>
1. JPL Transmitter Tube Requirements .....	1
2. JPL Transmitter System Requirements .....	4
3. Pierce/Wiggler Design Specifications .....	23
4. MIG Gun Design Specifications .....	25
5. Circuit Performance .....	37
6. Cavity Design .....	40
7. Harmonic Power Emission .....	57
8. Calculated Mode Output for $TE_{12} \rightarrow TE_{11}$ Converter .....	61
9. Percent Power in Modes .....	68
10. $TE_{11}^0$ Directional Coupler 1.75-Inch-Diameter Waveguide	88
11. $TE_{11}^0$ Directional Coupler 2.5-Inch-Diameter Waveguide .	89
12. Calculations for 1.75-Inch Waveguide .....	99
13. Calculations for 2.5-Inch Waveguide .....	100
14. Calculated AM Sensitivities .....	109
15. Calculated PM Sensitivities .....	110
16. Mechanical Tolerances .....	112



## I. INTRODUCTION AND TECHNICAL OVERVIEW

### A. OBJECTIVES AND SCOPE

This report describes the results of a study performed by the Varian Microwave Tube Division for the Jet Propulsion Laboratory under Contract No. SC-956813. The purpose of this work was to investigate the feasibility of using a gyrokystron power tube as the final amplifier in a 400 kW CW 34 GHz transmitter on the Goldstone Antenna.

The milestone schedule for this study is given in Figure 1. The program began on 23 February 1984 with the investigation of the conceptual design of the gyrokystron and overmoded waveguide components (Milestones A-C). The performance characteristics of the tube and transmission line were studied in the latter part of the program (Milestones D-I). This final report is represented by the last scheduled report milestone, Item #4.

### B. TRANSMITTER REQUIREMENTS

The 400 kW CW 34 GHz transmitter will be installed in one of three 16-foot high transmitter housings mounted on the 64-meter-diameter Goldstone Antenna as shown in the photograph in Figure 2. The transmitter tube requirements which have been specified by JPL are given in Table 1.

Table 1  
JPL Transmitter Tube Requirements

	<u>Goal</u>	<u>Requirement</u>
Center Frequency	--	34.0 GHz
Bandwidth (-1 dB)	--	> 0.1 %
Output Power	400 kW	200 kW
Duty	--	CW --
Efficiency	40 %	20 %
Saturated Gain	50 dB	-- --
Beam Power	--	< 1.0 MW
Beam Voltage	--	< 90 kV
Noise Figure	--	< -80 dB/MHz



varian

# MILESTONE CHART


 <b>varian</b>		<b>MILESTONE CHART</b>																							
PROGRAM	JPL 34 GHz GYROKLYSTRON	J.O.	DATE 7-20-84																						
TASK DESCRIPTION		REV. NO. 0																							
PROGRAM START 2-23-84		MONTH END																							
		1	2	3	4	5	6	7	8	9	10	11	12	13	14	15	16	17	18	19	20	21	22	23	
A. CIRCUIT DESIGN																									
B. REQUIREMENTS FOR ALL OTHER TUBE COMPONENTS																									
C. REQUIREMENTS FOR TRANSMISSION LINE COMPONENTS																									
D. SYSTEM CONFIGURATION & PERFORMANCE																									
E. ITERATE CIRCUIT DESIGN																									
F. ITERATE TUBE COMPONENTS																									
G. ITERATE TRANSMISSION LINE																									
H. INTEGRATE OVERALL CONCEPTUAL DESIGN																									
I. SENSITIVITY ANALYSIS																									
REPORTS AND REVIEWS																									
1. BIMEEKLY TRX REPORTS																									
2. DESIGN REVIEW A																									
3. DESIGN REVIEW B																									
4. FINAL REPORT																									

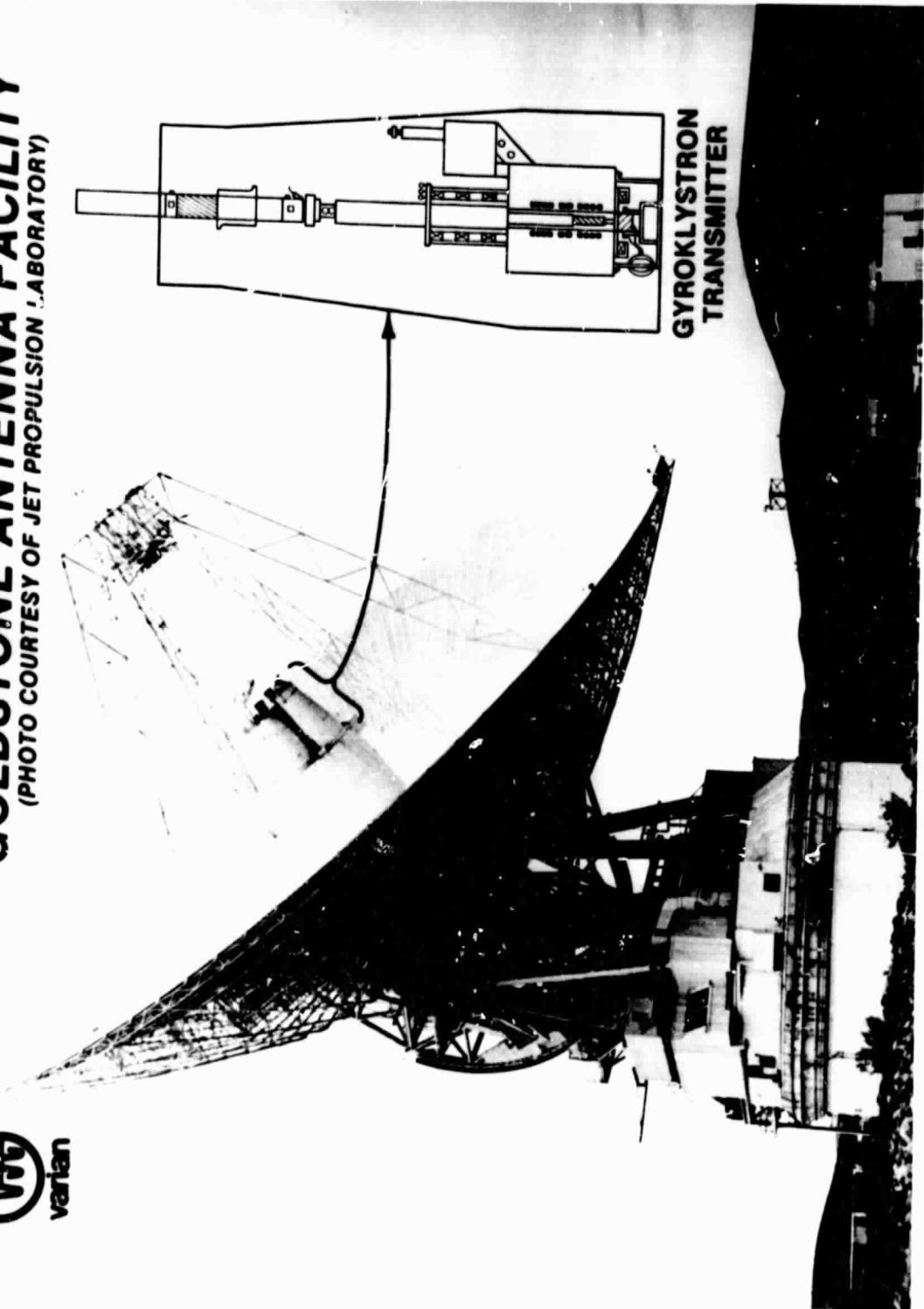
FIGURE 1. MILESTONE

2

ORIGINAL PAGE IS  
OF POOR QUALITY

# GOLDSTONE ANTENNA FACILITY

(PHOTO COURTESY OF JET PROPULSION LABORATORY)



GYROKLYSTRON  
TRANSMITTER

ORIGINAL PAGE  
BLACK AND WHITE PHOTOGRAPH

ORIGINAL PAGE  
BLACK AND WHITE PHOTOGRAPH

Additional system requirements which affect other portions of the transmitter are given in Table 2.

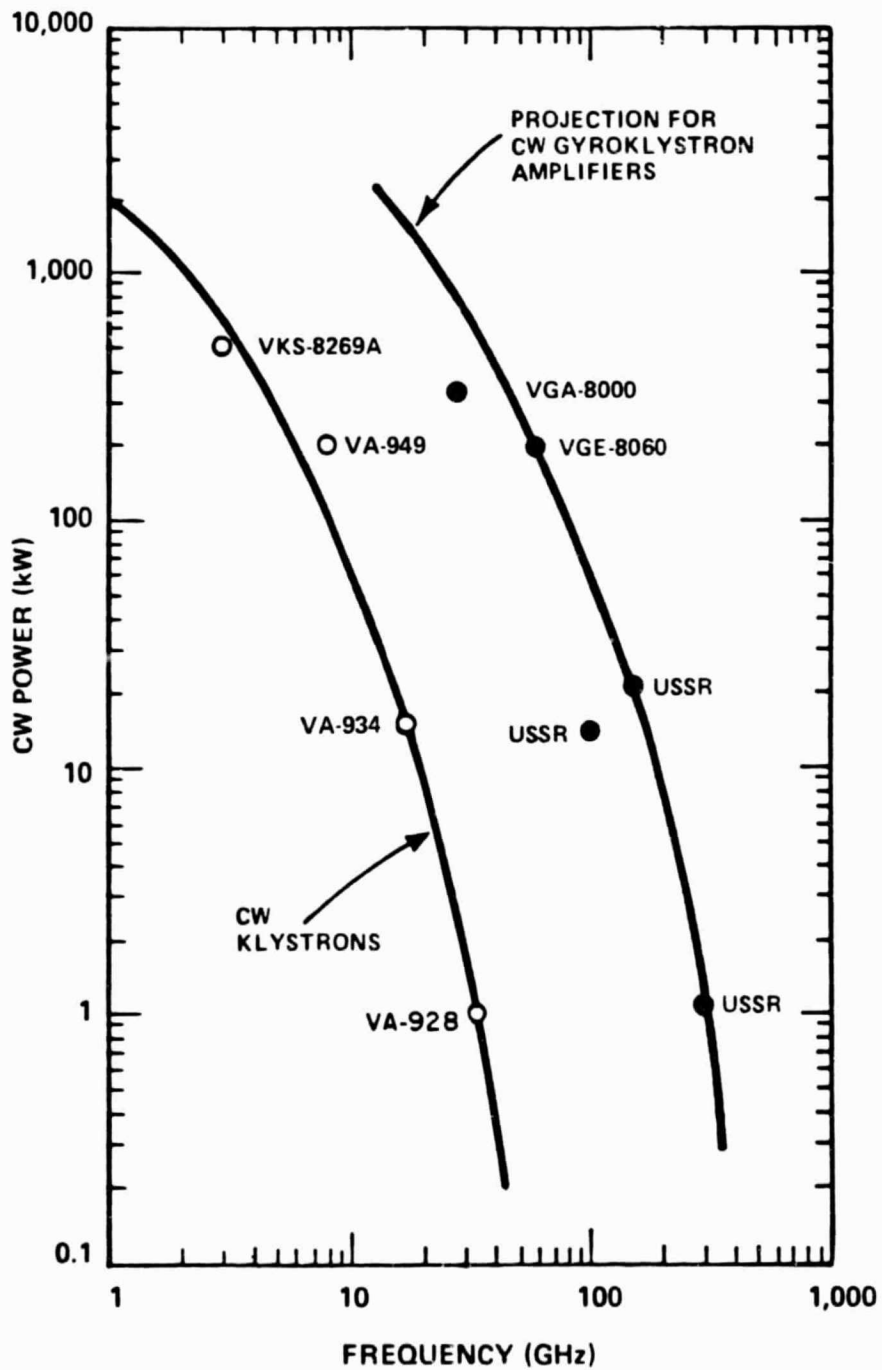
Table 2  
JPL Transmitter System Requirements

- Manageable AM/PM Sensitivities
- $TE_{11}^0$  Mode Purity Better than 99.9% at Feed
- Circular Polarization Within 1 dB at Feed
- Tilttable (Zenith to  $15^\circ$  Elevation)

C. CHOICE OF TRANSMITTER TUBE: GYROKLYSTRONS vs CONVENTIONAL TUBES

Before describing the conceptual design of the gyroklystron, it is worthwhile to briefly review why conventional klystron technology is inadequate for the requirement of 400 kW CW at 34 GHz. Capabilities of CW microwave power amplifiers are compared with klystrons and gyroklystrons in Figure 3. The technology limit for either type of tube at millimeter wavelengths is determined by the volume of conducting material available to absorb the rf power dissipated in the interaction circuit.

Symons has shown<sup>1</sup> that in this regime the power limit scales as the frequency to the minus five-halves power for a given circuit configuration. Indeed, curves with this slope may be drawn through the performance data for production klystrons given in Figure 3. At the frequency of interest, 34 GHz, power output of the order of one kilowatt is typical for production klystrons. A similar power versus frequency curve may be projected for gyroklystrons. The solid dots in Figure 3 represent performance of gyrotron oscillators demonstrated both in the United States and in the Soviet Union. The CW power levels achievable for gyroklystron amplifiers are bounded by the design limits of the same critical internal components used in gyrotron oscillators, namely circuits, collectors and windows. Therefore, a curve with the minus five-halves slope drawn through the gyrotron oscillator state-of-the-art data represents a conservative projection for CW gyroklystron amplifiers.<sup>2</sup> At 34 GHz, this projection implies that



- PRODUCTION CW KLYSTRON AMPLIFIERS
- DEMONSTRATED CW GYROTRON OSCILLATORS

FIGURE 3. POWER vs FREQUENCY FOR CW MICROWAVE AMPLIFIERS

gyroklystrons can achieve 830 kW CW, well in excess of the 400 kW CW JPL requirement.

#### D. TRANSMITTER LAYOUT

The layout of the proposed gyroklystron transmitter is given in Figure 4 as an enlargement of the schematic presented previously beside the photograph of the JPL Goldstone Antenna in Figure 2. The transmitter is housed in a silo which is 16-feet high. The inside diameter at the base is 7 feet, and the inside diameter at the top is 5 feet. A high voltage tank filled with insulating oil rests at the base of the silo and contains the high voltage connections for the gyroklystron tube. A solenoid is seated on top of the high voltage tank and contains electromagnets which focus the electron beam in the tube and provide the strong 12 kG field required for the cyclotron resonance interaction. The gyroklystron tube is supported by the solenoid and is approximately 8 to 10 feet long. The remaining height within the silo is allotted to the various overmoded transmission line components which connect the output waveguide flange of the tube to the bottom of the antenna feed horn. The entire transmitter must be capable of tilting with the antenna dish as it tracks through elevations from zenith to  $15^{\circ}$  above the horizon.

#### E. GYROKLYSTRON DESIGN

The preferred approach for the design of the gyroklystron amplifier tube itself is shown in Figure 5. The device configuration comprises a Pierce gun/wiggler beam optics system, an interaction structure made up of  $TE_{111}$  buncher resonators with a  $TE_{121}$  output cavity, a  $TE_{12}$  to  $TE_{11}$  mode converter, an electron beam collector, and a double-disc output window which separates the tube vacuum from the external waveguide. The mechanism for the microwave interaction, known as the "cyclotron resonance maser" or "gyrotron" interaction requires a strong axial magnetic field (12.5 kG at 34 GHz) and has been proven to be an efficient (>50%) means of microwave generation for CW power levels of hundreds of kilowatts at millimeter wavelengths.<sup>3</sup> Because of power handling considerations and mode integrity, the rf power cannot be extracted in the conventional manner

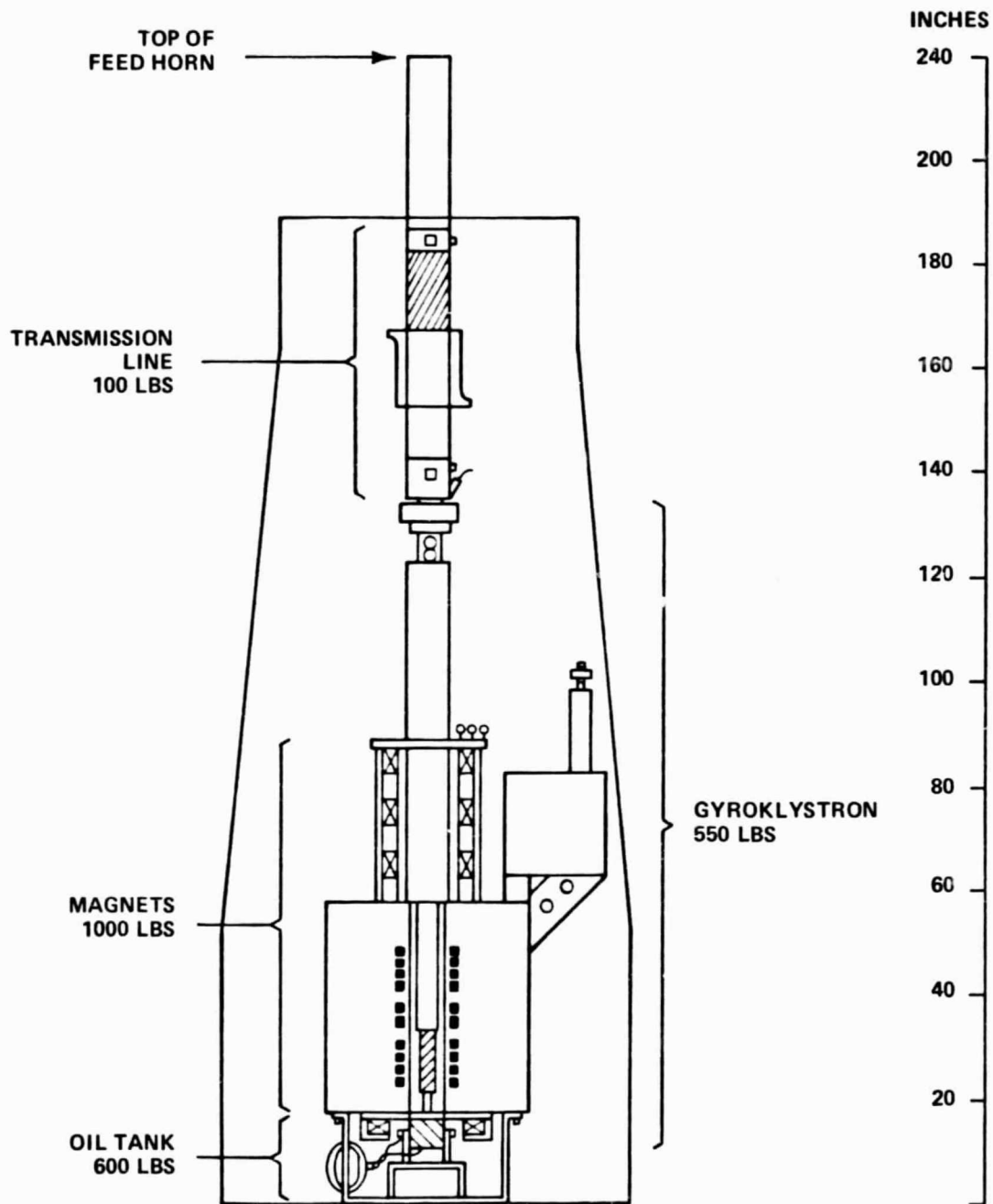


FIGURE 4. LAYOUT GYRCKLYSTRON TRANSMITTER (TO SCALE)

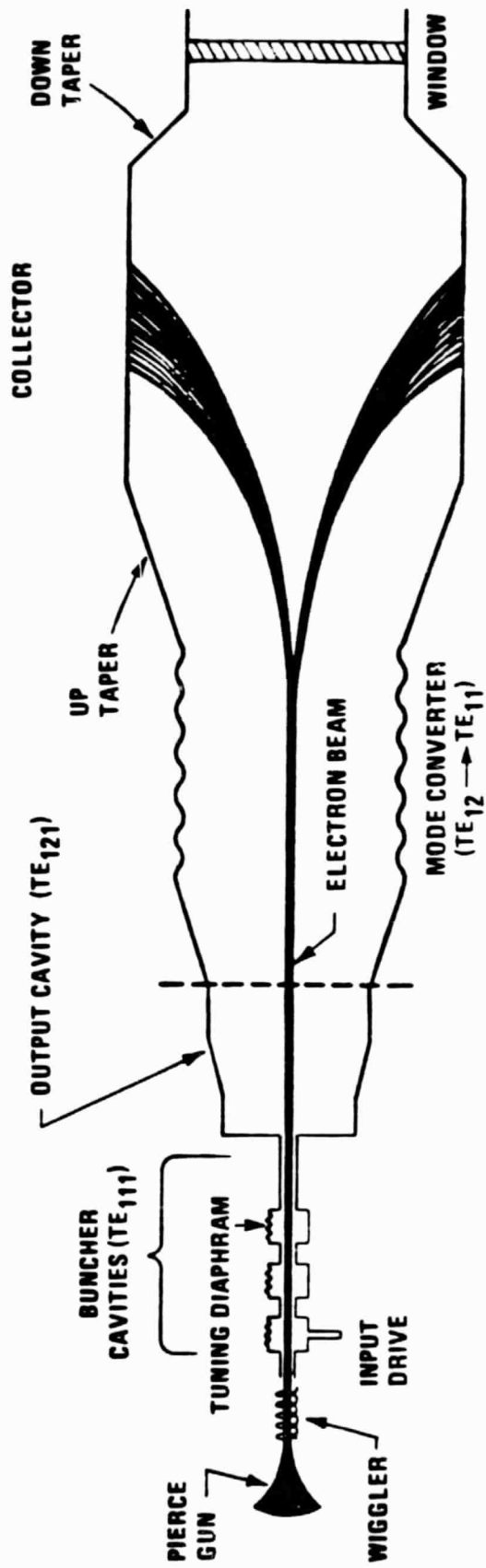


FIGURE 5. SCHEMATIC OF PROPOSED JPL GYROKLYSTRON



through a coupling hole at right angles to the device but must travel in line with the spent electron beam through an uptaper and collector region (see Figure 5). The beam is then made to impinge on the collector walls while the rf power continues on through an output window.

The lowest order compatible mode that can handle the rf power dissipation in the output cavity is the  $TE_{121}$  mode. The overall stability of the gyrokystron amplifier against the propensity to oscillate is ensured by using short enough cavities and low enough cavity Q's such that the threshold current required for each cavity to oscillate on its own is above the operating electron beam current. A sufficient number of resonator cavities are then used to achieve the required gain of 50 dB.

As in all gyro devices, the electron beam must carry 70-80% of its energy in rotational motion. The two methods used at Varian for producing such a beam are the magnetron injection gun (MIG) and the Pierce gun/wiggler configuration. In the latter configuration, which is the preferred approach for the JPL device, the solid beam from a Pierce gun drifts through a bifilar helix, or wiggler, acquiring transverse energy from the spatially rotating transverse magnetic field inside the helix. Adiabatic magnetic compression then increases the transverse energy to the desired value as the beam travels from the wiggler to the circuit. Unlike the magnetron gun, the wiggler configuration has not yet been used in oscillators and thus has not yet had the opportunity to demonstrate the capability of generating beams of high enough quality (low velocity spread) sufficient for high efficiency (> 50%). However, an important advantage of using the Pierce gun/wiggler instead of the magnetron gun in this application is that standard Pierce gun technology can be employed which ensures operation with a space charge limited (low noise) beam.

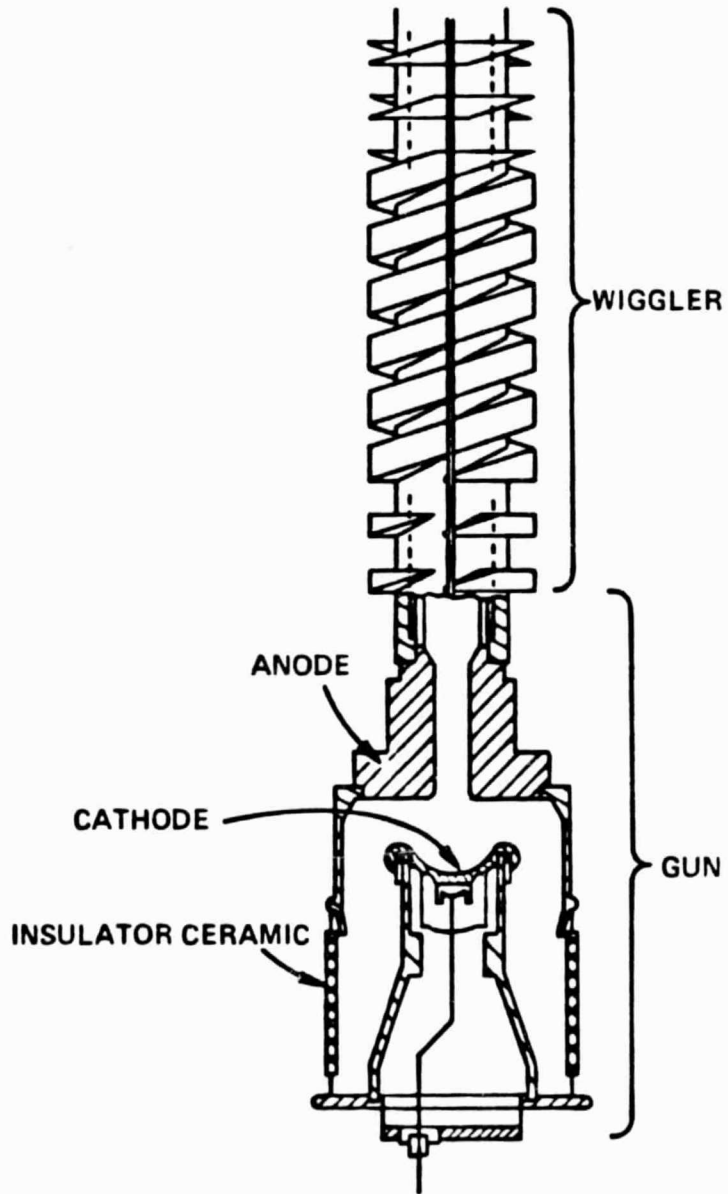
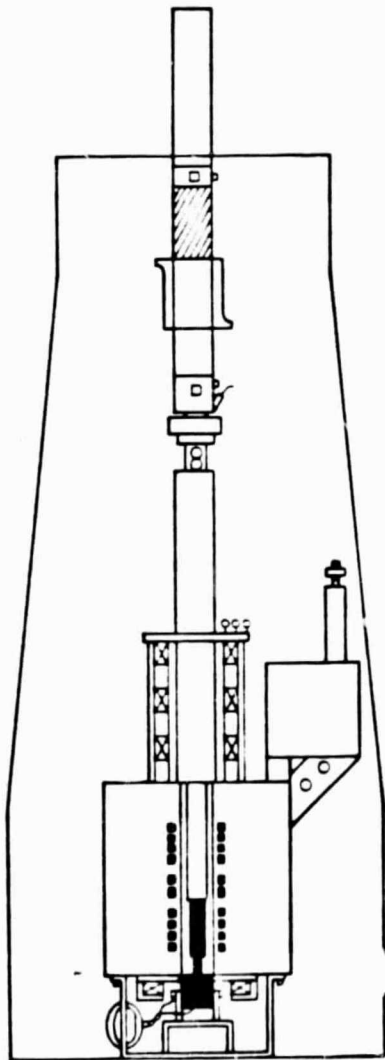
With the output cavity operating in the  $TE_{121}$  mode, power must be converted back into the desired  $TE_{11}$  mode and run into overmoded waveguide in order for the output window and collector to handle the CW power requirement. A symmetric rippled-wall mode converter is used to convert  $TE_{12}$  to  $TE_{11}$ . The converter is comprised of a set of small sinusoidal axisymmetric perturbations in the wall of the waveguide. The two most

likely locations for this converter are inside the tube adjacent to the output cavity, or outside the tube in the external transmission line. The beam collector must be at least 4 inches in diameter for reliable power handling capabilities during operation with 1 MW CW of beam power. This requires that the waveguide taper up to 4 inches in diameter and then back down to the 2.5-inch diameter output window. Unique designs for modified nonlinear gaussian tapers have been developed which can maintain ~95% mode purity in these tapered sections. A mode filter is then required in the external transmission line to remove the last ~5% of undesired modes consisting primarily of  $TE_{12}$ ,  $TE_{13}$  as well as  $TM_{11}$ ,  $TM_{12}$ ,  $TM_{13}$ , and  $TM_{14}$  modes. An overmoded mode-selective directional coupler is also used in the transmission line to provide an accurate real time measurement of the power radiated by the antenna.

#### F. ORGANIZATION OF REPORT CONTENTS

The following sections of this report describe conceptual designs for each of the major sections of the tube, for the solenoid magnet, and for the critical overmoded waveguide components. The design sections are arranged in the order in which each component interacts with the electron beam or the microwave signal. Each section is introduced with a reproduction of the transmitter layout (Figure 4), highlighted to show the location and configuration of the hardware under discussion. The discussion begins with the beam optics in Section II followed by descriptions of the solenoid, interaction circuit, mode converter, collector, window, directional coupler, and mode filter (Sections III-IX). The sensitivity of the transmitter performance characteristics to small variations in control parameters is reviewed in Section X. The areas of technical risk for the development of the transmitter hardware are summarized in Section XI and technical approaches are described for solving anticipated problems. Details regarding the requirements for an injection locked oscillator for the JPL transmitter are described in Appendix A. A listing of the directional coupler design code, developed for this study program, is given in Appendix B. Finally, details of the sensitivity calculations are given in Appendix C.

# BEAM OPTICS



## II. ELECTRON BEAM OPTICS

### A. PIERCE GUN/WIGGLER CONFIGURATION

An electron beam with power approaching one megawatt is required in order that the gyrokystron circuit can emit at least 400 kilowatts of microwave power (40% efficient). Efficient gyrotron interaction requires that at least 70-80% of the beam energy be in rotational motion, that all electrons have essentially the same velocities (minimal velocity spread) and that the beam fill factor be less than 50% (~120-mil-beam diameter at 34 GHz). The required electron beam can be generated using either a Pierce gun with wiggler or a magnetron injection gun. In either configuration, one requires that the space charge effects be minimized to keep velocity spreads low. This requires as high a voltage and as low a current as possible (low perveance) within the constraints of available power supplies, beam power requirements and low arcing probability. We have chosen the beam voltage to be 80 kV and beam current 12.5 amps for purposes of this design feasibility study. In the Pierce/wiggler configuration shown in Figure 6, a solid beam is emitted from a Pierce gun with velocity  $v_z$  and then focused with an axial field  $B_A$  into a dc rotating helical transverse magnetic field  $B_T$  given approximately by:

$$B_T = B_W \left\{ \hat{e}_x \sin(2\pi z/p) + \hat{e}_y \cos(2\pi z/p) \right\}$$

where the pitch  $p$  of the field is chosen so that it matches the cyclotron pitch of the electrons rotating in the axial field  $B_A$ .

$$p \approx 21.2 \sqrt{\text{voltage}/B_A} .$$

This helical field can be produced by using a wiggler which consists of a mandrel upon which is wound bifilar helical windings carrying opposing currents as illustrated in Figure 7. Upon traversing a wiggler of length  $L$ , the beam electrons acquire a small amount of transverse velocity  $v_\perp$  given by:

$$\alpha = v_\perp/v_z = (2\pi L/p)B_W/B_A \quad (\text{see Figure 8})$$

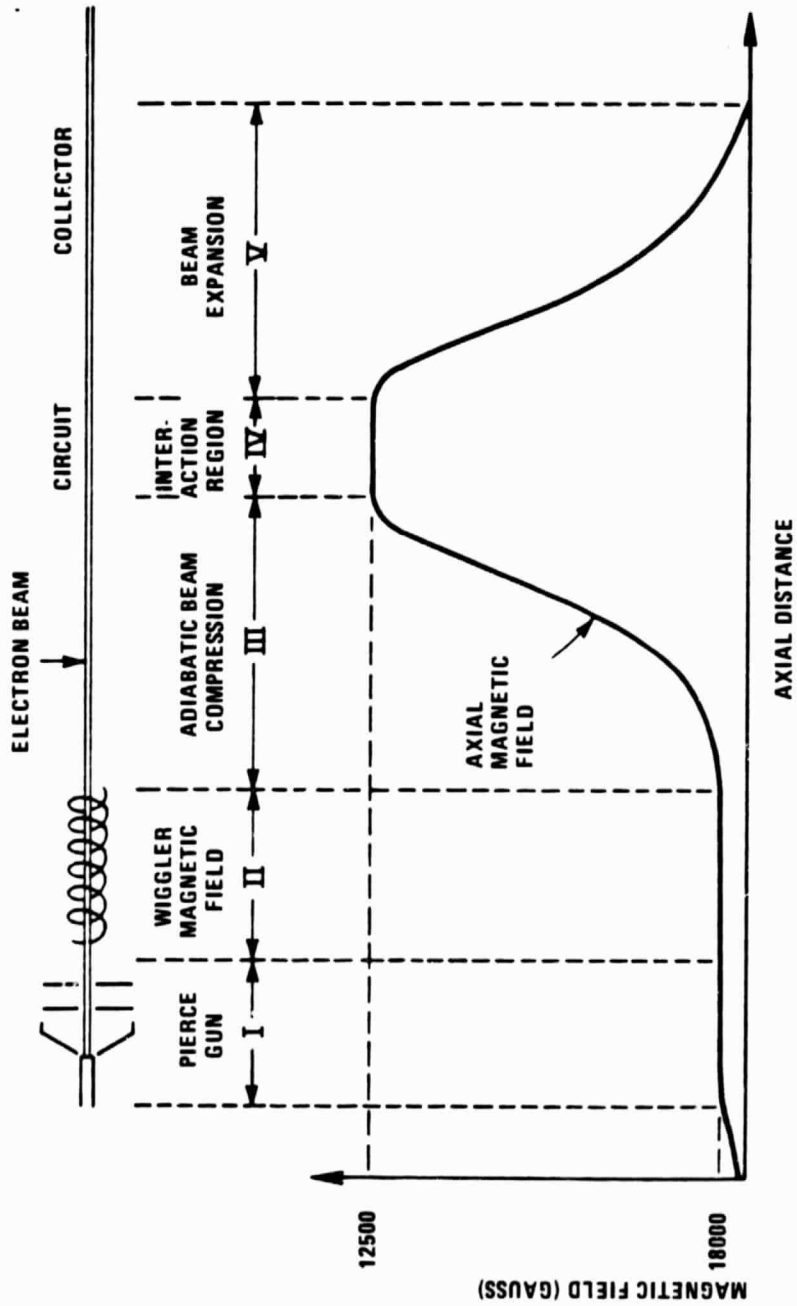


FIGURE 6. SCHEMATIC FOR PIERCE/WIGGLER CONFIGURATION

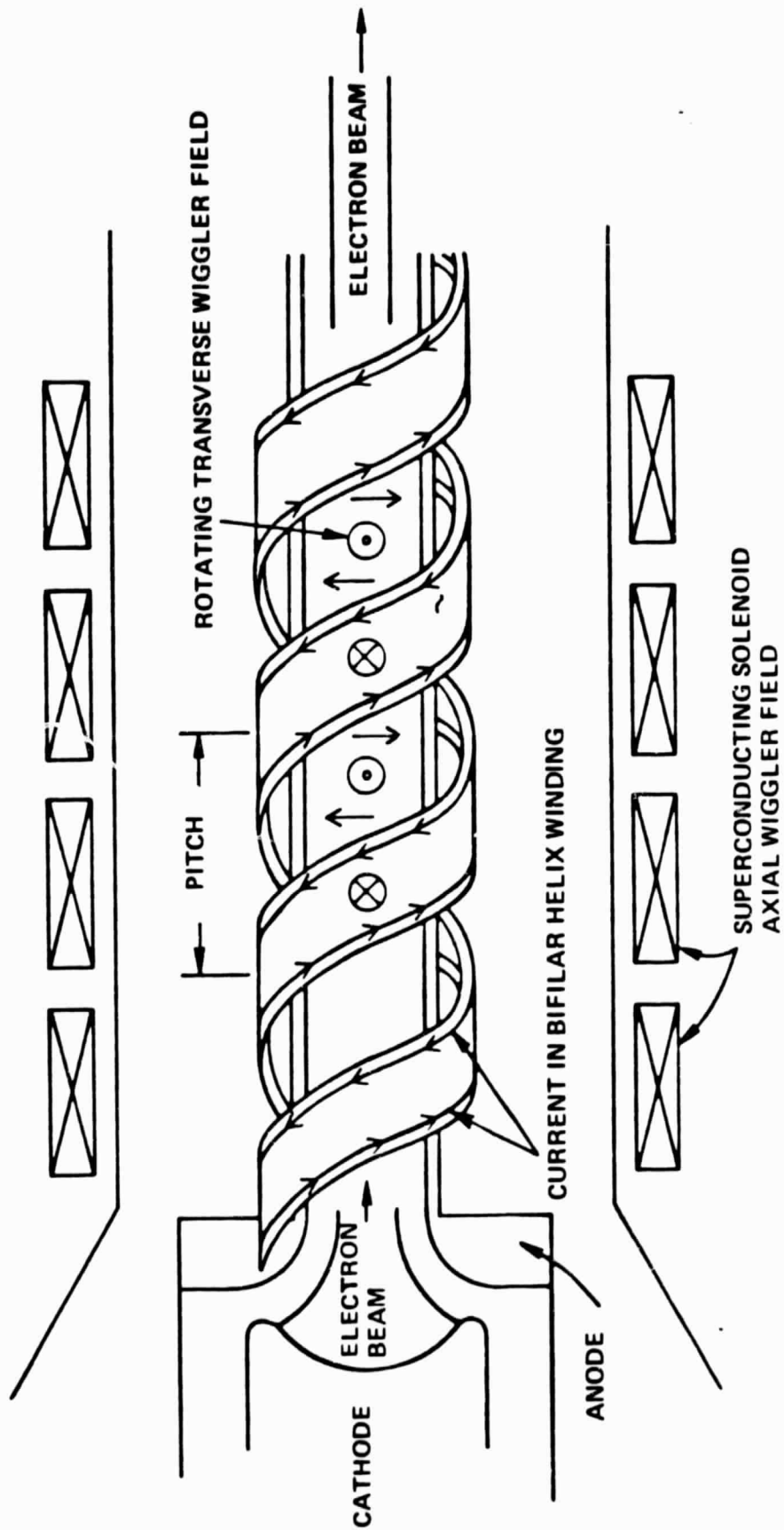


FIGURE 7. WIGGLER CONFIGURATION

The rotational energy is increased to the final value as the beam drifts towards the circuit through a region of rapidly increasing axial field due to the constancy of the adiabatic invariant  $v_{\perp}^2/B$ .

#### B. VELOCITY SPREAD EFFECTS

Ideally it is desirable for all electrons to have the same final rotational velocity since spreads in the electron distribution degrade interaction efficiency. There are non-ideal effects both in the wiggler and the electron beam which lead to velocity spreads. The fact that the bifilar helical windings must start and end causes some electrons to experience different fields than others. This can be remedied by gradually tapering the winding density over several pitch lengths at the entrance and exit to the helix. Non-uniformities in the transverse helix field increase as one moves away radially from the axis. If the pitch is made large enough compared to the beam radius, sufficient uniformity of the transverse fields is maintained across the beam diameter. Space harmonic contributions coming from helical windings may also distort the fields. This effect is eliminated by not allowing the pitch to become too large compared with the helix radius.

Our studies indicate that the most important causes of velocity spread are the space charge and ripple characteristics of the electron beam entering the wiggler. To address the problems imposed by space charge and ripple effects, a study of the overall integrated design of the Pierce gun, wiggler, and final beam parameters must be made. It can easily be shown that since the rotational velocity of an electron in a Pierce beam is roughly proportional to radius (ignoring edge effects), a perpendicular velocity spread of  $\sim 35\%$  is inherent in the beam emanating from a Pierce gun. The only way this velocity spread can be reduced is if all electrons acquire additional perpendicular velocity in the wiggler which is much larger than the rotational velocities any of the electrons had when they first entered the wiggler (Figure 8).

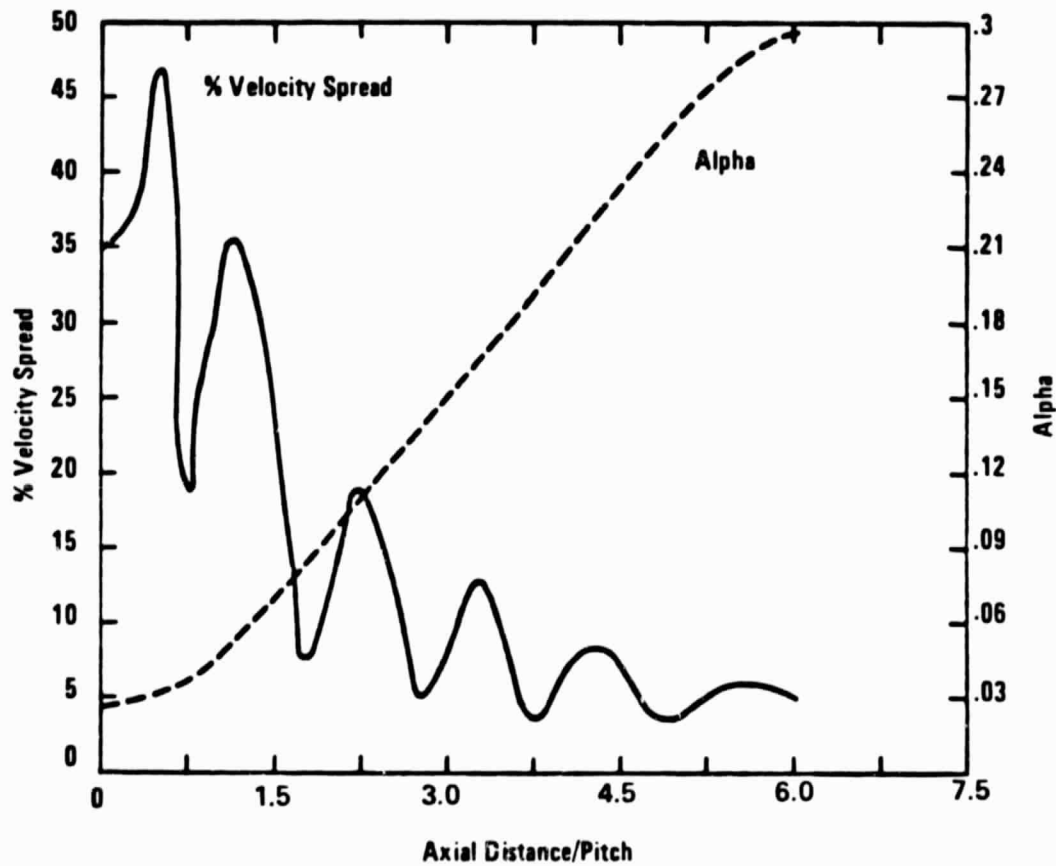


FIGURE 8. VELOCITY SPREAD AND ALPHA ( $v_{\perp}/v_z$ ) vs DISTANCE



It can be shown that the ratio of the maximum rotational velocity of an electron in the Pierce gun to the rotational velocity acquired in the wiggler is given by:

$$\left| \frac{v_{\perp \text{ pierce}}}{v_{\perp \text{ wiggler}}} \right| \sim \sqrt{\left[ 1 - \sqrt{1 - 1/M^2} \right]^2 + (2\Delta)^2}$$

where  $\Delta$  is the fraction of beam ripple present and  $M$  is the ratio of the actual field used to the Brillouin field. It is evident that velocity spread will be minimized by reducing the beam ripple as much as possible and operating as high above Brillouin as practically possible. Computer particle simulations using the computer program WIGGLER.FORT bear out these conclusions as illustrated in Figure 9 which shows an example of velocity spread contours as a function of  $M$  number and beam ripple. The velocity spread contours shown in this figure are those extrapolated to the circuit region, and are a factor of two greater than those occurring in the wiggler due to the adiabatic compression of the beam.

It should be noted that for the same axial fields in the wiggler, higher  $M$  numbers are obtained with higher beam voltages and lower currents. The limitation on maximum  $M$  number occurs when it is physically impossible to wind helical coils on mandrels of smaller and smaller pitch with sufficient amp turns. It is evident that one requires a low perveance Pierce gun which can create a confined flow beam with very little ripple or scalloping. The electrode shapes and spacings necessary to produce an 80 kV beam carrying 12.5 amps are illustrated in Figures 10 and 11 which show the predicted electrostatic fields and beam trajectories in the cathode anode region. Figure 12 shows the optimized magnetic profile required to minimize beam ripple. A finite element magneto-static code is then used to synthesize the pole piece shapes necessary to produce this optimized magnetic field (Figure 13). A first design attempt based on the above considerations was carried out for the Pierce/wiggler for the JPL gyrokystron and led to the design parameters quoted in Table 3. A possible hardware realization is illustrated in Figure 14.

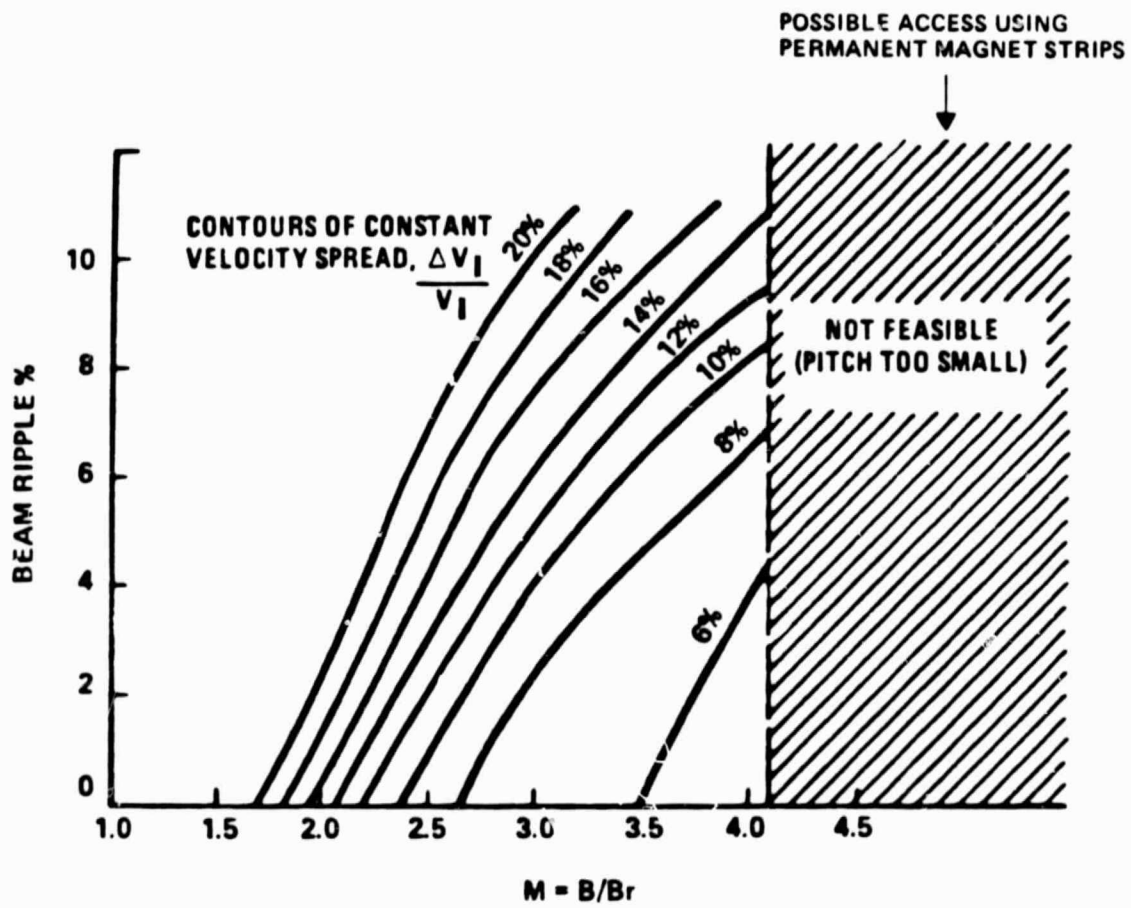


FIGURE 9. CRITERIA FOR OPTIMAL DESIGN OF PIERCE/WIGGLER SYSTEM

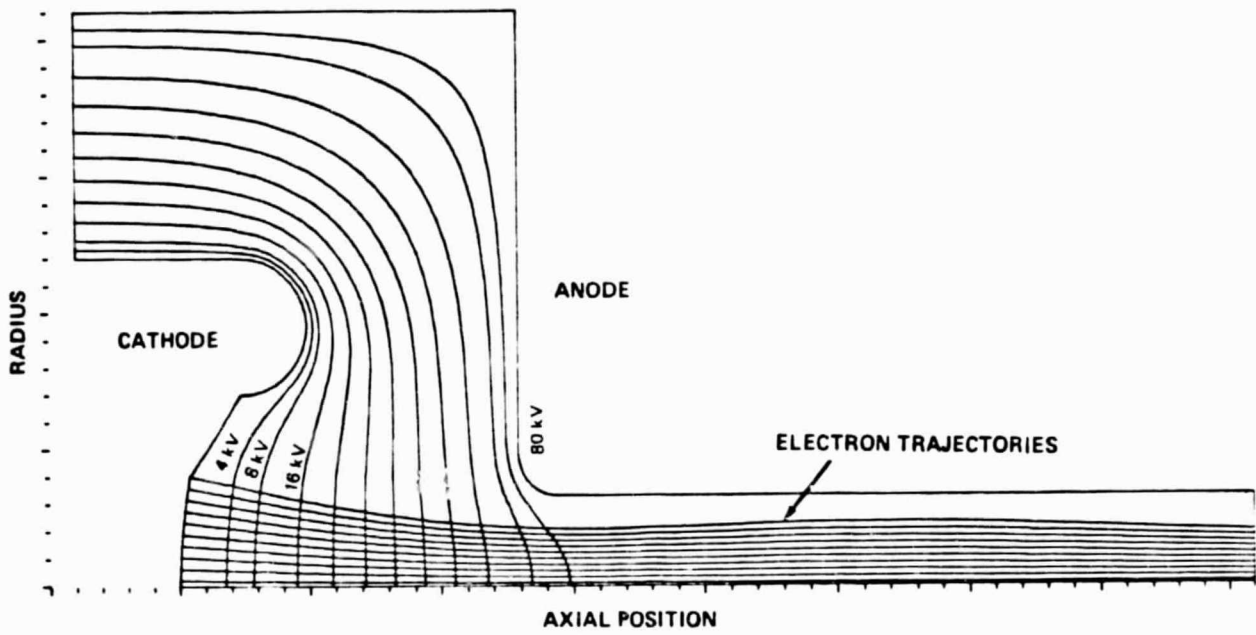


FIGURE 10. BEAM OPTICS FOR 80 KV PIERCE GUN

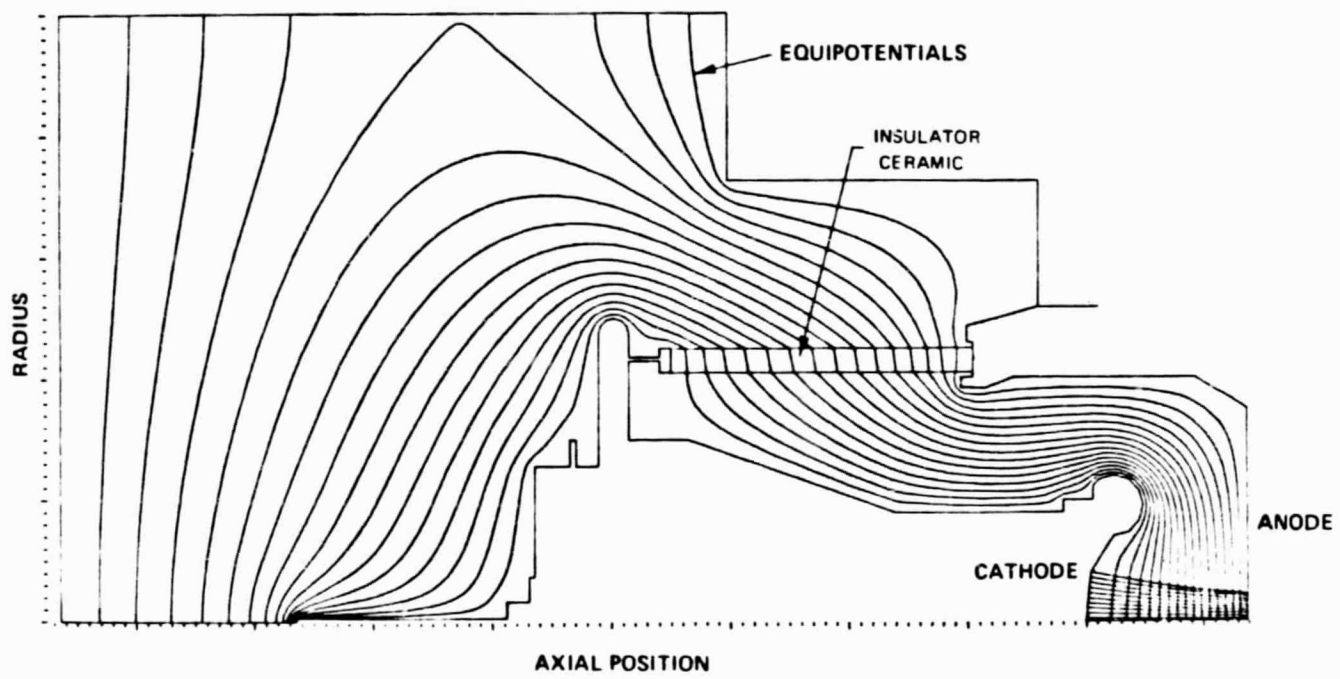


FIGURE 11. ELECTROSTATIC FIELDS IN GUN

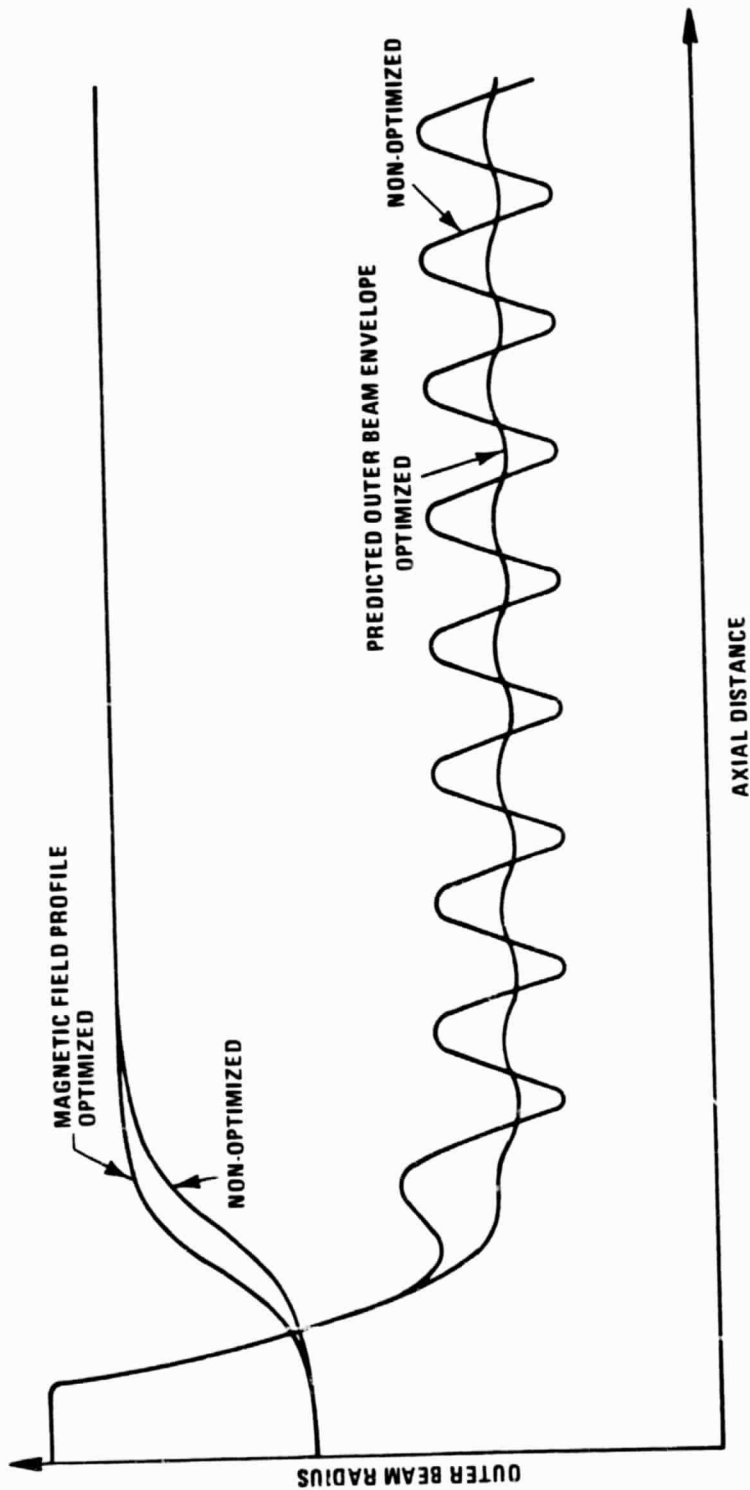


FIGURE 12. MAGNETIC PROFILE SHAPING TO REDUCE BEAM RIPPLE

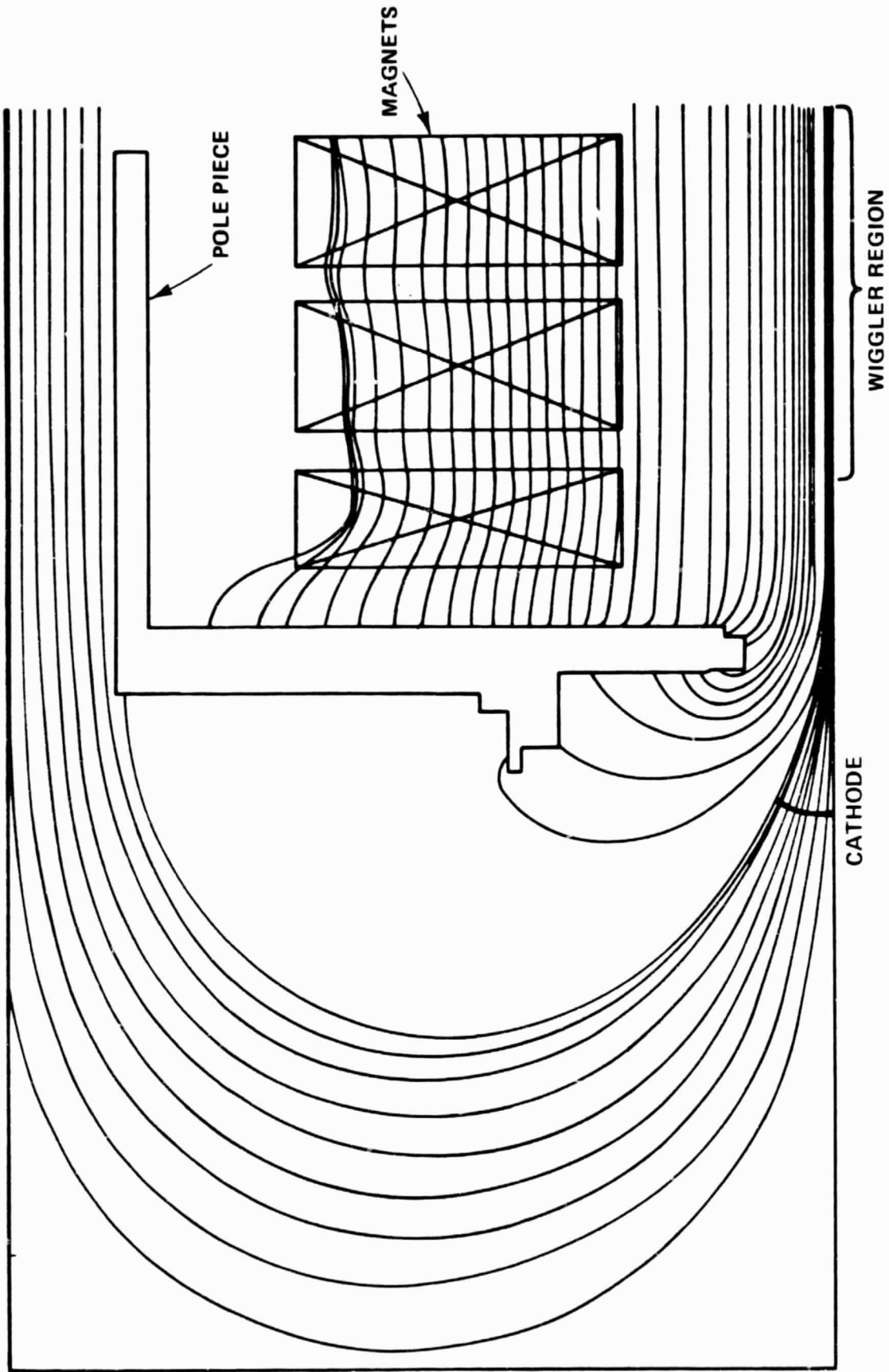


FIGURE 13. POLE PIECE CONFIGURATION FOR OPTIMIZED MAGNETIC FIELD PROFILE

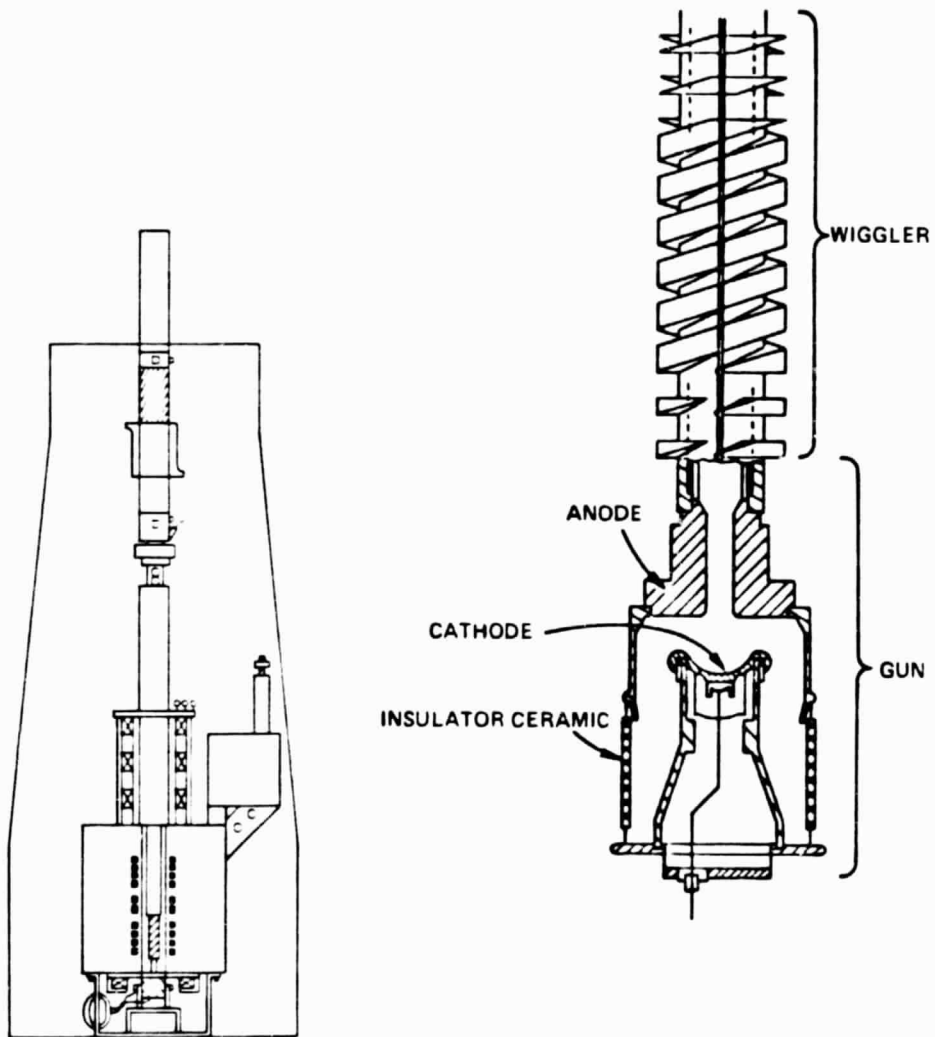


FIGURE 14. REALIZATION OF PIERCE/WIGGLER DESIGN

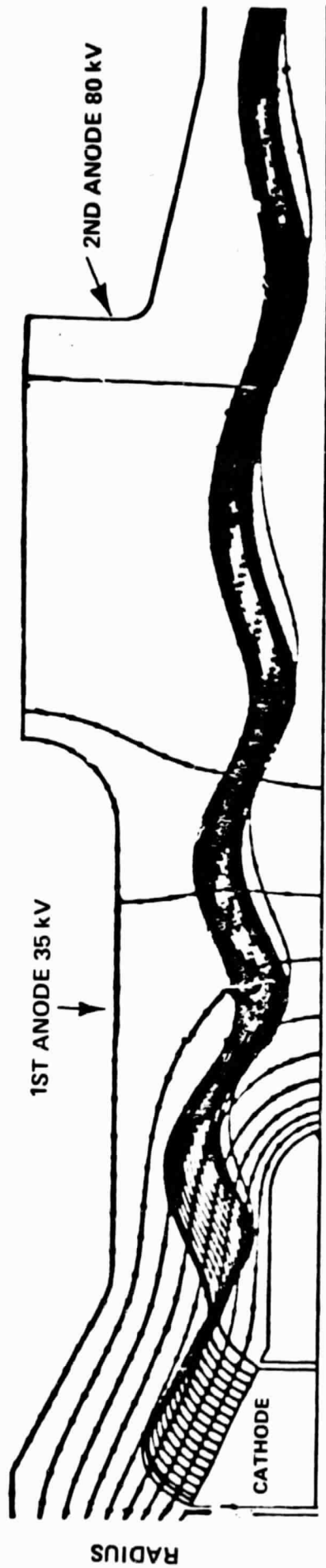
Table 3  
Pierce/Wiggler Design Specifications

Pitch	3.66 cm
Radius	3.83 cm
Length	22 cm
Amp Turns	~ 770
Axial B Field	1770 gauss
Wiggler Field	13.6 gauss
Beam Voltage	80 kV
Beam Current	12.5 amps
M Number (X Brillouin)	3.3
Cathode Loading	3.8 A/cm <sup>2</sup>
Perpendicular/Parallel Velocity	0.30 (In Wiggler)
% Velocity Spread	5.1% (~ 10% In Circuit)
Beam Radius $R_w$ in Wiggler	0.385 cm
Pierce Gun Compression	~ 7:1
Adiabatic Compression	7.35:1

C. MAGNETRON INJECTION GUN

The other approach to creating a suitable electron beam is to use a magnetron injection (MIG) gun illustrated in Figure 15. This gun would produce a hollow beam within the required 50% fill factor. Crossed electric and magnetic fields over the cathode give the beam its initial rotational energy. The beam is then accelerated to 80 kV and then finally adiabatically compressed as in the Pierce/wiggler scheme. Low velocity spread (<10%) is ensured only by making the cathode radius small (higher cathode loading) and optimally shaping the electrodes. Key design parameters for the MIG gun are given in Table 4.





AXIAL POSITION

FIGURE 15. BEAM OPTICS FOR 80 KV MIG GUN

ORIGINAL PAGE  
BLACK AND WHITE PHOTOGRAPH

RADIUS

Table 4  
MIG Gun Design Specifications

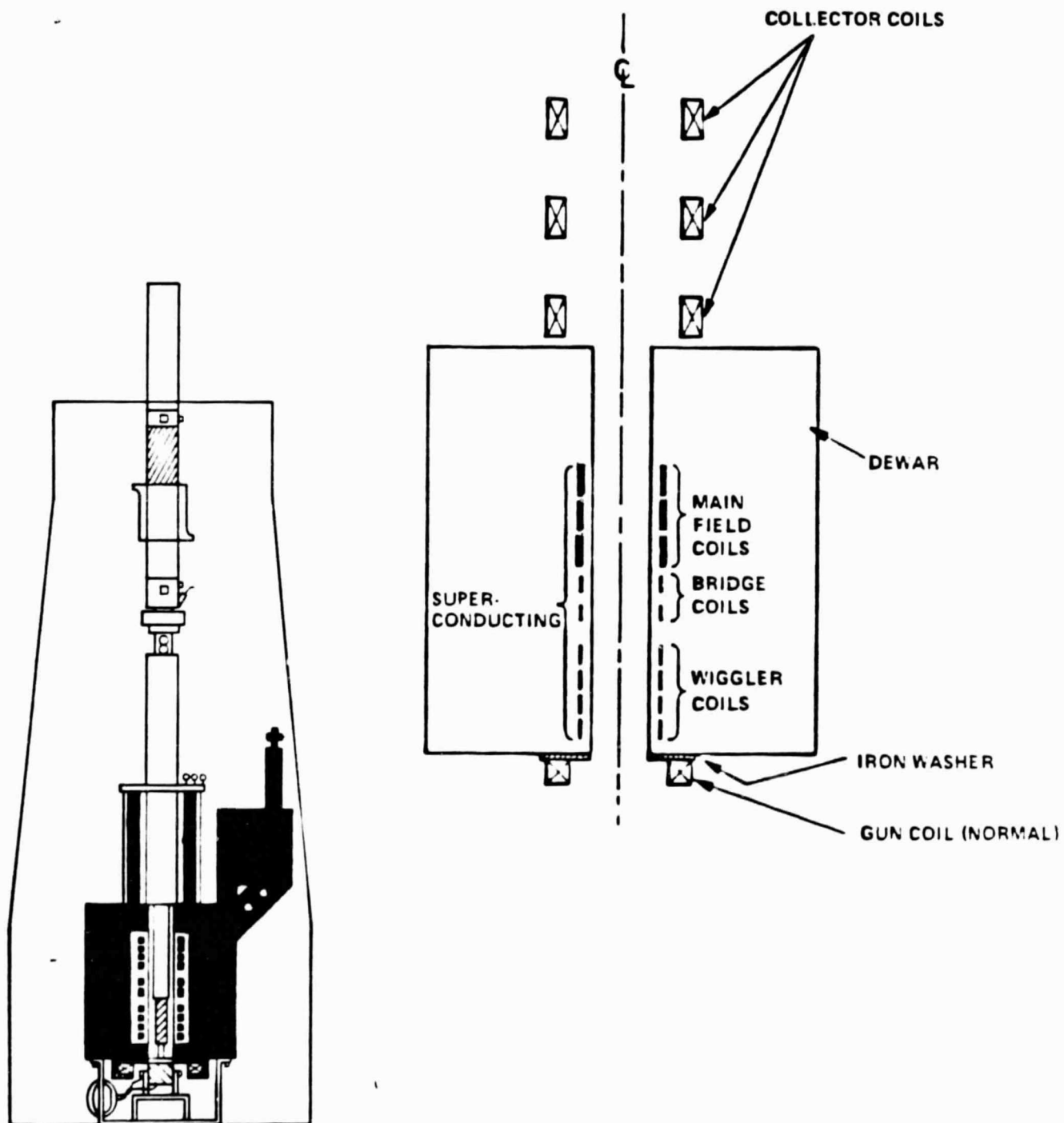
Beam Current (temperature limited)	12.5 amps
Mod Anode Voltage	35 kV
Anode Voltage	80 kV
Cathode Magnetic Field	1103 gauss
Cathode Radius	0.44 cm
Cathode Length	0.565 cm
Cathode Angle	15°
Cathode Loading	8 A/sq cm

The Pierce/wiggler was selected as the preferred design approach because the Pierce gun operates space charge limited (as opposed to temperature limited for the MIG gun) which greatly reduces shot noise. A more detailed discussion of shot noise will be given in the section on circuit design (Section IV). The required cathode loading can be about one-half that for the MIG gun giving greater reliability. The disadvantage of the Pierce/wiggler approach is that there has been limited experience in using the Pierce/wiggler in gyrotrons compared with MIG guns which are used extensively in gyrotron oscillators. Also, the wiggler increases the overall tube length by 6 - 12 inches and requires additional solenoid coils.

D. FEASIBILITY SUMMARY - BEAM OPTICS

In summary, the Pierce/wiggler is the preferred approach to generate the electron beam required for the JPL gyrokylystron, but it would be desirable to develop designs for the MIG gun as a backup.

# SOLENOID AND DEWAR



### III. SOLENOID AND DEWAR

#### A. CONCEPTUAL DESIGN

A typical on-axis magnetic field profile for a gyrokystron using a magnetic wiggler is shown in Figure 16. This field can be produced by the proposed magnet set shown in Figure 17. Nine solenoid coils produce the required profile. The large number of coils give the required versatility in an experimental tube in that the gun field and circuit field profiles can be varied independently. The number of coils could be reduced on subsequent magnets after further gyrokystron test experience is obtained. A superconducting solenoid design is favored for its advantages of low prime power consumption and low current ripple (which allows the required phase stability, as discussed in Section IV). The correct magnetic flux through the cathode is achieved with an iron pole piece and either a normal gun coil or iron rings. The correct profile in the collector region is obtained with three normal coils.

Key specifications for the coil set and dewar are:

1. The system is to be tiltable from vertical to  $75^{\circ}$  away from vertical (i.e.,  $15^{\circ}$  from horizontal) during operation;
2. a constant field of approximately 12,500 gauss is to extend over the circuit region; if a magnetic wiggler is used, a constant field of approximately 1800 gauss is to extend over the wiggler region;
3. maximum alignment errors, quantified by the ratio of the transverse magnetic field to the axial magnetic field, are to be less than 0.2% (i.e.,  $B_{\text{transverse}}/B_{\text{axial}} < 0.2\%$ );
4. the operating hold time of the liquid helium is to be 48 hours.

Vendor response to these specifications has been favorable. The last three specifications are considered standard. The capability to tilt the

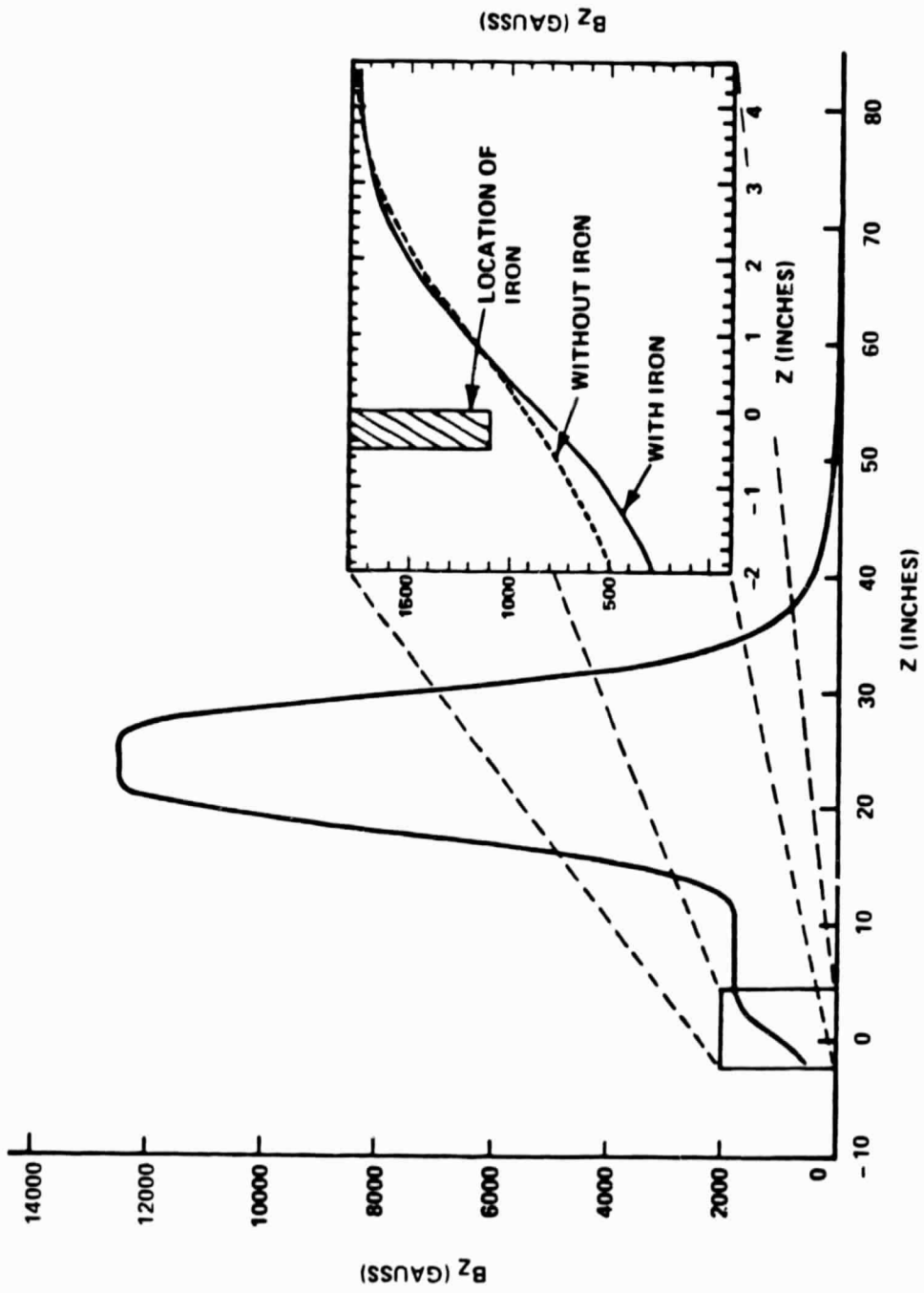


FIGURE 16. AXIAL MAGNETIC FIELD PROFILE,  $B_z$

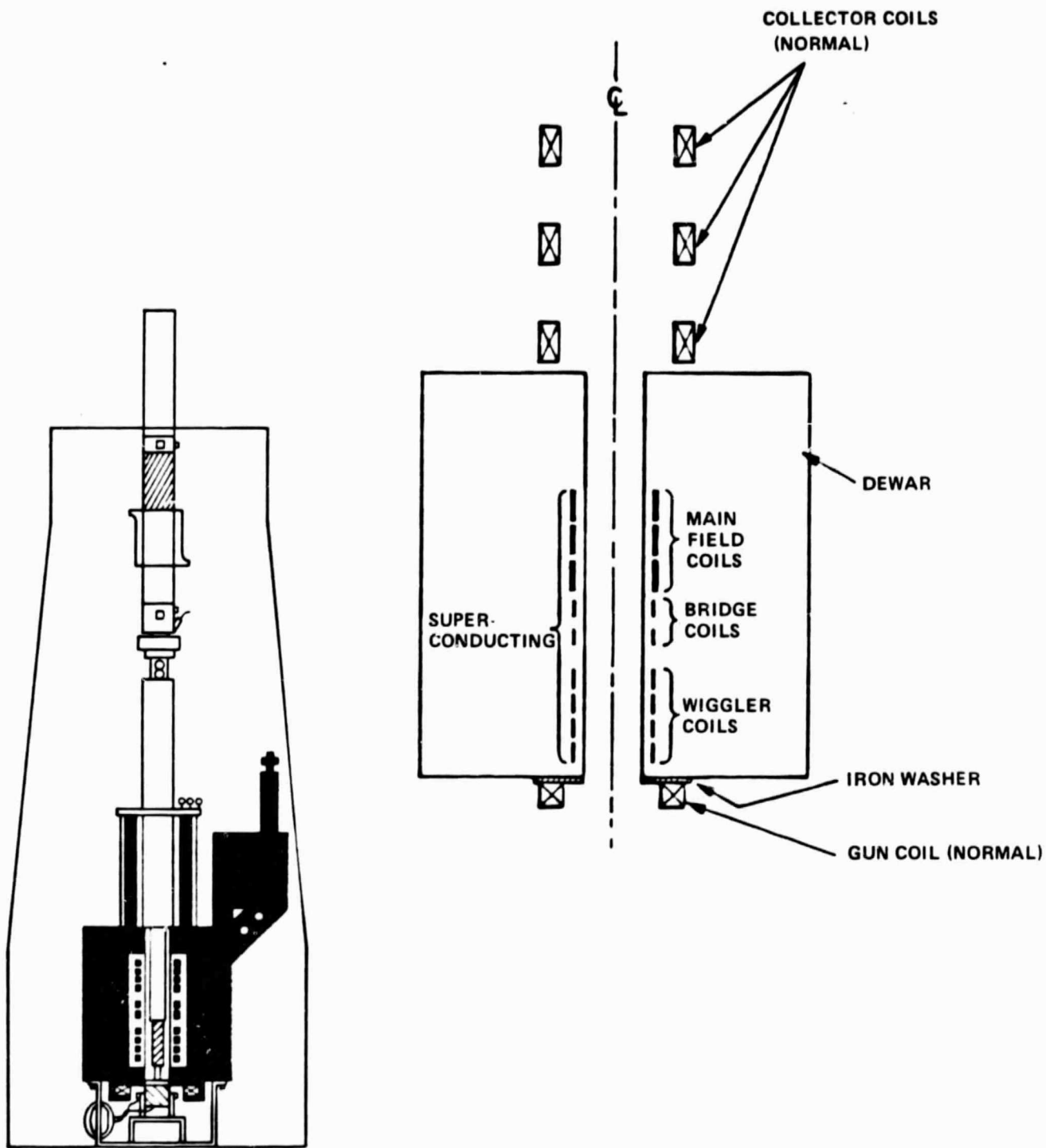


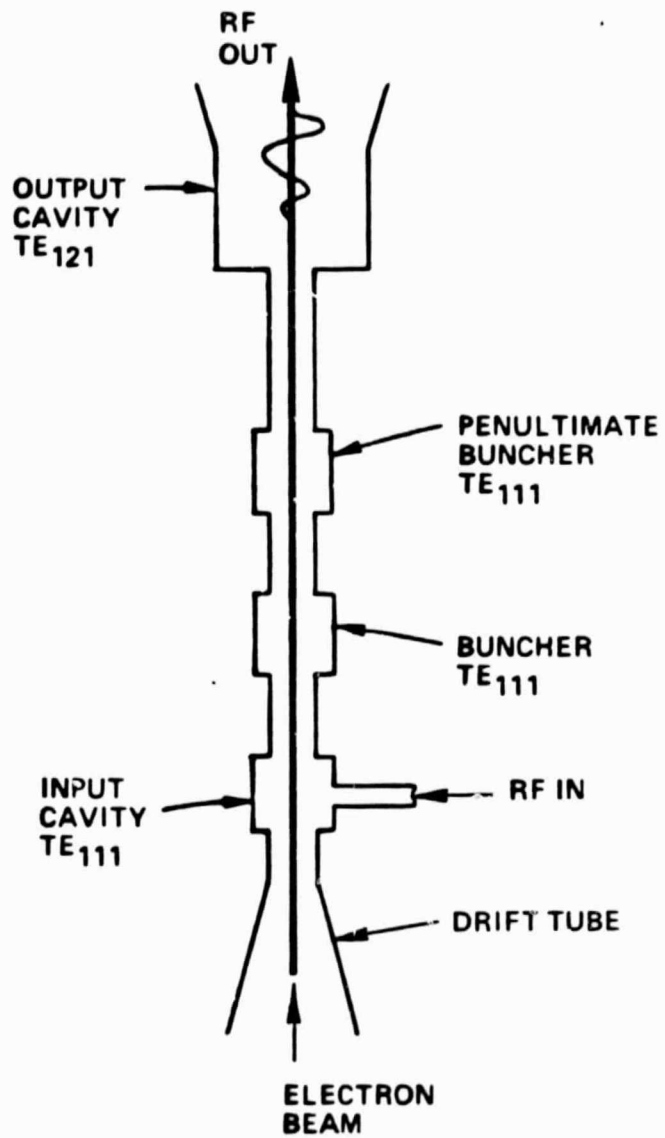
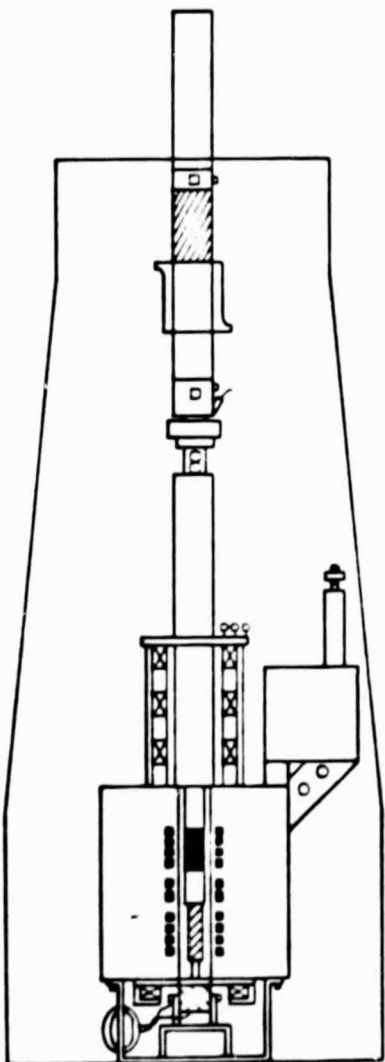
FIGURE 17. SOLENOID AND DEWAR

system is nonstandard; however, American Magnetics Inc., Magnetic Corporation of America and Intermagnetics General Corporation have each built at least one system that tilts.

B. FEASIBILITY SUMMARY - SOLENOID AND DEWAR

The proposed coil system is flexible, compatible with either magnetron injection gun or Pierce gun/wiggler operation. Coil specifications are consistent with present systems, and the ability to tilt adds to dewar complexity but is within the state of the art.

# GYROKLYSTRON CIRCUIT





## IV. GYROKLYSTRON CIRCUIT

### A. CHOICE OF RESONATOR MODES

The gyroklystron interaction circuit consists of a series of input resonant cavities operating in a TE cylindrical cavity mode connected by drift tubes which serve to prebunch the electrons in the transverse direction but with little energy exchange. The electron beam is assumed to have a large fraction of its energy in rotational motion. The prebunched beam can then be made to give up a large fraction of its energy to microwave radiation in the output cavity which is an open irregular low-Q resonator operating in an overmoded TE mode. Because of power handling considerations and mode integrity, the rf power cannot be extracted conventionally through a coupling hole at right angles to the device but must travel in line with the beam through an up taper and collector region. Gyrotron devices can operate at high powers and high frequencies due to the fact that electrons can interact in overmoded cavities. When the cavities are overmoded, however, the problem is introduced of suppressing unwanted modes in the cavities whose cutoff frequencies are close to the desired mode. Since the desired output mode for this program is  $TE_{11}$ , the dominant lowest order mode, it would be desirable to choose this operating mode for the entire gyroklystron to rule out the possibility of mode competition. While it would be feasible to operate the buncher cavities, where the power dissipation is low, in the  $TE_{111}$  mode, the requirement of 200 to 400 kilowatts of CW output power at 34 GHz demands a larger and therefore overmoded output cavity to limit the power density dissipated in its walls, as will be discussed later.

The use of  $TE_{111}$  mode buncher cavities has a number of advantages besides the fact that they would be operating in a single mode. Of significant importance is the fact that the interconnecting drift tubes between the cavities can be cut off to all modes, thus eliminating the problem of unwanted interaction in the drift tubes, a problem in previous gyroklystrons built at Varian<sup>4</sup>. In addition, tunable  $TE_{111}$  cavities are readily realiable.

With the bunchers operating in the  $TE_{111}$  mode, the output cavity must be of a  $TE_{1n1}$  type, i.e., the azimuthal index 1 must be the same as for the  $TE_{111}$ . As will be discussed below, the output cavity for this tube can be small enough to operate in the  $TE_{121}$  mode. Therefore, to obtain the required  $TE_{11}$  right-circularly-polarized output from the tube, only one mode converter, from  $TE_{12}$  to  $TE_{11}$ , will be needed in the output section of the gyrokystron.

Disadvantages to using  $TE_{111}$  buncher cavities are that the beam diameter must be small ( $\cong \lambda/4$ ), and that non-symmetric mode conversion is possible in the overmoded output sections of the tube.

As an alternative, it would be possible to use buncher cavities which operate in the  $TE_{011}$  mode. Advantages of these bunchers are that the beam diameter can be larger ( $\cong \lambda/2$ ), and that there would not be any TM modes present in the cavities. Disadvantages would be that the buncher cavities would be overmoded, thus allowing mode competition in them; the drift tubes between cavities would not be cut off to all modes, which raises the possibilities of interaction with the beam in the drift tubes and unwanted coupling between the buncher cavities; and that tuning of these cavities would require motion of their end walls, which presents mechanical difficulties. Also, with the bunchers operating in the  $TE_{011}$  mode, the output cavity would need to operate in the  $TE_{021}$  mode. Then to obtain a  $TE_{11}$  right-circularly-polarized output signal, it would be necessary to have three converters in the output section of the tube or transmission line: one to convert from the  $TE_{02}$  mode to the  $TE_{01}$  mode, one to convert from the  $TE_{01}$  mode to the  $TE_{11}$  mode, and a third to obtain the right circular polarization.

With either  $TE_{111}$  mode or  $TE_{011}$ -mode bunchers, a beam from either a MIG or a Pierce/wiggler gun configuration could be used to excite the circuit.

The preferred approach chosen for this program is to use  $TE_{111}$ -mode buncher cavities and a  $TE_{121}$ -mode output cavity, as shown in Figure 18. This ensures no mode competition in the bunchers or drift tubes since only the  $TE_{111}$  mode can exist in the bunchers and the drift tubes can be cut off

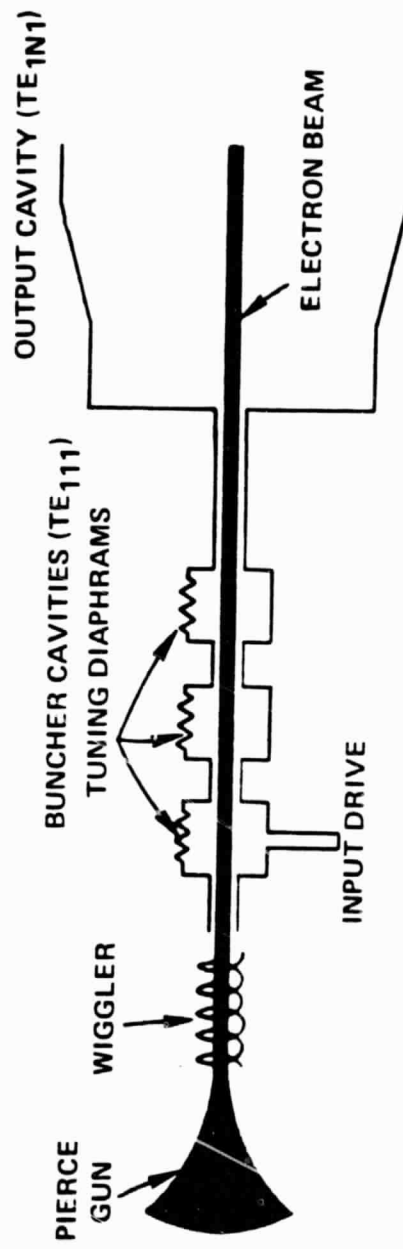


FIGURE 18. SCHEMATIC OF PROPOSED GYROKLYSTRON CONFIGURATION

to all modes near 34 GHz. The output  $TE_{12}$  mode can be easily converted to the antenna feed mode ( $TE_{11}$ ) by means of a single  $TE_{12}$ -to- $TE_{11}$  mode converter.

The power dissipated in a  $TE_{1n1}$ -mode output cavity is given by

$$P \text{ (W/cm}^2\text{)} = 4.838 \times 10^{-5} \left[ \frac{f_o^{5/2} P_o Q_{\text{ext}}}{k_{mn}^2 (L/\lambda_o) (1 - m^2/k_{mn}^2)} \right]$$

where  $f_o$  = frequency (GHz)  
 $P_o$  = output power (kilowatts)  
 $Q_{\text{ext}}$  = output cavity external Q  
 $k_{mn}$  = transverse mode number for  $TE_{mn}$  mode  
 $L/\lambda_o$  = cavity length in units of free space wavelengths

In order to stay within the limits of proven heat transfer technology at this time, the power dissipated in the cavity walls must be less than  $1 \text{ kW/cm}^2$ . The lowest order mode that can satisfy this criterion in a  $TE_{1n1}$  cavity is the  $TE_{121}$  mode. The most pessimistic estimate for the power in this mode at 34 GHz is obtained by assuming an output power  $P_o = 400$  kilowatts,  $Q < 400$  (a requirement to achieve bandwidth of 0.1%) and  $L/\lambda_o \leq 3$  (for reasons of efficiency). Then the maximum power dissipated for operation in the  $TE_{121}$  mode is  $P_{\text{max}} = 635 \text{ W/cm}^2$ , which is well below the maximum allowed  $1000 \text{ W/cm}^2$ .

A possible competing mode to the  $TE_{121}$  mode would appear to be the  $TE_{411}$ , since  $k_{41} (5.318) \approx k_{12} (5.331)$ . However, the threshold currents required to excite this mode will be much higher than the operating current since the beam's special bunching pattern of  $\cos \theta$  created by the buncher cavities will be incompatible with the required  $\cos 4\theta$  pattern for the  $TE_{411}$  mode. Further assurance against mode competition comes from the fact that the fields of the  $TE_{411}$  mode are essentially null near the axis where the beam is located while the fields of the  $TE_{121}$  mode attain their maximum value on axis.

A detailed circuit design for the gyrokystron consists of choosing the cavity lengths, drift tube lengths, cavity frequencies and cavity cold Q's such that when an electron beam of the desired voltage, current and rotational energy is made to pass through the circuit, the required gain, bandwidth and efficiency will be obtained while maintaining circuit stability against oscillation in either the  $TE_{111}$  or  $TE_{121}$  modes.

Note that the  $TE_{mn}^0$  cavity modes (with  $m \neq 0$ ) are degenerate in the sense that the fields for any particular mode can be expressed as an arbitrary linear combination of a pair of modes which have identical topology but are orthogonal in the x-y plane. Depending on the phase between this degenerate pair the cavity field structure can be right or left circularly polarized (RCP or LCP), linearly polarized (LP) or elliptically polarized. However, because the electrons on the beam rotate in the right hand sense, only RCP cavity fields will experience positive gain. For this reason, the output signal itself is inherently RCP also.

For mechanical convenience, our gyrokystron input buncher cavity is fed by a single input waveguide through a single slot and thus LP fields are excited in the input buncher. Since an LP wave is a combination of RCP and LCP waves of equal amplitude only one-half of the input power is available for amplification when the input cavity is excited in this manner. Thus there is 3 dB less signal gain than would be achieved if an RCP wave was excited in the cavity directly. We account for this effect in the circuit design by assuming that a pure RCP wave is launched in the input buncher but then requiring that the total circuit provides an additional 3 dB gain beyond the specified 50 dB. All calculations of gain presented later in this section have been corrected to include this effect and indicate the true gain as would be measured by the gyrokystron transmitter operator.

## B. STABILITY CRITERIA

The circuit characteristics are chosen using both small and large signal gyrokystron theories developed at Varian. It can be rigorously shown that the same equivalent circuit used for many years in describing klystrons can be used to describe gyrokystrons if the transadmittance and

beam loaded Q's are redefined<sup>5</sup>. In particular, the expression for the gain of an N cavity gyrokystron takes the same form as that for a conventional klystron, namely;

$$\text{Gain} \approx \frac{F(\omega, \Omega_c)}{\left| (1 - 2i\delta_1 Q_1) \right|^2 \left| (1 - 2i\delta_2 Q_2) \right|^2 \dots \left| (1 - 2i\delta_n Q_n) \right|^2}$$

where  $\delta_n = (\omega - \omega_n^N) / \omega_n^N$   
 $\omega_n$  = resonant frequency of cavity n.  
 $\Omega_c$  = cyclotron frequency

The major difference is that the circuit elements such as beam loaded Q and transmittance can have a strong dependence on magnetic field and frequency compared with conventional klystrons as shown in Figure 19. Even with these differences, general design strategies from conventional klystrons are carried over into gyrokystron design. The buncher cavities are designed to have positive beam loading while the output cavity has negative beam Q of sufficient absolute magnitude to prevent oscillation (i.e., oscillation threshold currents are factor of 2 higher than operating current). This allows bunching with no energy exchange, critical for CW operation while allowing maximum efficiency at the output. Positive beam loading also allows operation with the required total Q's for the buncher cavities without excessively loading them with loss; an important consideration in actual cavity manufacture. The use of a buncher cavity next to the output cavity but tuned outside the band is also used to enhance efficiency (penultimate cavity). Feedback from one cavity to another is eliminated by choosing the drift tubes long enough so that at least 25 dB isolation exists from one cavity to the next.

### C. CIRCUIT DESIGN DETAILS

After a number of iterations, a circuit design was devised for the JPL gyrokystron with the basic performance characteristics shown in Table 5. The design consists of 3 input bunchers and an open output resonator. Linear theory was used to determine the cavity lengths, drift tube lengths and cavity external and beam loaded Q's.<sup>5</sup> Large signal theory was required

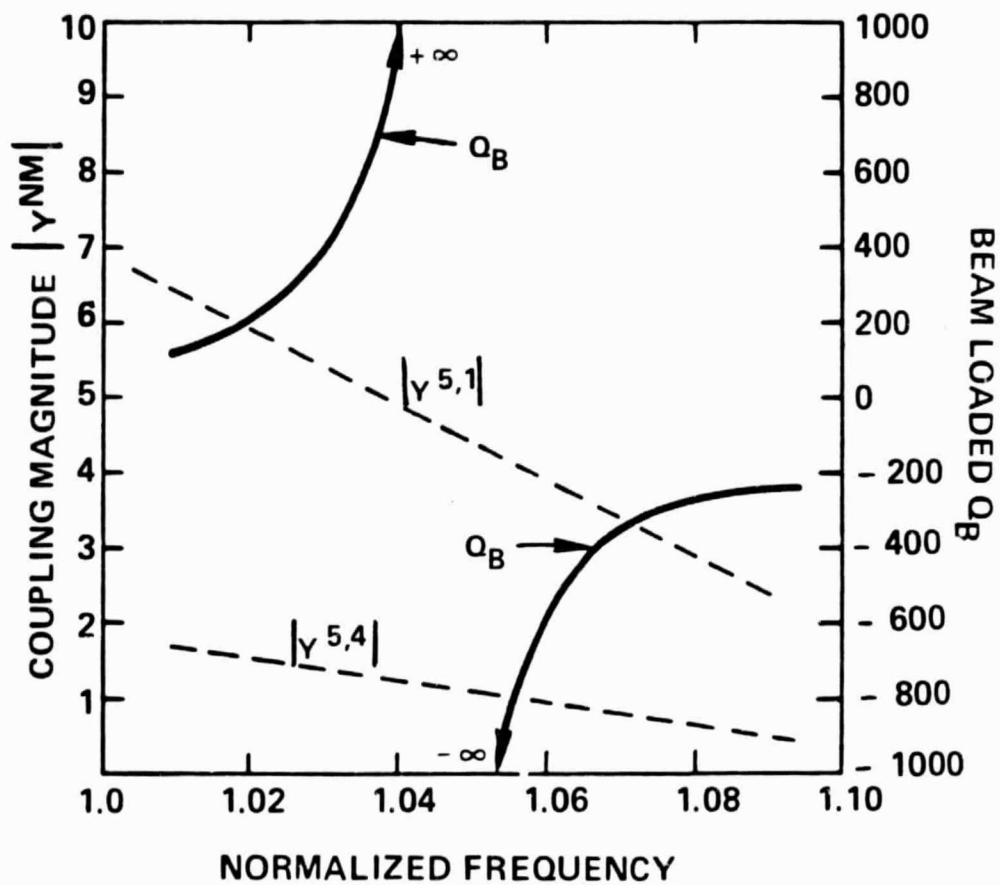


FIGURE 19. BEAM LOADED  $Q_B$  AND "TRANSADMITTANCE"  $Y^{5,4}$ ,  $Y^{5,1}$  vs FREQUENCY

to determine the exact cavity frequencies, output cavity Q and exact output cavity length in order to maximize efficiency. The gyrokystron circuit parameters are given in Table 6. Short input cavities were required to keep the beam loading positive. Even so, external cold Q's of 300 and 400 give an added safety margin in preventing the bunchers from oscillating. The output cavity Q of 120 is almost one-half of the absolute value of the beam loaded  $Q_B$  ensuring that the output will not oscillate. To actually realize an external Q of 120, a shaped iris is required, as illustrated in Figure 20, which is determined by examining mode solutions in arbitrary shaped open resonators. The drift tube just before the output is made longer to give extra isolation of the output cavity which contains high levels of microwave power. A physical realization of the circuit is illustrated in Figure 21.

Table 5  
Circuit Performance

Power Output	450 kW
Wall Loading in Output Cavity	400 Watts/sq cm average
Frequency	34.03 GHz (center)
Saturated Bandwidth	0.29%
Linear Gain	57 dB
Saturated Gain	50 dB
Efficiency	45%



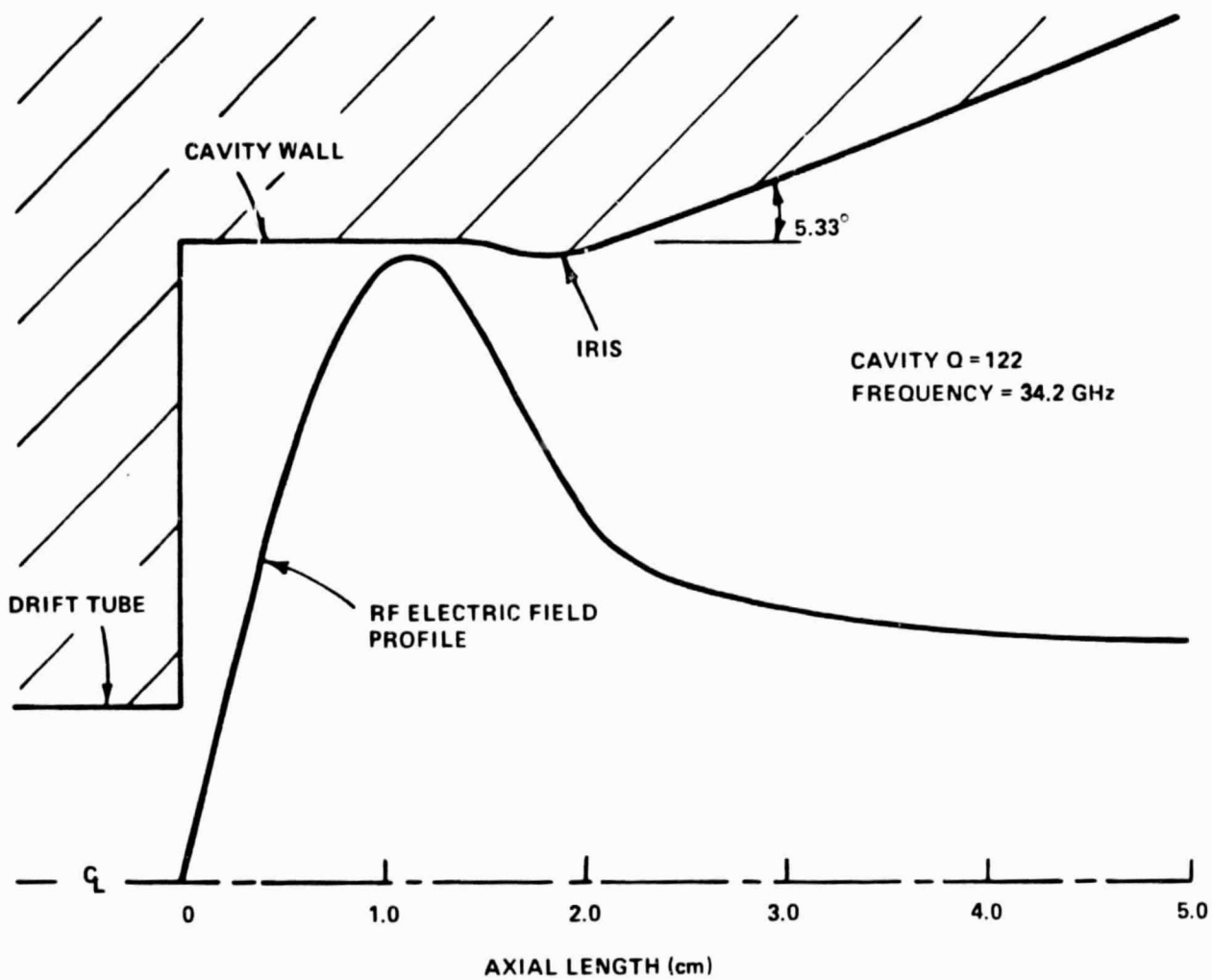


FIGURE 20. ELECTRIC FIELD PROFILE FOR TE<sub>12</sub> OUTPUT CAVITY

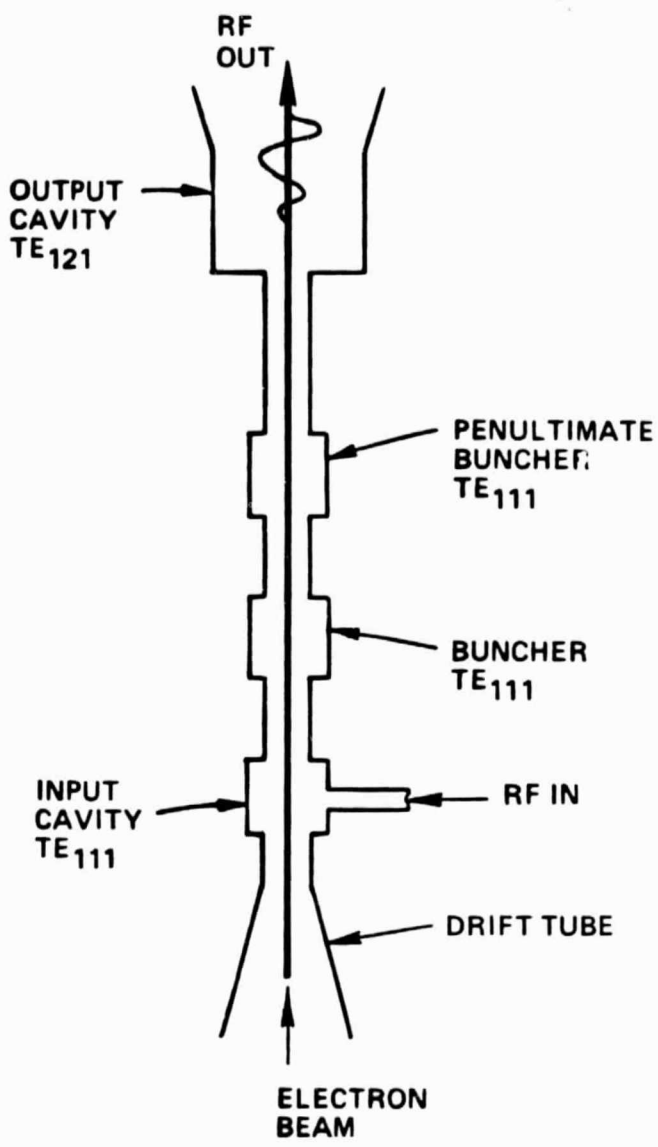
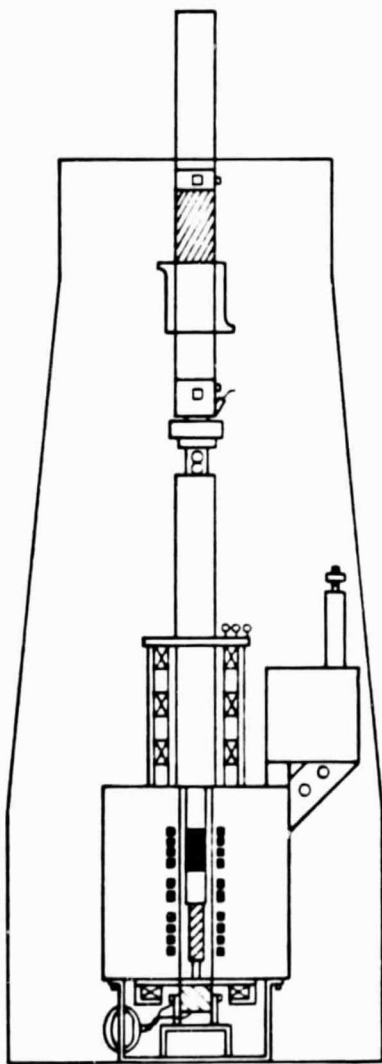


FIGURE 21. GYROKLYSTRON CIRCUIT

Table 6  
Cavity Design

Voltage	80 kV
Current	12.5 Amps
$v_{\perp}/v_{\parallel}$	1.5 (~ 75% rotational energy)
Beam Radius	0.146 cm
Magnetic Field	~ 12,500 gauss

Cavity No.	Type	Cold Q	Loaded Q	Freq (GHz)	Length (cm)	Drift Tube (cm)	Radius (cm)
1	TE <sub>111</sub> Input	300	156	33.90	0.784	—	0.3137
2	TE <sub>111</sub> Buncher	400	180	33.68	0.784	0.784	0.3167
3	TE <sub>111</sub> Penultimate	400	180	33.60	0.784	0.784	0.3178
4	TE <sub>121</sub> Output	120	263	34.19	1.7254	2.196	0.7693

D. CALCULATED CIRCUIT PERFORMANCE

The following results (Figure 22 through 32) give a detailed performance of the circuit behavior. Figure 22 shows linear gain and phase versus frequency. The phase varies almost linearly with frequency within the 0.33 percent linear bandwidth range. Figure 23 shows power out versus frequency for four input drive power levels. At 4 watts of drive power, the 1 dB saturated bandwidth is ~0.3 percent. Figure 24 shows power out versus power in for different frequencies. Different frequencies saturate at various power levels. This illustrates the sensitivity of the gyrokystron to the difference between the operating frequency and the cyclotron frequency. Figure 25 illustrates the variation of power and phase with voltage. The sensitivity shown is actually coming from the change in rotational energy that results when the change in voltage puts the wiggler off resonance which then gives the beam less rotation. Figure 26 shows how the power and phase vary with beam current. Changes in beam current modify the beam loaded Q's which change the effective bandwidth in the cavities and thus the output power and phase. Figure 27 illustrates the change in phase and power with the circuit magnetic field. This extreme sensitivity to

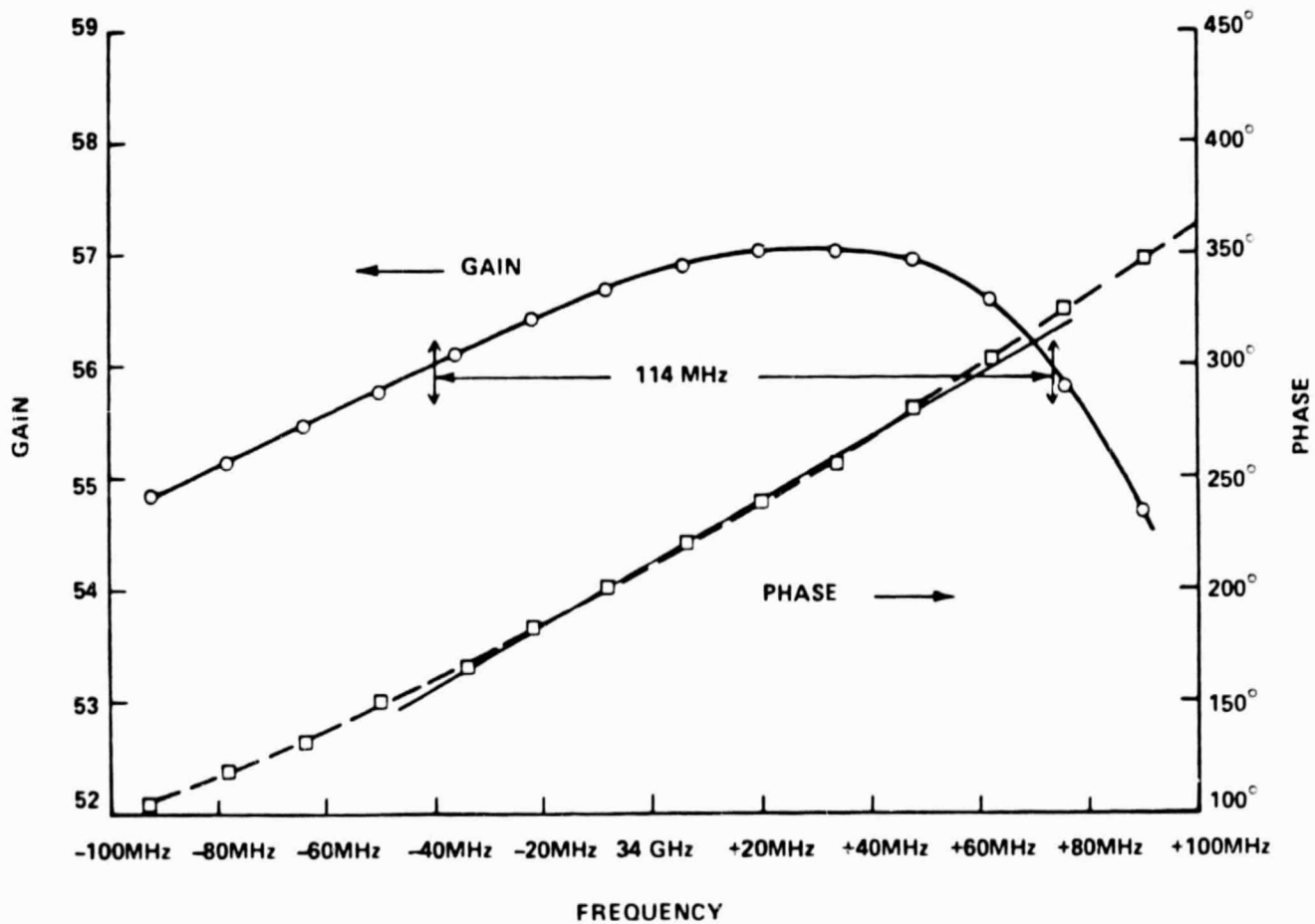


FIGURE 22. LINEAR GAIN AND PHASE vs FREQUENCY

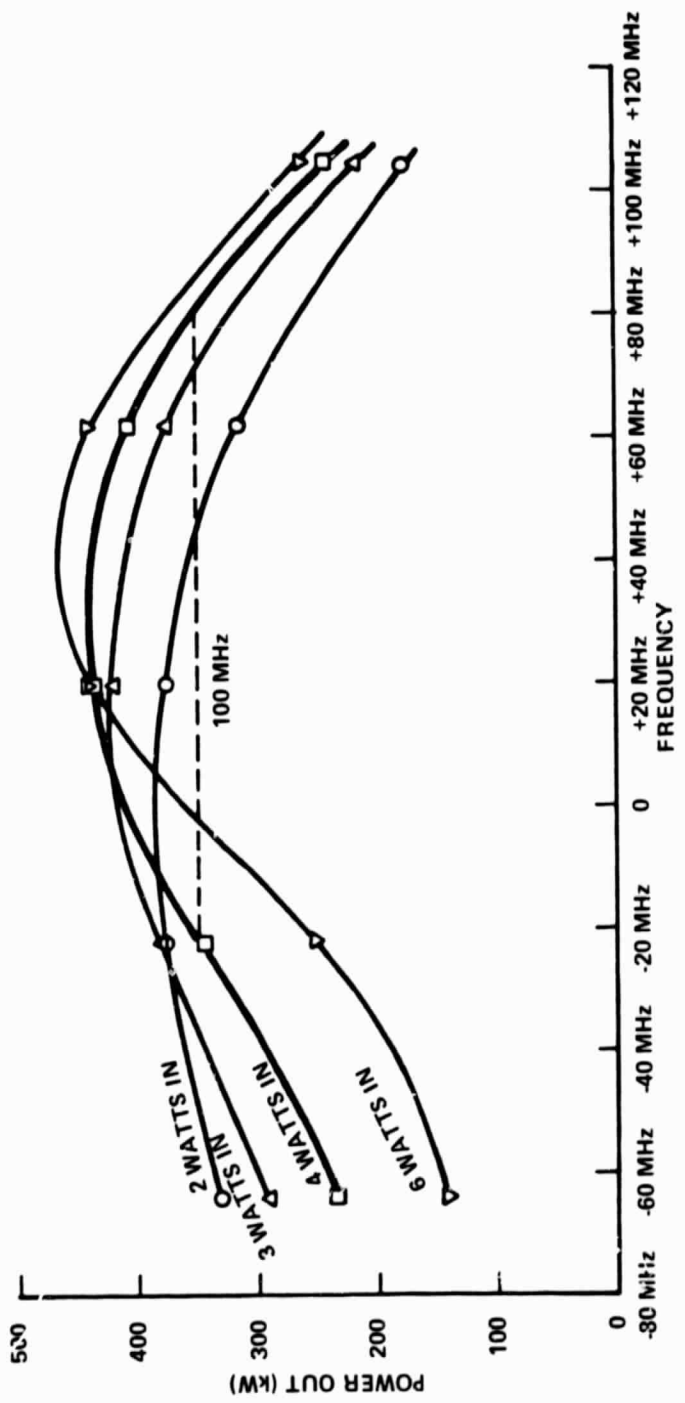


FIGURE 23. POWER OUT vs FREQUENCY AND DRIVE LEVEL

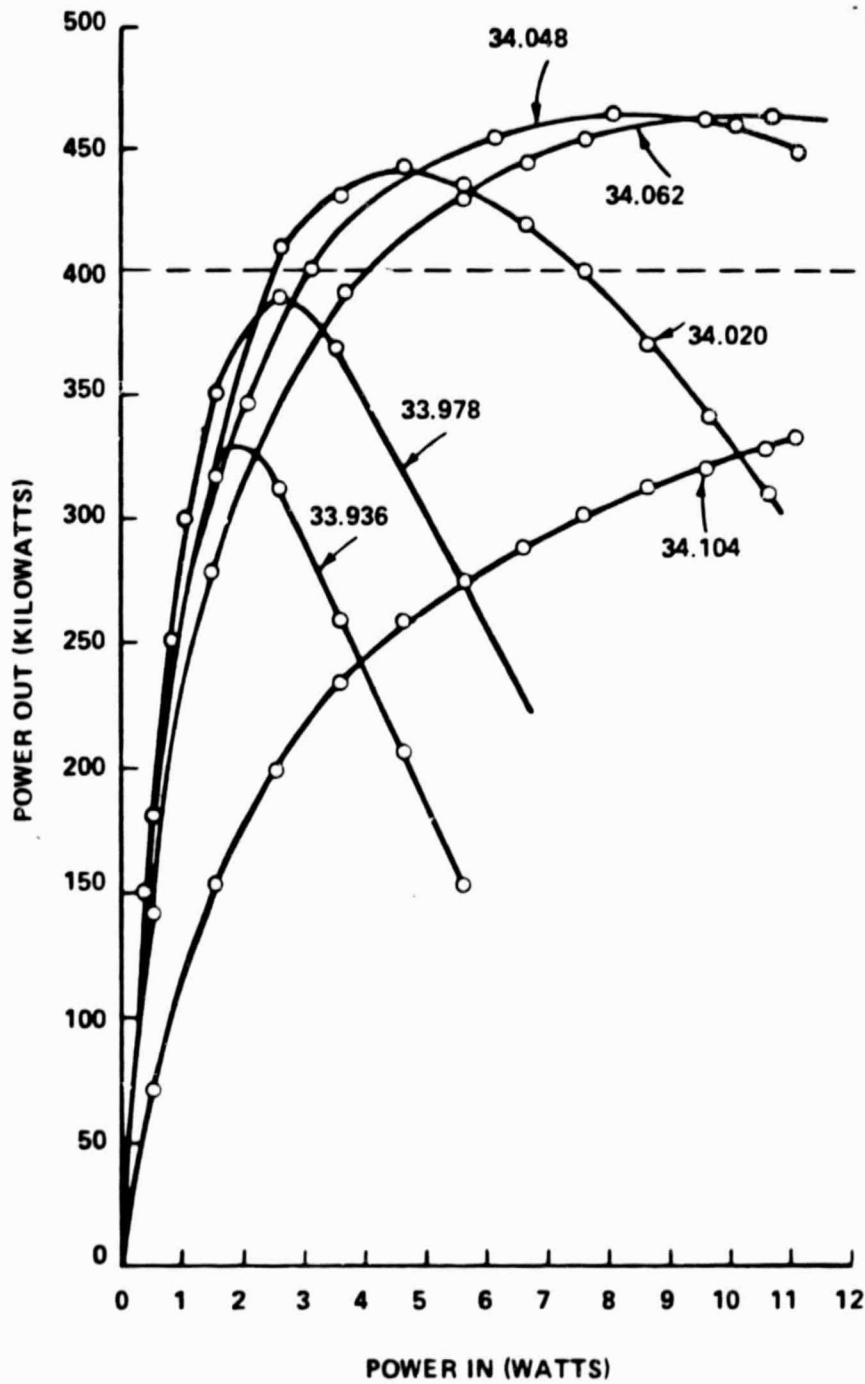


FIGURE 24. POWER OUT vs POWER IN (DIFFERENT FREQUENCIES)

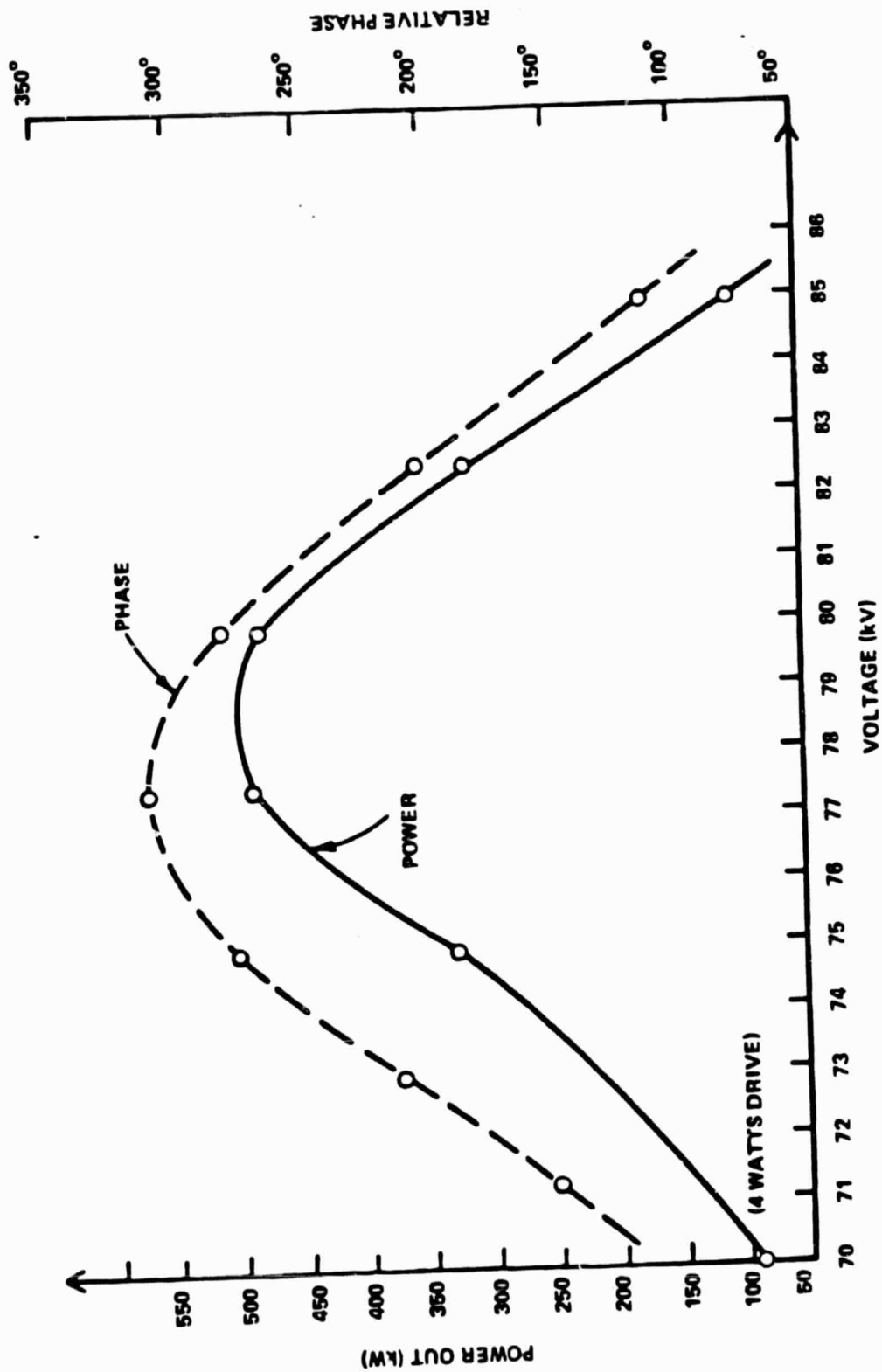


FIGURE 25. POWER OUT AND PHASE vs VOLTAGE

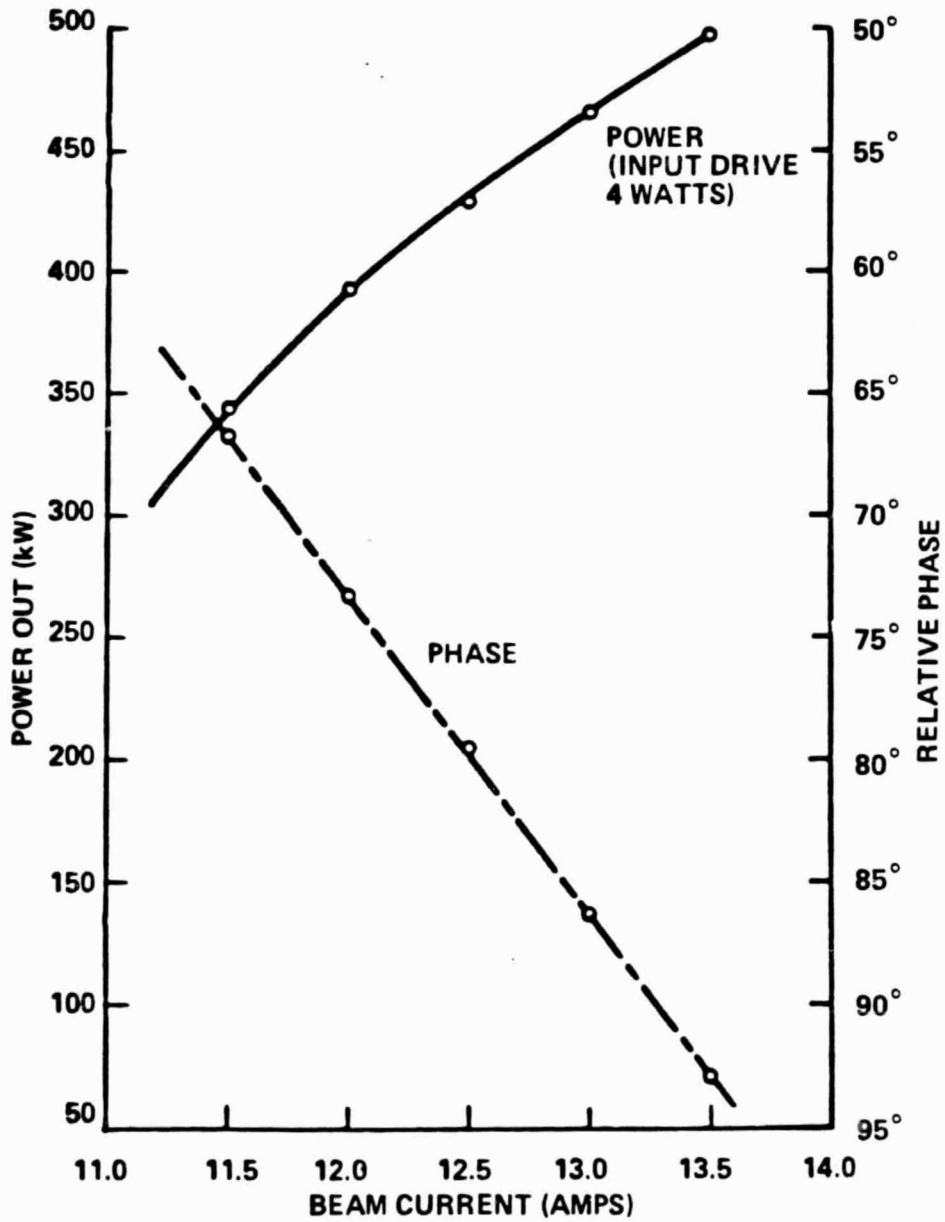


FIGURE 26. POWER OUT AND PHASE VS BEAM CURRENT



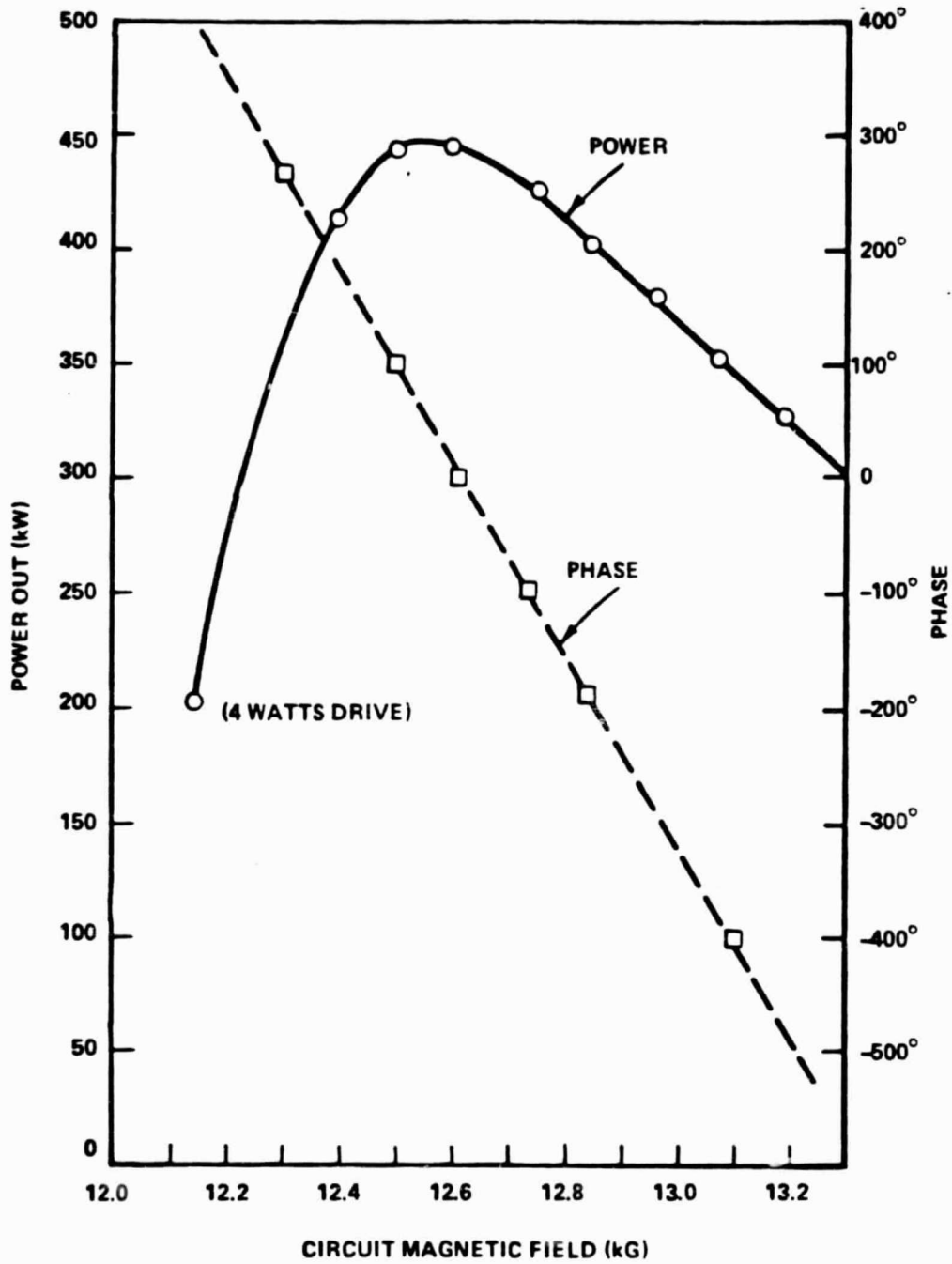


FIGURE 27. POWER OUT AND PHASE VS CIRCUIT MAGNETIC FIELD

magnetic field is again a unique characteristic of gyrokystrons and reflects the fact that the beam interacts with a cyclotron wave, not a space charge wave. This sensitivity need not cause problems since the fields are produced from superconducting magnets which have virtually no fluctuation in the coil currents. Figure 28 shows how power and phase vary with  $\alpha$  (ratio of perpendicular to parallel velocity). This variation actually results from variations in either the transverse or axial wiggler fields. Superconducting coils eliminate fluctuations in the axial field. Permanent magnet wigglers can eliminate fluctuations in the transverse fields. Load mismatches at the tube output cause problems by modifying the effective external Q of the output cavity. Figure 29 shows how the power out is modified by having the effective Q go from 120 to 180. This is an extreme case indicating a mismatch with a VSWR of 2 and the most unfavorable phase. The sensitivity to cavity tuning is illustrated in Figures 30 and 31. Figure 30 shows the effect of tuning all cavity resonant frequencies by  $\pm 0.25$  percent as a result of cavity heating. It should also be noted that the power can drop 15 percent. This indicates the desirability for accurate tunable cavities as exist for conventional klystrons. Figure 31 shows how to enhance efficiency by tuning the penultimate buncher cavity below the circuit passband.

#### E. VELOCITY SPREAD EFFECTS

In Figure 32, the effect of beam velocity spread on output power is shown. Note that a 10 percent velocity spread can almost cut the tube output power and efficiency in half. On-going studies suggest a number of solutions to the deterioration of performance with velocity spread. If one operates at higher voltages (90-95 kV) and lower currents, it is possible to reduce space charge effects (higher M number) and reduce velocity spreads. Use of permanent magnets for the wiggler and increasing the taper lengths for the transverse field may improve beam quality, reducing spreads. Further design work on the MIG may show that it is possible to generate higher quality beams in this way rather than with the Pierce/wiggler. The circuit can be made with longer cavity lengths so that the resonant frequencies are closer to the cavity cut off giving lower axial wave numbers ( $k_z$ ). Since velocity spread effects are in part due to doppler shifts of

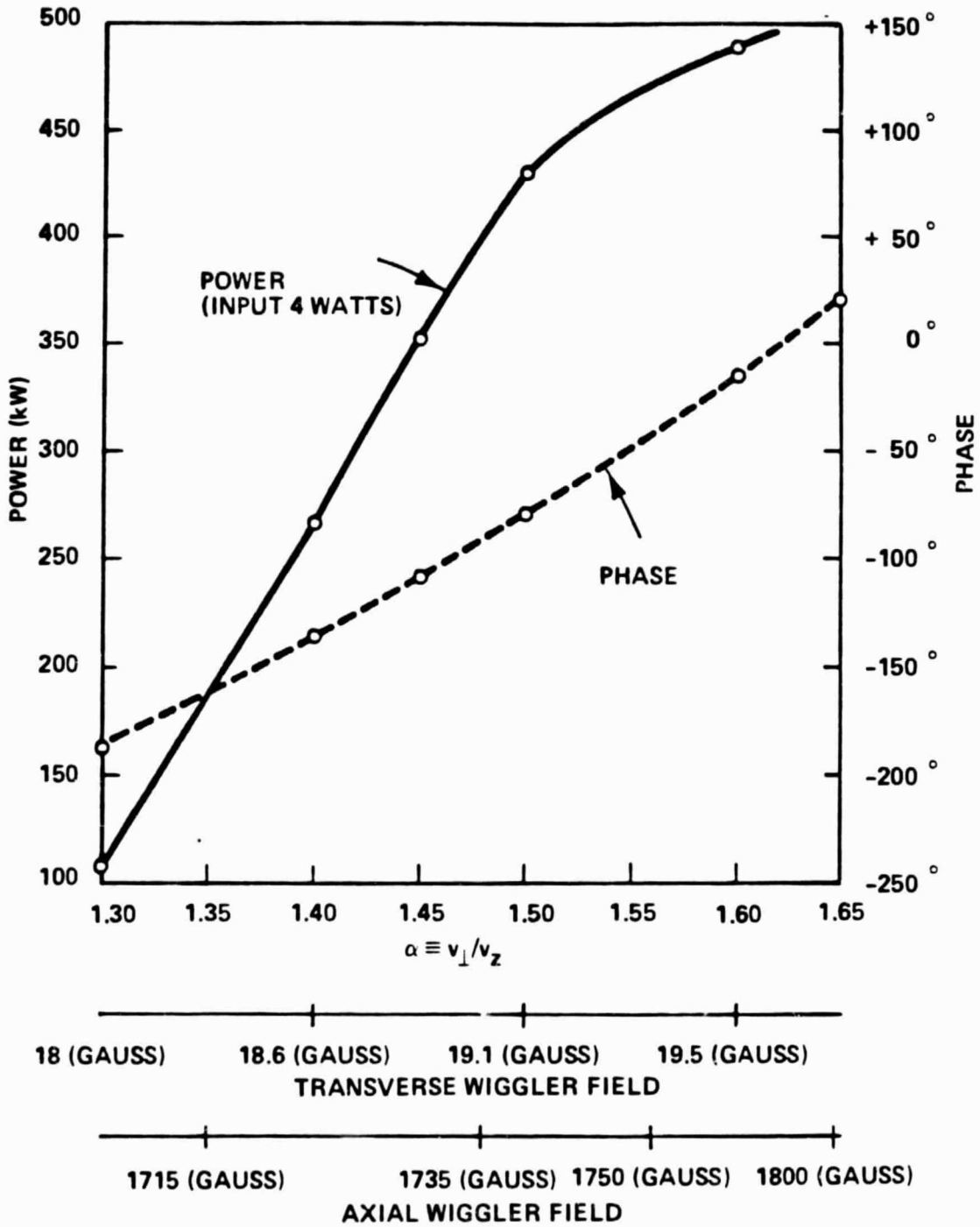


FIGURE 28. POWER OUT AND PHASE vs ALPHA (WIGGLER FIELDS)

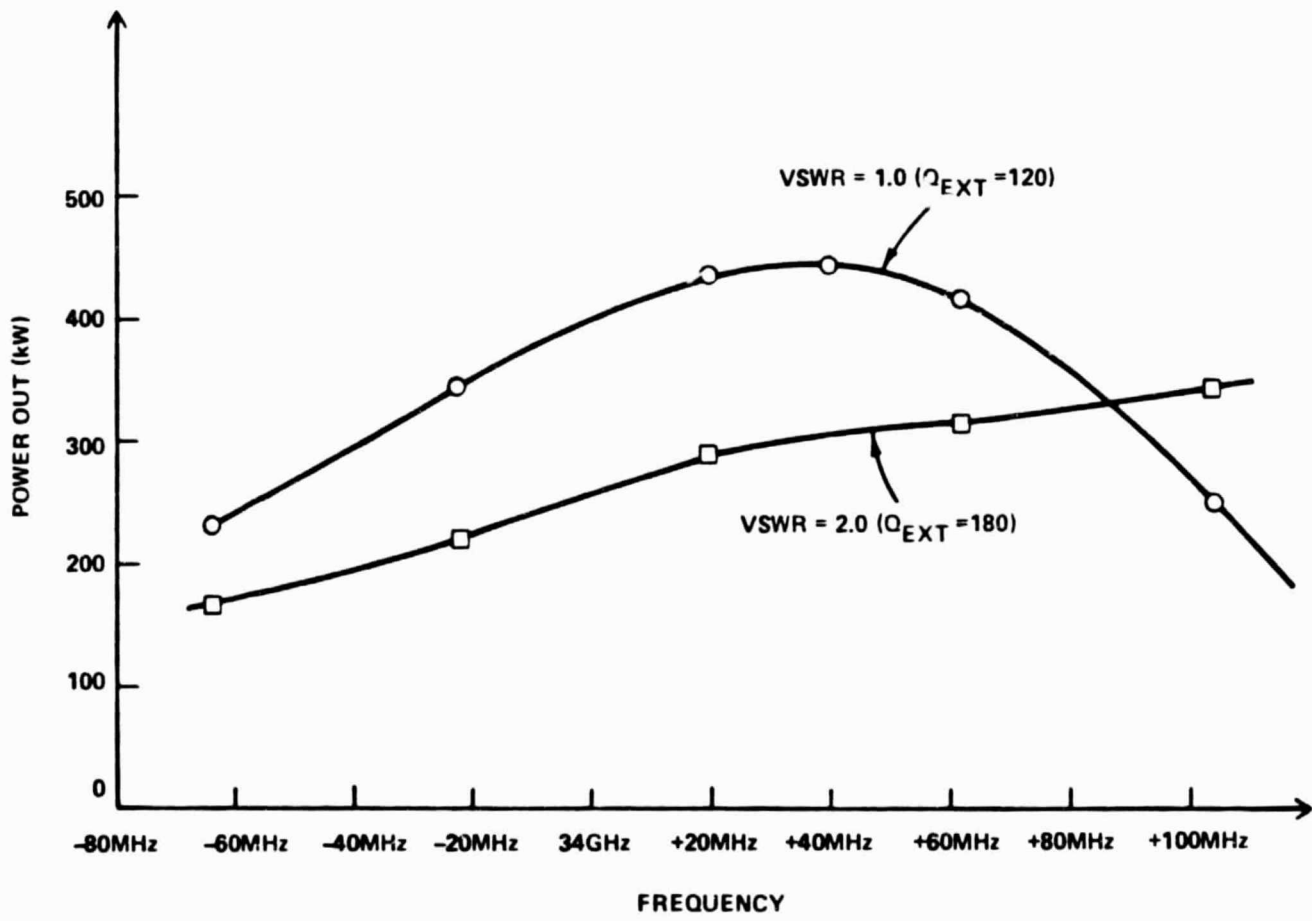


FIGURE 29. EFFECT OF LOAD MISMATCH

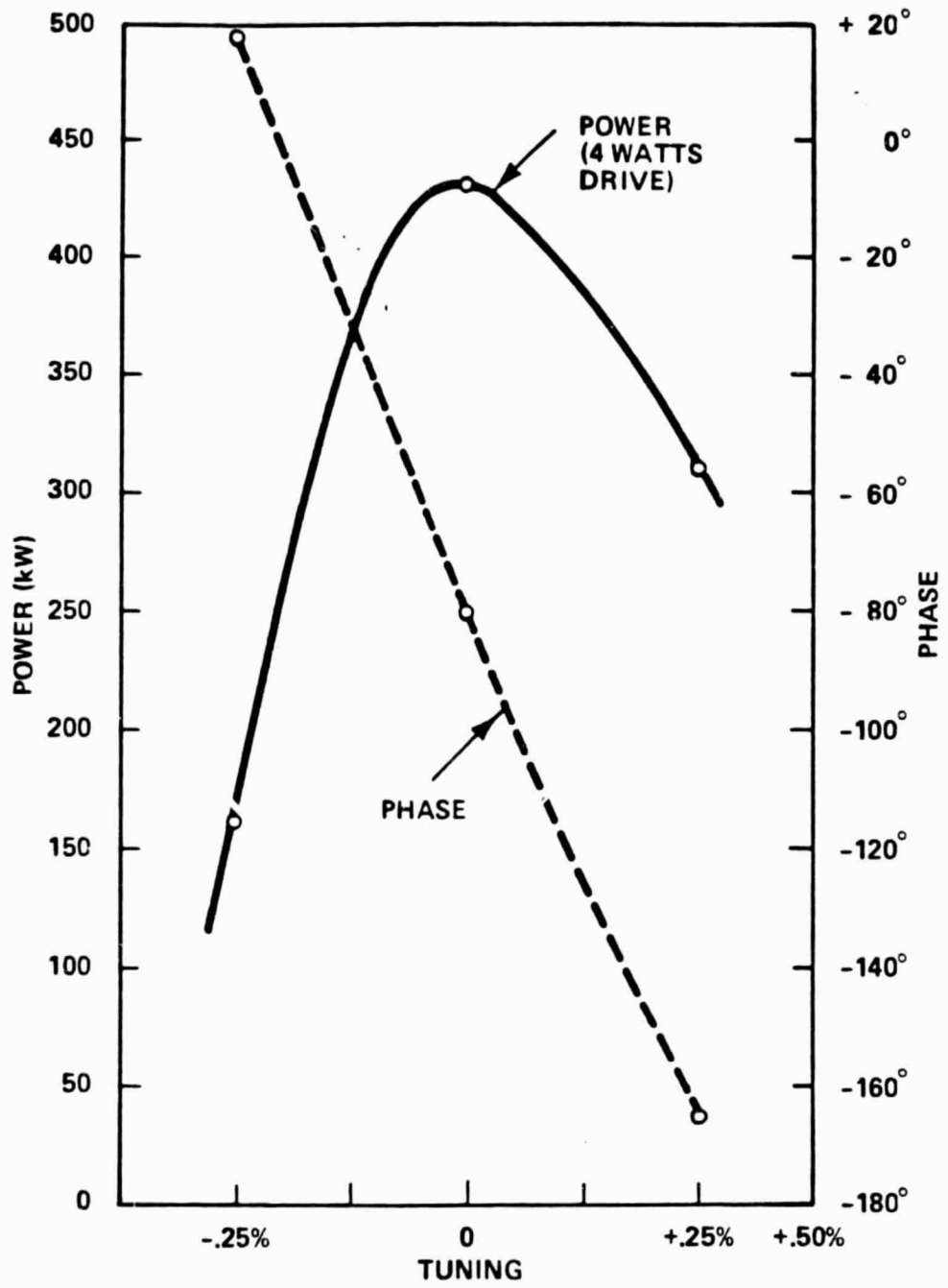


FIGURE 30. POWER OUT AND PHASE VS CAVITY HEATING (SHIFT OF RESONANT CAVITY FREQUENCIES)

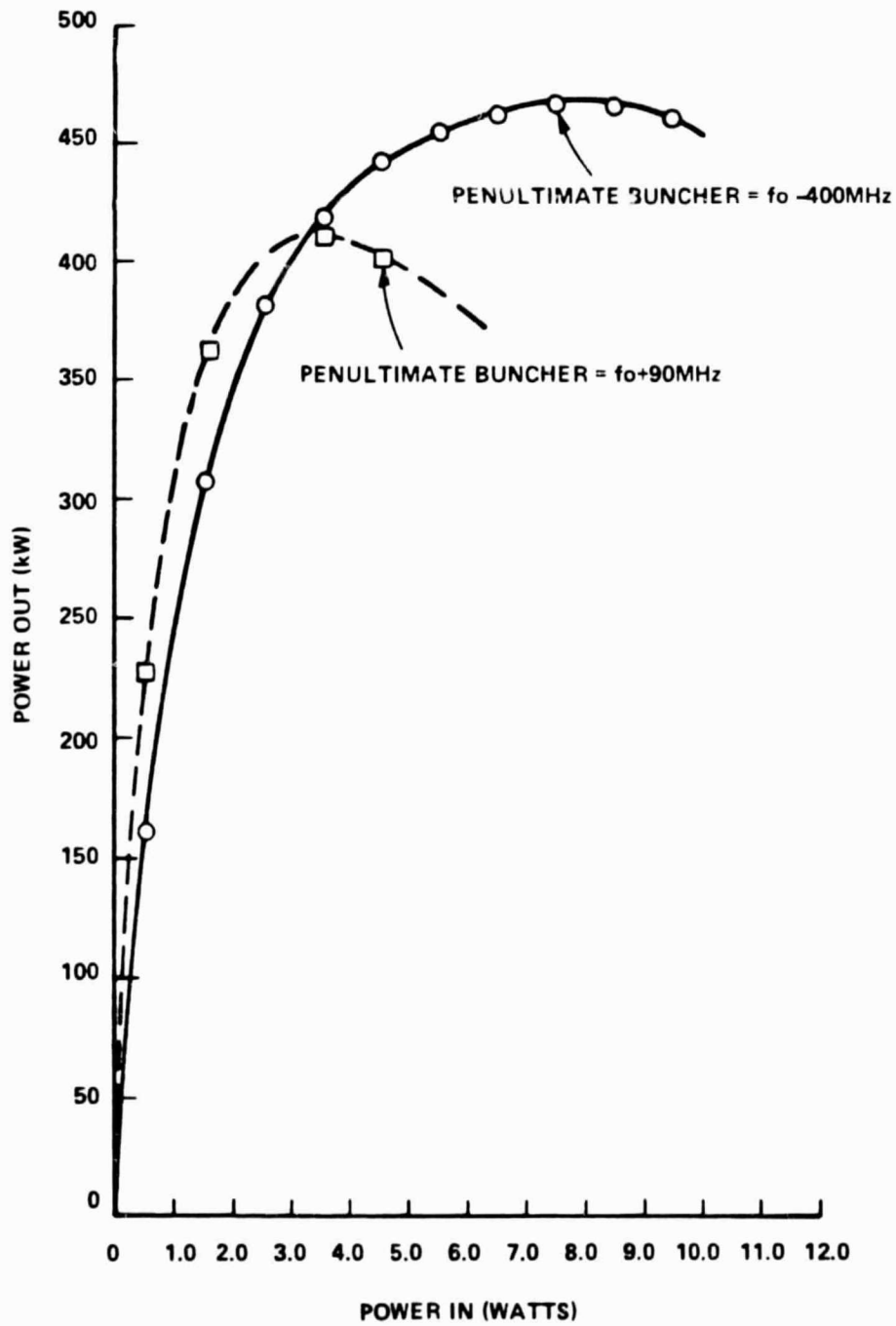


FIGURE 31. TUNING PENULTIMATE CAVITY FOR EFFICIENCY

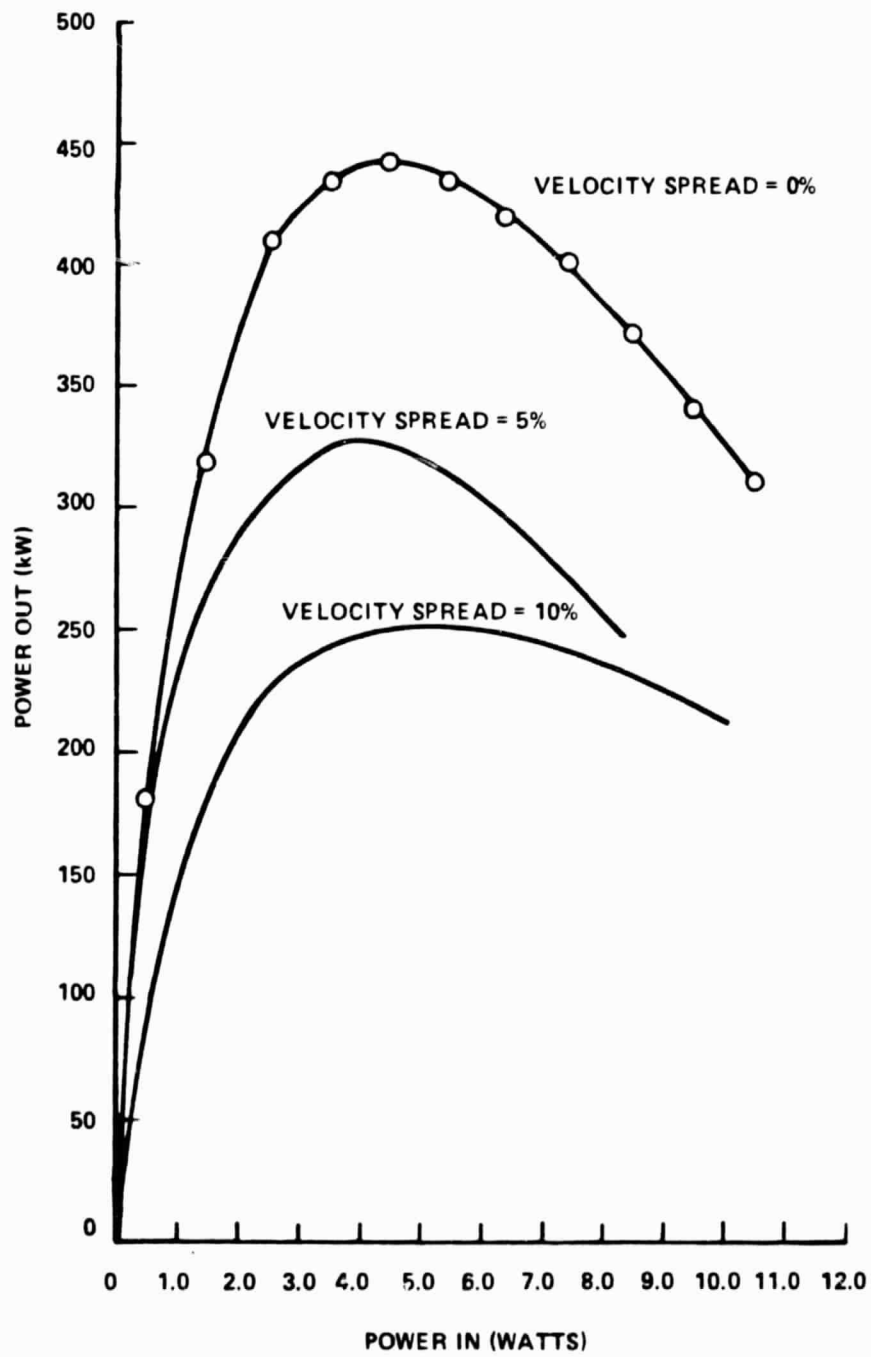


FIGURE 32. EFFECT OF VELOCITY SPREAD

the frequency seen by an electron (proportional to  $k_z v_z$ ), lower  $k_z$  means less sensitivity to variations in axial velocity  $v_z$ . Finally, optimizing the penultimate cavity may reduce velocity spread problems since the effect of this cavity is to reconstitute or tighten the electron bunch before the output, thus increasing efficiency.

#### F. POLARIZATION

The polarization at the output of the circuit is pure right circular. However, over the length of the tube and transmission line, a change in polarization can result from the offset at the 35 to 40 joints that occur. Each section of the tube and transmission line can be modeled as an elliptical waveguide of length  $L$  with major axis the diameter,  $d$ , of the section and minor axis  $(d-\Delta d)$ , where  $\Delta d$  is the tolerance for offset at each joint. The total phase change from a series of  $N$  such elliptical waveguides is

$$\Delta\phi \cong 1.09L \lambda_o \sqrt{N \left[ \frac{1}{(d-\Delta d)^2} - \frac{1}{d^2} \right]}$$

The ellipticity ratio is

$$\epsilon \cong 10 \log_{10} \left[ \frac{E_{\max}}{E_{\min}} \right]^2 = 10 \log_{10} \left[ \tan \left( \frac{\Delta\phi + \frac{\pi}{2}}{2} \right) \right]^2 .$$

Using an average joint-to-joint length,  $L = 5"$ , an average joint diameter,  $d = 2"$ , and a conservative offset tolerance  $\Delta d = 0.005"$ , with  $N = 40$ ,  $\lambda_o = 0.347"$ , we calculate a spurious polarization ellipticity ratio of  $\epsilon = 0.13$  dB. The design goal was to have the ellipticity ratio less than 1 dB. Therefore, the polarization purity requirement can be met without any stringent requirements on tolerances of offsets at joints.



## G. NOISE FIGURE

A first effort at determining the shot noise for a gyrokystron is to apply formulas for conventional tubes but substituting the appropriate circuit element values. Spangenberg<sup>6</sup> gives the shot noise power generated in an electron beam device which is space charge limited by:

$$\text{Noise power (watts)} = [2eI_o \Delta f R_s \Gamma^2 G_s]$$

where

$$e = 1.6022 \times 10^{-19} \text{ coulombs}$$

$$I_o = \text{current (amps)}$$

$$R_s = \text{effective resistance (ohms) of 1st stage}$$

$$G_s = \text{small signal gain}$$

$$\Delta f = \text{bandwidth}$$

$$\Gamma^2 = \text{space charge smoothing factor}$$

$$\text{The factor } \Gamma^2 = 1.5 \times 10^{-4} T_c / V_o$$

$$\text{where } V_o = \text{beam voltage (volts)}$$

$$T_c = \text{cathode temperature (}^\circ\text{K)}$$

Temperature limited beams have noise powers which are  $(1/\Gamma^2)$  larger than for space charge limited beams because of the absence of the shielding mechanism provided by space charge effects. Noise characteristics are defined according to the following definitions established at Varian in characterizing klystron devices<sup>7</sup>.

$$\text{Noise figure (dB)} = 10 \log \left[ \frac{\text{noise power}/(\text{gain} \cdot \text{bandwidth})}{\text{thermal noise power}} \right]$$

$$\text{Noise-to-power ratio (dB/kHz)} = 10 \log \left[ \frac{\text{noise power (watts/kHz)}}{\text{carrier power (watts)}} \right]$$

The thermal noise at room temperature is  $4.1 \times 10^{-21}$  watts/Hz. Symons<sup>1</sup> has attempted to define the effective resistance of a TE<sub>11</sub> gyrokystron cavity through the definition:

$$R_s = \frac{161.2 Q (\lambda_0/a)^2}{(L/\lambda_0)} \quad (\text{ohms})$$

where

Q is the total cavity Q

$\lambda_0$  is free space wavelength

a is cavity radius

L is cavity length

For a cavity length  $L = 0.78428$  cm,  $\lambda_0 = 0.88174$  cm,  $a = 0.31371$  cm and a total Q of 150 (proposed gyrokystron design of 1st cavity) the effective resistance is given as  $2 \times 10^5$  ohms. Assuming a beam voltage of 80 kV and cathode temperature of 1273°K, the space charge smoothing factor is  $r^2 \approx 2.4 \times 10^{-6}$ . Assuming a current of 12.5 amps and a gain of 50 dB one obtains the following noise characteristics for the Pierce/wiggler gyrokystron configuration operating at 400 kW.

$$\text{Noise figure} = 10 \log (468) = 26.7 \text{ dB}$$

$$\text{Noise-to-power ratio} = 10 \log \frac{9.6 \times 10^{-11} \text{ watts/kHz}}{400000 \text{ watts}} = -156.2 \text{ dB/kHz}$$

The absence of the space charge smoothing factor in temperature limited beams would apparently cause the MIG gun configuration to have a noise figure of 83 dB and a noise-to-power ratio of -100 dB/kHz.

It should be noted that it may be invalid to apply the linear beam formula to gyro devices since the strong magnetic fields over the cathode (MIG gun case) and noise generated in wiggler (Pierce/wiggler case) are not taken into account. Further investigation is needed to clarify the results,

but our initial estimates show that the proposed JPL gyrokystron circuit configuration will satisfy the noise requirement of -80 dB/MHz.

#### H. HARMONIC OUTPUT

Harmonic emission from gyrokystrons can only be estimated at this time from experimental results obtained from gyrotron oscillators. Theoretical estimates are far too ideal and incomplete to be of great value.

Experiments at MIT (100 kW at 140 GHz) and Varian (150 kW at 28 GHz) suggest second harmonic levels at -20 to -30 dBc.

When an efficient gyro amplifier radiates at its fundamental frequency, harmonic components in the highly non-linear bunched currents may radiate at cyclotron harmonics. The amount of power radiated requires a detailed multi mode analysis,<sup>8</sup> the results of which are still not conclusive.

Experimental measurement of harmonic output from high power gyrotron oscillators has been limited for several reasons:

- Until recently, stringent specifications for mode and harmonic purity have not been required by users, as long as the power in the desired mode is high;
- large output powers at the fundamental cause a poor signal to noise environment for measuring harmonics;
- the weak theoretical basis makes calibration of directional couplers and other measuring equipment difficult; the harmonic waveguide modes, and coupling coefficients are not well understood.

A summary of experimental measurements of harmonic emission is shown in Table 7.<sup>9,10</sup> The qualitative conclusion from these measurements is that when conditions for one frequency are optimized, other frequencies are depressed. The harmonic output from a gyrokystron would probably be

-20 dBc or less. Harmonic filters before the feed could eliminate this unwanted radiation.

Table 7  
Harmonic Power Emission

<u>Source</u>	<u>Fundamental Frequency and Power</u>	<u>2nd Harmonic</u>	<u>3rd Harmonic</u>
MIT	100 kW @ 140 GHz	-20 to -30 dBc Typically <-40 dBc with care	Not measured
MIT	100 - 200 kW @ 28 GHz	-20 to -30 dBc	Not measured
Oak Ridge	10 - 100 kW @ 28 GHz	Not Measured	Detected; Power Unknown

#### I. FEASIBILITY SUMMARY - GYROKLYSTRON CIRCUIT

The problem which may require the most attention is tube stability. All the stability criteria imposed so far have been small signal (linear) criteria. In a gyrotron oscillator, hard excitation regions exist which allow the device to oscillate at currents below the small signal threshold if microwave power already exists in the cavity (Figure 33). It is conceivable that as the output power of the tube increases, the output cavity could start to oscillate even if the operating currents were below the linear thresholds. Further investigations into this problem using particle simulation codes<sup>11</sup> are required although actual operating devices will be needed to fully address the stability question. Only a gyroklystron circuit is capable of generating 400 kW CW at 34 GHz. Particle simulation, theory and analogies to conventional klystrons so far indicate that efficient stable circuit performance is feasible.

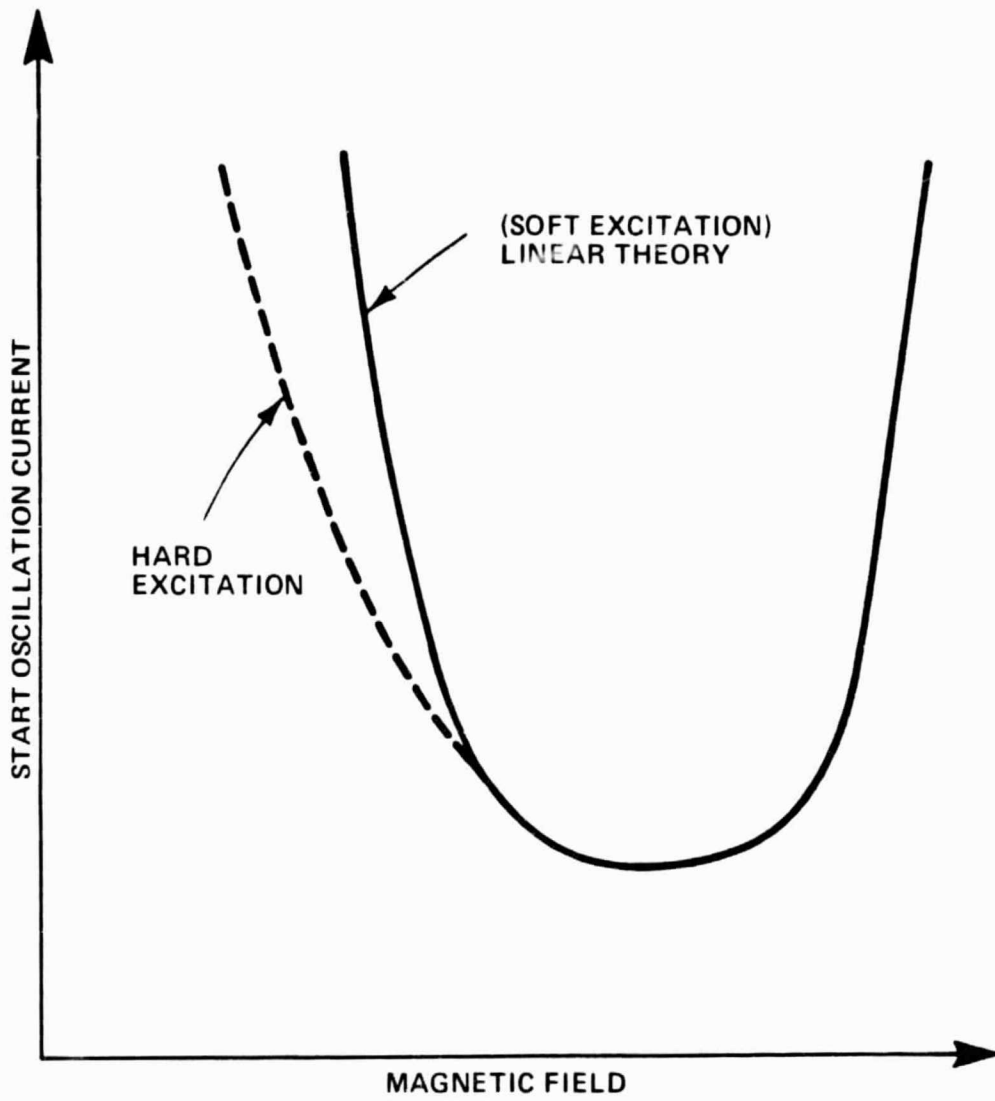
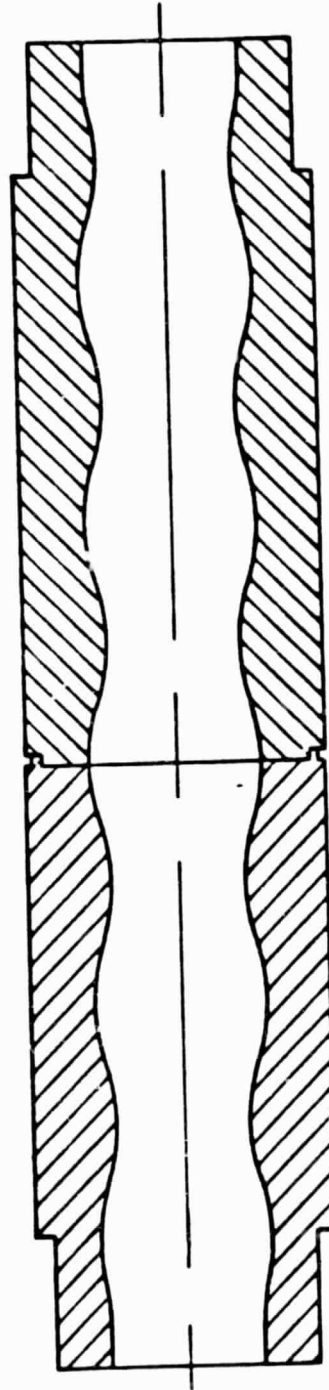
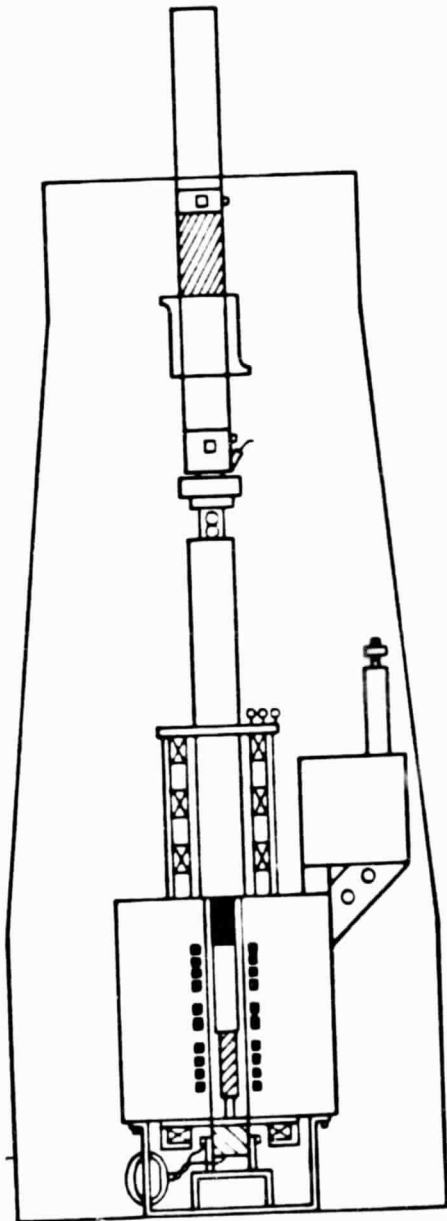


FIGURE 33. HARD AND SOFT EXCITATION OF GYROTRON OSCILLATOR

# MODE CONVERTER



## V. MODE CONVERTER

### A. DESIGN APPROACH

The power emitted from the output cavity is in the  $TE_{12}$  mode, and therefore a mode converter must be designed to convert to the desired  $TE_{11}$  mode. Since the azimuthal index of the two modes are the same ( $m=1$ ) a relatively simple cylindrically symmetric mode converter can be designed.<sup>12</sup> This consists of a section of waveguide which has a sinusoidal variation of the wall radius  $a(z)$ , with distance (Figure 34). That is,

$$a(z) = a_0 + \delta a \sin(2\pi z/\lambda_b) ,$$

where  $a_0$  is the average wall radius,  $\lambda_b$  is the wavelength of the ripples and  $\delta a$  is the amount of maximum wall perturbation.

Mode conversion is accomplished by choosing the ripple wavelength equal to the beat wavelength between the  $TE_{11}$  and  $TE_{12}$  mode,

$$(2\pi/\lambda_b) = (2\pi/\lambda_{11}) - (2\pi/\lambda_{12}) .$$

The optimum converter length to obtain complete conversion is given approximately as:

$$L_c = \frac{0.638 \lambda_b}{\delta a/a_0}$$

The question arises as to where the mode converter should be placed, at the output of the circuit inside the vacuum envelope, or in the 1.75-inch-diameter transmission line outside of the vacuum envelope.

### B. CONCEPTUAL DESIGN

As an example of a reasonable choice, with the converter inside the vacuum envelope, we selected a converter radius  $a_0$  of 1 cm which is about 20-30 percent above cutoff of the  $TE_{121}$  cavity, making the beat wavelength

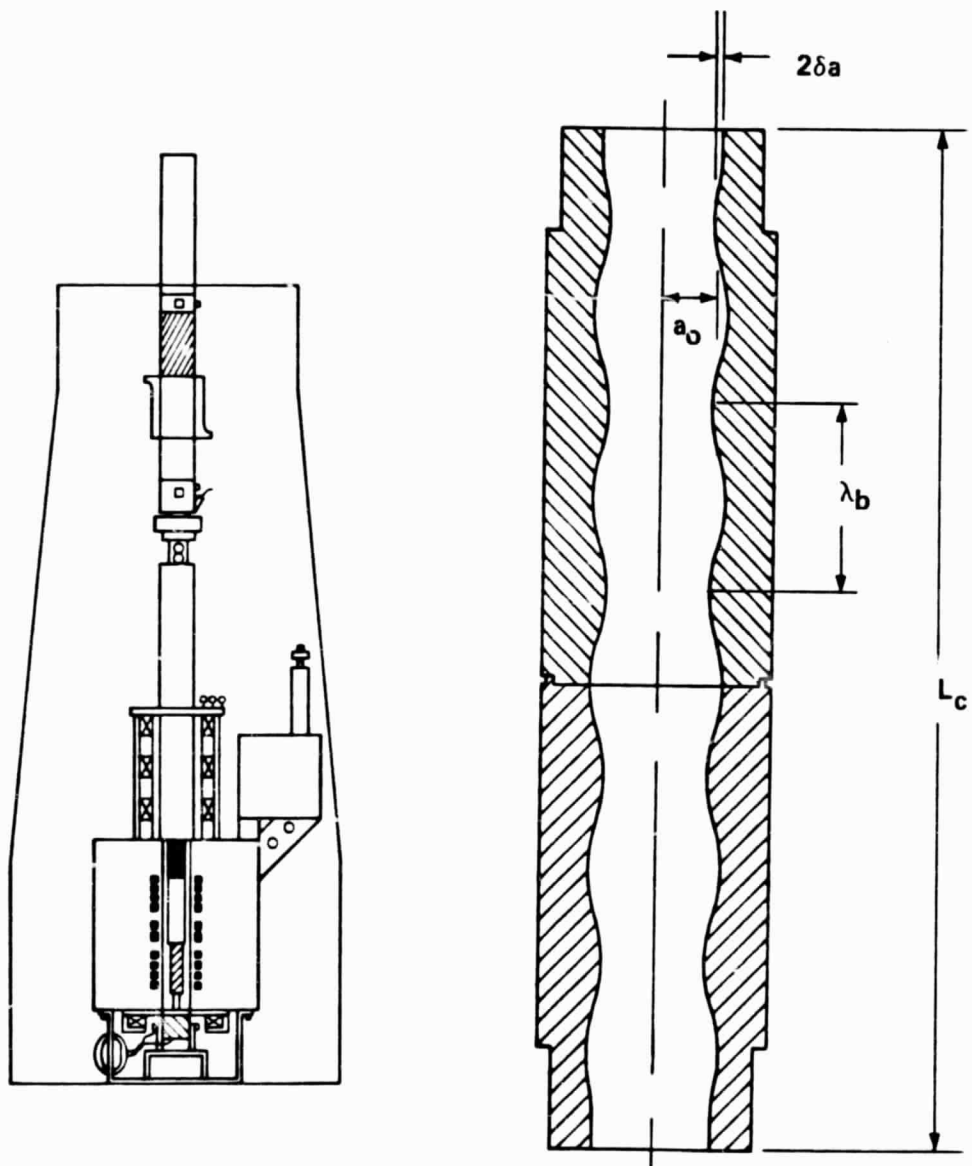


FIGURE 34. MODE CONVERTER



equal to 2.915 cm and the total converter length about 7 inches long. The design was checked by using the computer code MULTIMODE.FORT which solves, exactly, the set of reduced Maxwell's equations (20 coupled telegraphers equations) inside a waveguide of arbitrary wall profile.<sup>13</sup> The code solves for the mode conversion occurring from the  $TE_{12}$  mode to all other modes with the same azimuthal symmetry  $m=1$  which are the only conversions allowed in a symmetric converter. Figure 35 shows the results of such a calculation.

As expected, almost all the power is converted to the desired  $TE_{11}$  mode (Table 8) at approximately 6.9 inches (17.5 cm), as predicted by the simple theory, although the optimum ripple wavelength,  $\lambda_b$ , was changed from the predicted wavelength because it was calculated assuming  $a_0$  as the radius, not taking into account the effect of the rippled wall on the beat wavelength.

Table 8  
Calculated Mode Output for  $TE_{12} \rightarrow TE_{11}$  Converter  
Length = 6.9 Inches

Mode	% Power
$TE_{11}$	97.98%
$TE_{12}$	0.28%
$TM_{11}$	0.32%
$TM_{12}$	1.42%

Although the mode conversion is adequate for this design, the calculation predicts an 8 percent energy loss caused by the partial cutoff of the  $TM_{12}$  mode. The  $TM_{12}$  mode is cutoff in the ripples. It is the closest mode to  $TE_{12}$  and thus power can be easily transferred to it. Because it is cutoff by the ripples, strong reflection of the wave and absorption in the wall occurs. One shortcoming of the computer code is that it does not include reflected waves. In the future, in order to fully analyze and design the mode converter, the code can be made to include the dominant reflected wave with little complication.

A mode converter was built according to the design for which calculated results are presented in Table 8. The mode conversion properties of the converter were inferred from a transmission cold test measurement. A pure

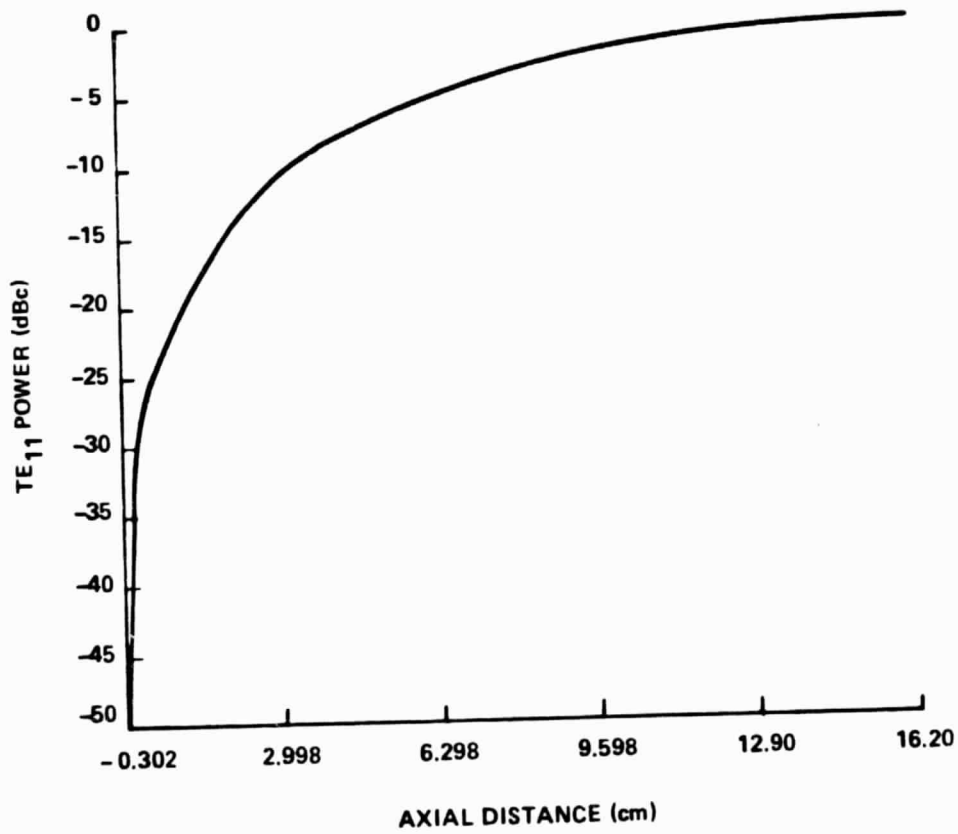


FIGURE 35. MODE CONVERTER TE<sub>12</sub> → TE<sub>11</sub> (34 GHz)

$TE_{11}^{\circ}$  mode was launched at one end of the converter under test and a conventional  $TE_{11}^{\circ}$ -to- $TE_{10}^{\square}$  converter connected the far end of the converter under test to a crystal detector. A baseline measurement for the transmitted signal was obtained by replacing the converter under test with an equal length of straight copper pipe of inner diameter  $a_0$ .

The transmission results for the converter itself are compared with theory in Figure 36. In the cold test set up, zero received  $TE_{11}^{\circ}$  signal, corresponding to "100% power transmission" in Figure 36, implies that all the power exiting the converter under test is in another mode, the  $TE_{12}$ , as desired. It is also possible, however, that some of the power has been absorbed in the converter under test, due to the presence of the rippled wall structure. The test results in this figure imply that a combination of  $TE_{11}^{\circ}$  to  $TE_{12}^{\circ}$  conversion ( $\approx 95\%$ ) and power absorption ( $\approx 1-2\%$ ), has taken place in the mode converter. We conclude from these cold test results that the first cut design works reasonably well, with better than 95% conversion efficiency, but that an improved theoretical treatment of the  $TM_{12}$  absorption in the converter is necessary in order to obtain good agreement between theory and cold test measurements.

One possible way to alleviate the problem of trapped modes is to modify  $a_0$  slightly to eliminate some of the reflected power. If the converter is kept at a small diameter, the mode control is good. With the converter inside the vacuum envelope, the collector tapers would be optimized for the  $TE_{11}$  mode, which requires greater length for a given mode purity than  $TE_{12}$  collector-tapers (see Section VI).

The alternative is to place the mode converter on the outside of the tube. There will always be one mode that goes through cutoff, however; when the waveguide becomes more overmoded, the coupling to the partially cutoff mode will be smaller since it will be further removed from the  $TE_{11}$  and  $TE_{12}$  modes. Additional investigation into a 1.75-inch-diameter converter must be done. One could also try different radii of the converter when it is on the outside of the tube to find the optimum radius to make the converter as short as possible. With a smaller diameter, the power handling ability of the converter outside the tube will have to be addressed. If the converter

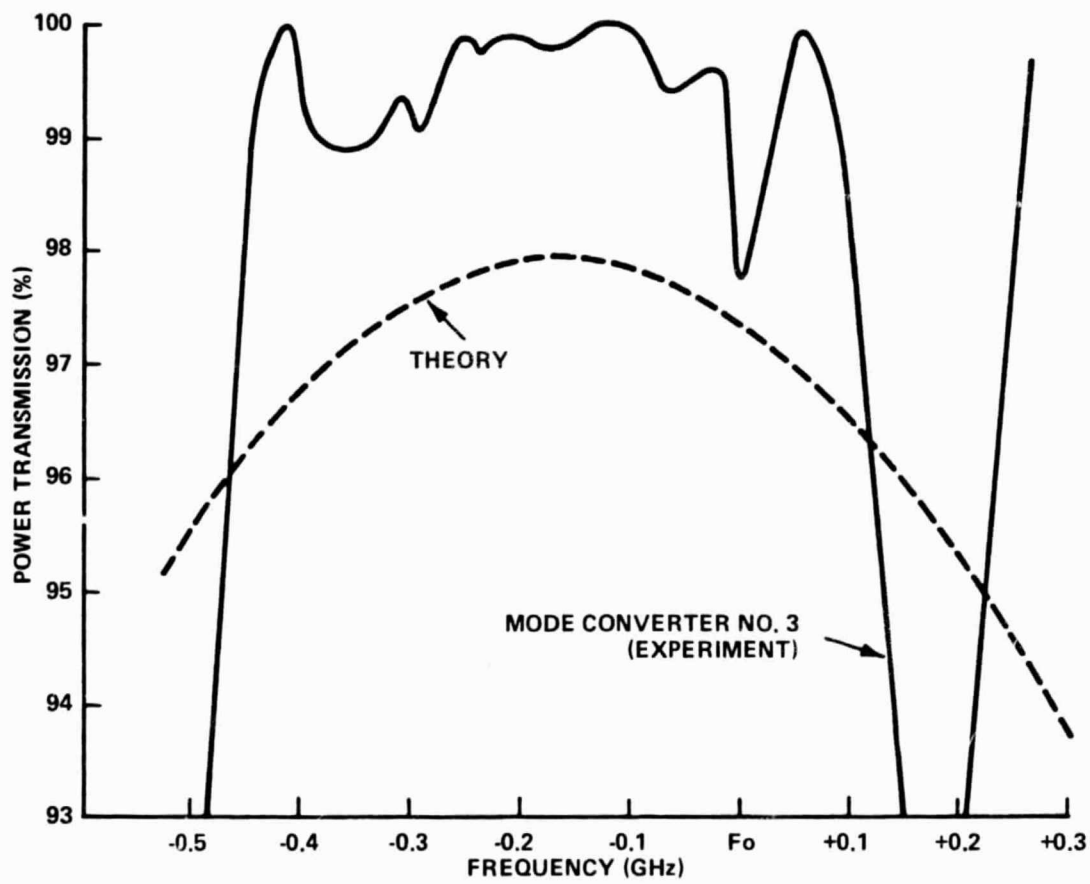


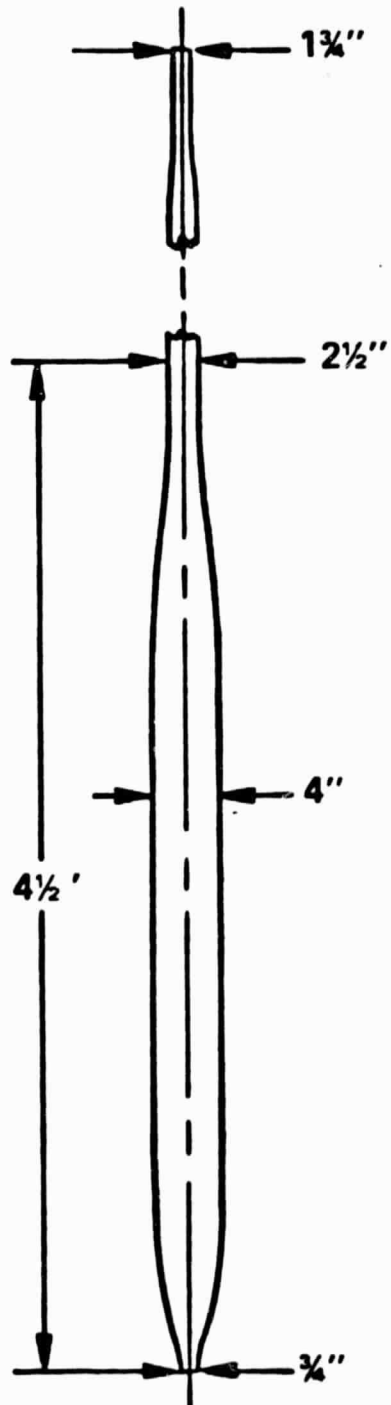
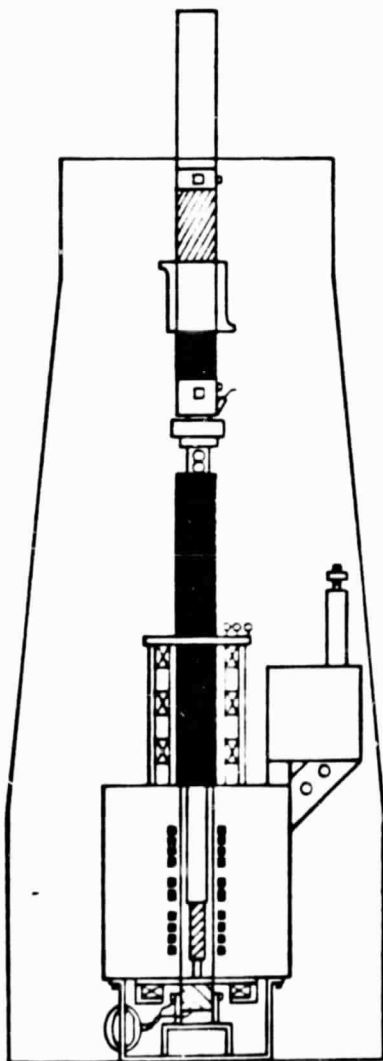
FIGURE 36.  $TE_{12} \rightarrow TE_{11}$  MODE CONVERTER PASSBAND

is outside the vacuum envelope at the larger diameter, there is an increased possibility of exciting unwanted modes. However, there would be little conversion to the mode cutoff in the ripples. The collector-tapers would be made to optimize for  $TE_{12}$ , which have reasonable lengths for good mode purity.

### C. FEASIBILITY SUMMARY - MODE CONVERTER

It is not clear what diameter would be best for the converter, or whether it should be inside or outside the vacuum envelope. At this point, the preference would be to put the converter outside the tube so that the converter development would be separate from the tube development. All possible diameters between the 1-inch circuit output and the 1.75-inch transmission line will have to be considered to find converter dimensions that have high mode purity in the  $TE_{11}^0$  mode and low energy transfer to the trapped mode. The converter codes must be upgraded to properly handle reflected waves. Finally, a compromise will have to be made between the optimum dimensions of the converter and the length and power handling requirements of the tube.

# COLLECTOR AND TAPERS



## VI. COLLECTOR-TAPERS

The diameter of the circuit at the far end of the output cavity will be 0.75 inch. To limit the maximum beam power density dissipated on the collector wall to 1000 watts/cm<sup>2</sup>, it was determined that the collector inside diameter should be 4 inches. Existing output window designs are for 2.5-inch-diameter waveguide, and the selected waveguide diameter for the output components is 1.75 inch (see Sections VIII and IX). Tapers will be required between these diameters, as shown in Figure 37, and these tapers must be designed for minimum mode conversion.

### A. TAPER DESIGN APPROACH FOR MINIMAL MODE CONVERSION

Designs related to the theory of Unger<sup>14</sup> were evaluated using MULTIMODE.FORT which solves for the simultaneous coupling of the TE<sub>11</sub> mode to as many TE<sub>1n</sub> and TM<sub>1n</sub> modes as necessary to model the problem. The TM<sub>1n</sub> modes are required because the main TE<sub>1n</sub> mode is asymmetric. This makes the design of TE<sub>1n</sub> taper more difficult than symmetric TE<sub>on</sub> tapers. The usual two-mode theories in the literature<sup>15</sup> tend to give results which are far too optimistic for large diameter overmoded guides, and thus the exact multimode theory is essential.

An empirical form for the tapers, which is easy to specify, consists of two arcs and a possible straight section that are smoothly connected. The resulting tapers can be made to be as optimum as Unger's raised cosine tapers. They have the advantage of being specified much more easily. Designs of both TE<sub>11</sub> and TE<sub>12</sub> tapers were considered. A comparison of tapers and power models are expressed in Table 9 while Figure 38 shows the collector-tapers mode conversion. With the same length of taper, the TE<sub>12</sub> tapers provide much better mode purity than the TE<sub>11</sub> tapers. For the TE<sub>12</sub> tapers, the relative mode spacing is further apart, and as Unger's analytic theory predicts, the tapers can be made shorter.

- It is possible to design longer TE<sub>11</sub> tapers (4 feet for the uptaper) which would provide adequate mode purity, however, length requirements of the tube make these tapers impractical.

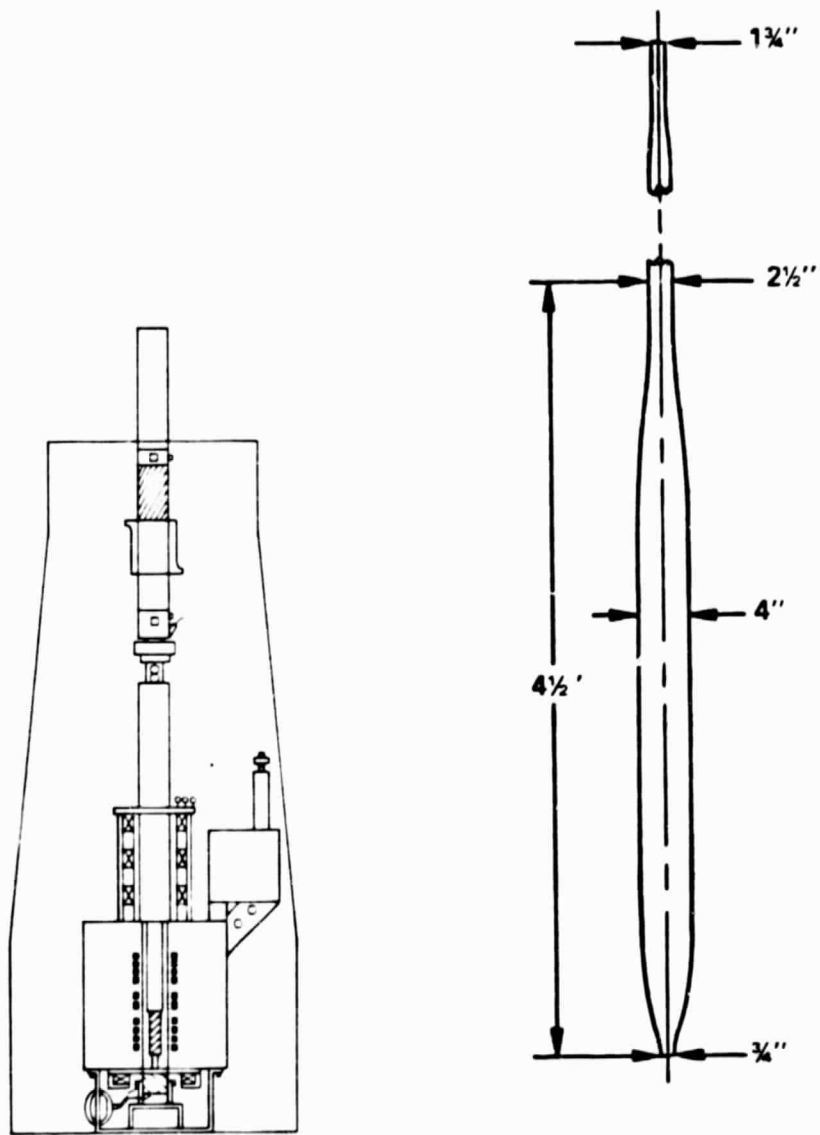


FIGURE 37. COLLECTOR AND TAPERS



For overall mode purity, the worst case estimate is to add the spurious mode levels for each taper. The total length of the collector-tapers can be used to an advantage. The length between the tapers can be adjusted slightly so that the phase change resulting can cause reconversion and the result is increased mode purity.

The collector-tapers can be designed to give adequate mode purity in reasonable lengths. The preferred design would be for  $TE_{12}$  tapers.

Table 9  
Percent Power in Modes

	Uptaper 2' <u>0.75 in + 4 in</u>	Downtaper 2-1/2' <u>4 in + 2.5 in</u>	Downtaper 1' <u>2.5 in + 1.75 in</u>
$TE_{12}$ Tapers			
$TE_{11}$	0.57	0.02	0.22
$TE_{12}$	98.95	99.47	99.27
$TE_{13}$	0.07	0.19	0.30
$TM_{11}$	0.25	0.29	0.18
$TE_{12}$	0.16	0.02	0.05
$TE_{11}$ Tapers			
$TE_{11}$	97.62	96.88	97.41
$TE_{12}$	0.09	0.64	0.69
$TM_{11}$	2.29	2.48	1.90

#### B. COLLECTOR BEAM POWER DENSITY CALCULATIONS

Collector performance was evaluated using COLLECTOR.FORT. Calculations indicate that thermal wall loading of the electron beam collector will be within the designed capabilities of the tube. As a first approximation a

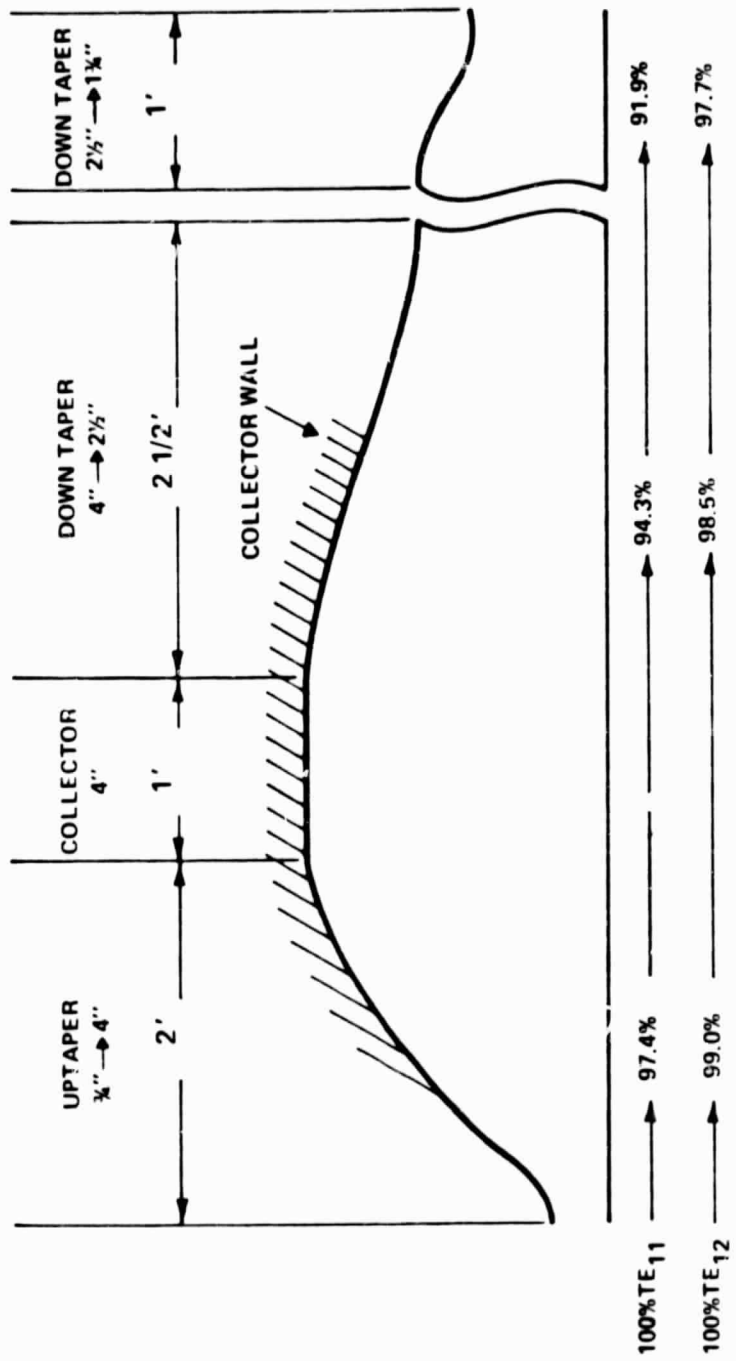


FIGURE 38. MODE CONVERSION IN COLLECTOR-TAPERS

"fat" hollow beam with inner radius 40 percent of the outer radius was used to model the electron beam. A typical simulation of particle trajectories in the tube for such a beam is shown in Figure 39. The calculated wall power density profile is shown in Figure 40. These results can be considered nearly correct for the actual solid beam configuration which is proposed for this tube.

The peak wall loading is approximately  $1 \text{ kW/cm}^2$ , which is commensurate with the demonstrated capabilities of high power gyrotron collectors. As shown in Figure 40 the location and extent of the beam power deposition can be varied by the collector magnets.

Modifications of computer software are needed to accurately model a solid electron beam (Cartesian coordinates); however, the results of such a calculation should not be qualitatively different from calculations made to date. The main difference expected from such a calculation is that some small fraction of the beam will go the length of the tube to the output window. It is standard practice even with hollow beam tubes to protect the output window with permanent transverse magnets which deflect stray electrons to the wall.

#### C. FEASIBILITY SUMMARY - COLLECTORS AND TAPERS

By using a 4-inch-diameter collector, the dissipated beam power densities will be no greater than those already demonstrated in the Varian CW gyrotrons and other Varian high power CW tubes.

The required tapers between the circuit and the collector as well as between the collector and the output components can be designed to give adequate mode purity in reasonable lengths.

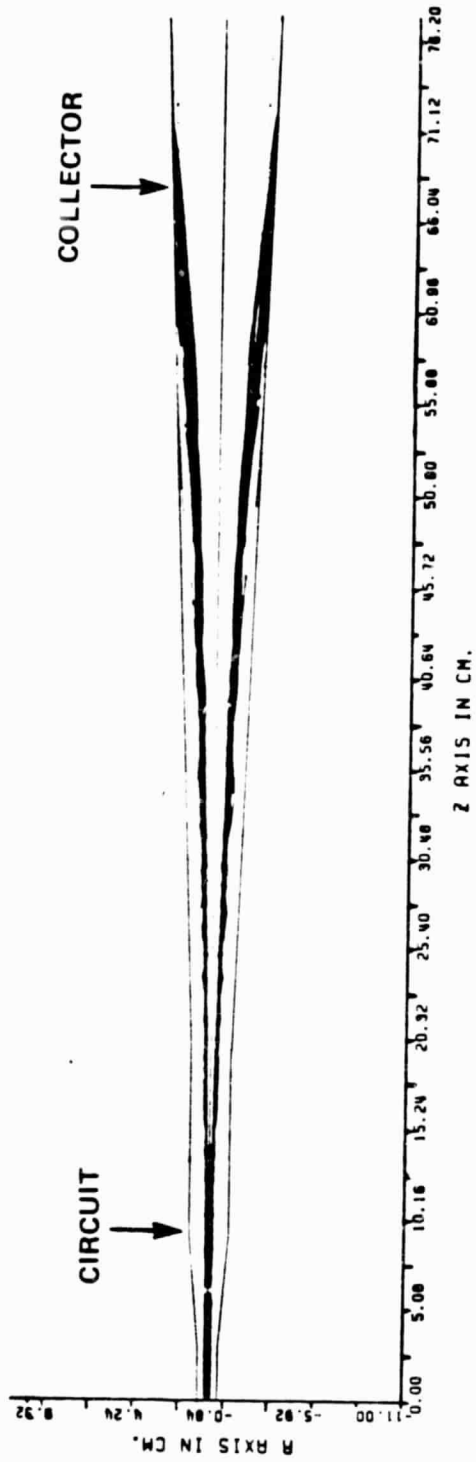


FIGURE 39. TYPICAL SIMULATION OF PARTICLE TRAJECTORIES FROM OUTPUT CAVITY TO COLLECTOR

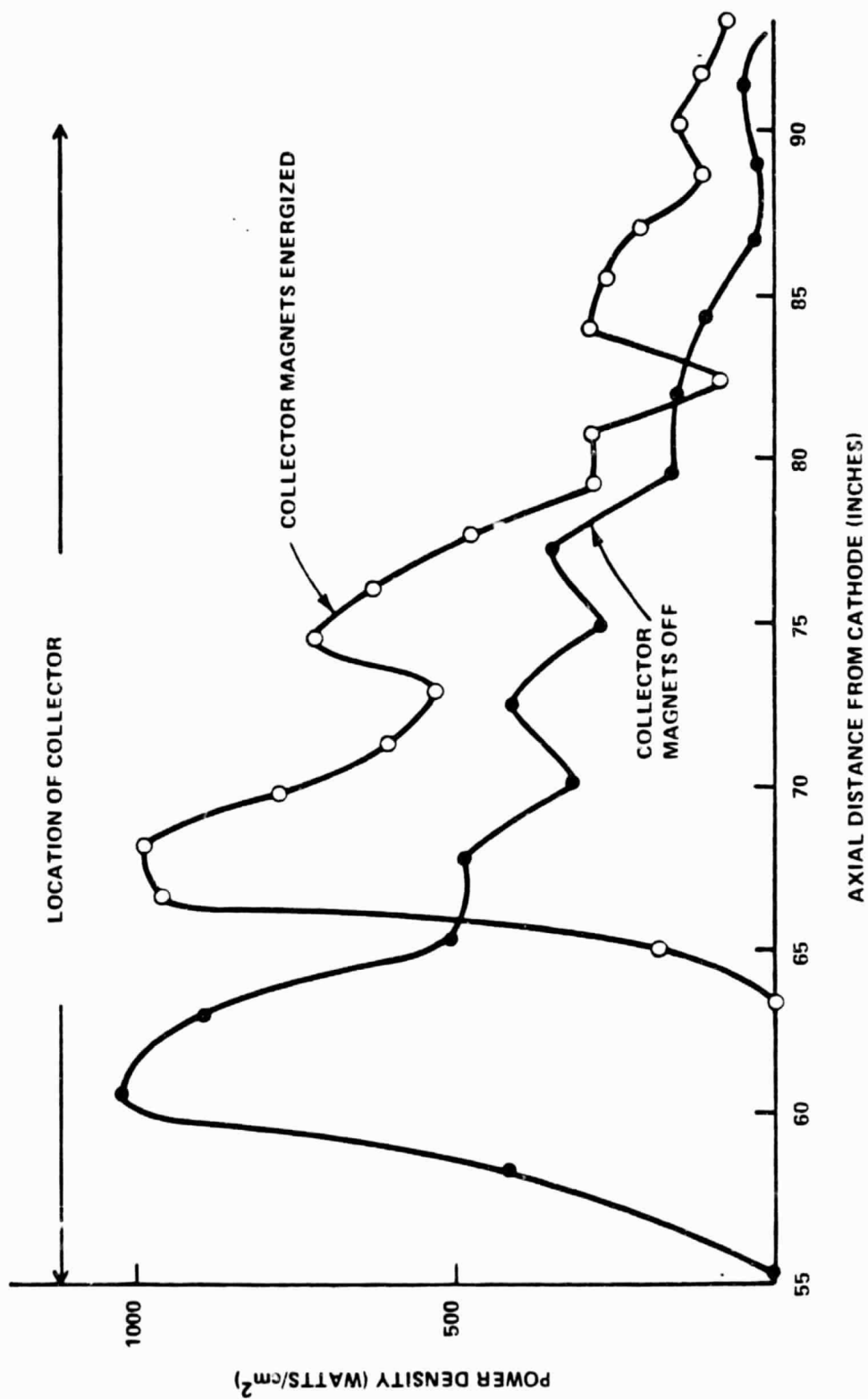
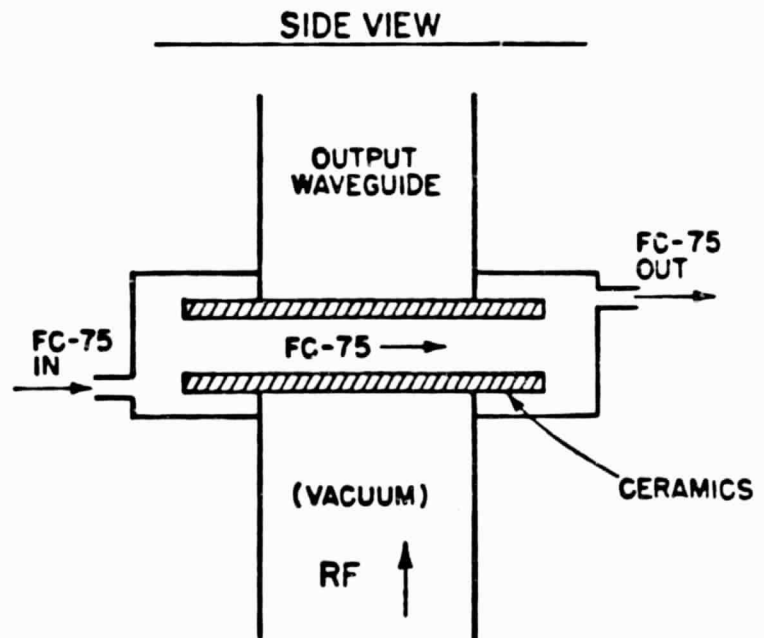
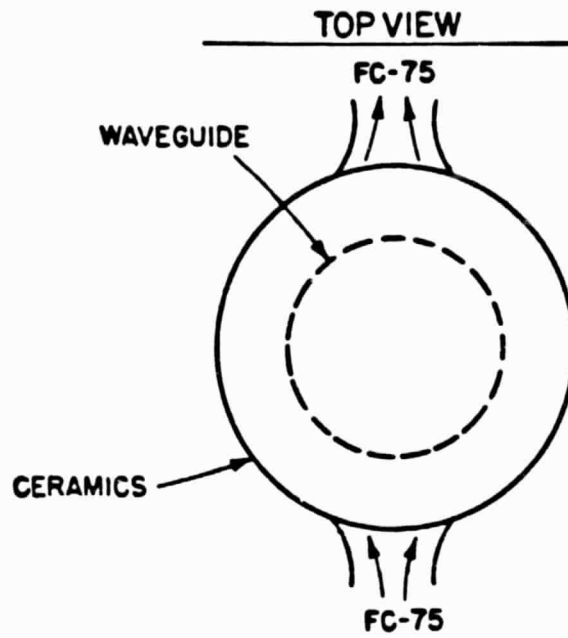
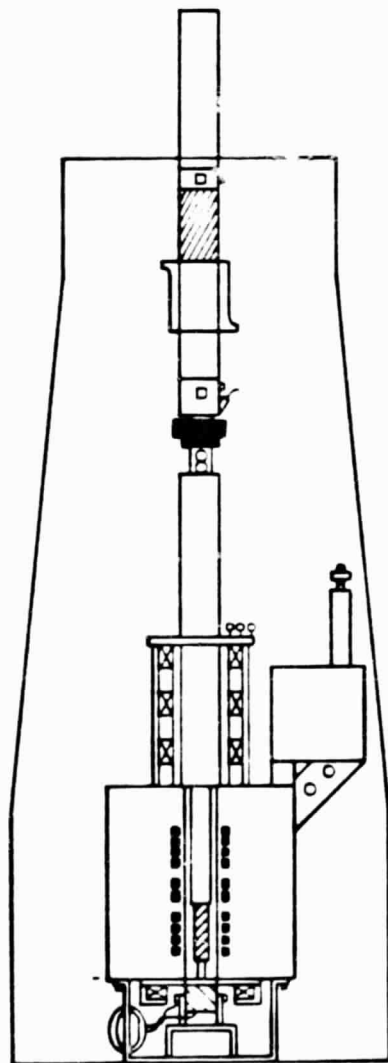


FIGURE 40. WALL POWER DENSITY PROFILE IN THE COLLECTOR REGION

# OUTPUT WINDOW



## VII. CW OUTPUT WINDOW

### A. DESIGN APPROACH

The fundamental requirements for the output window are to provide a reliable, high quality vacuum seal and to transmit the microwave energy with minimal power absorption, reflection and mode conversion.

The primary approach investigated was the double-disc window, shown schematically in Figure 41. The window assembly consists of two circular sapphire discs separated by a thin layer of fluorocarbon fluid, FC-75<sup>T</sup>. (FC-75 is a registered trademark of the 3M Company.) It is designed to allow the cooling fluid to flow directly over the heated area of the discs, giving high heat flux capabilities. The discs are face-brazed to the waveguide wall and are larger in diameter than the waveguide for stress distribution considerations.

Varian has many years of experience with double-disc windows, and has successfully operated windows at 340 kW CW 28 GHz and at 200 kW CW 60 GHz, in the TE<sub>02</sub> mode<sup>16</sup>.

One of the positive attributes of the double-disc window is that the FC-75 gap can be adjusted to give the best possible dielectric match for the exact operating frequency of the tube. Figure 42 shows a computer calculation of the VSWR of a window designed to match at 34 GHz. The humped curve is characteristic of double-disc windows. A VSWR of 1.5 or less is reasonable for steady operation of the tube, so this window has a bandwidth of about 1 GHz.

Figure 43 shows the mesh used to make finite element calculations with the computer code MARC. The deformation of the mesh, which is greatly exaggerated in this figure, is caused by the high fluid pressure ( $\approx 2$  atm) necessary to drive high velocity coolant through the narrow gap.

Figure 44 shows the actual window deflection due to the combined effects of fluid pressure loading and thermal expansion. These small

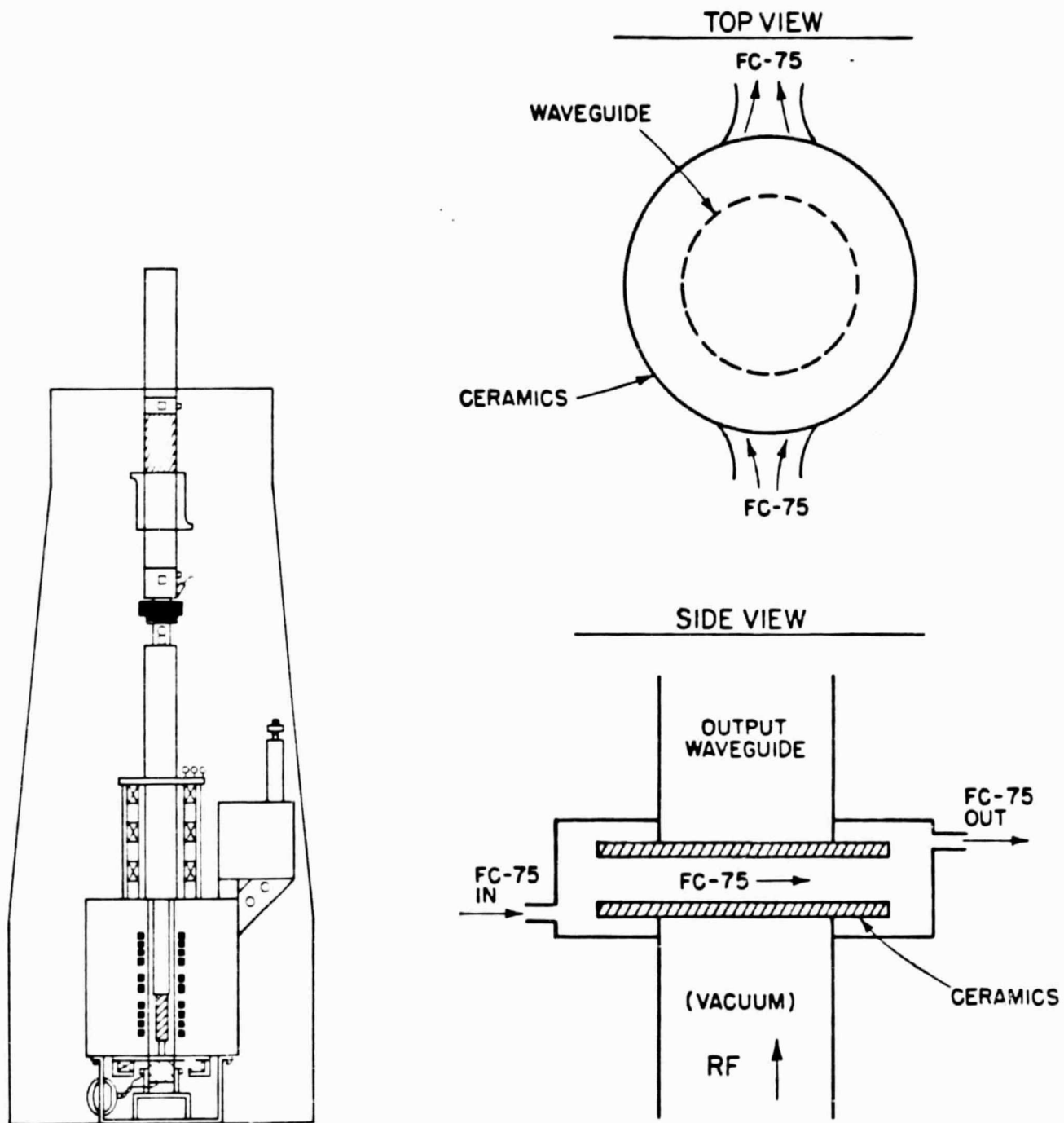
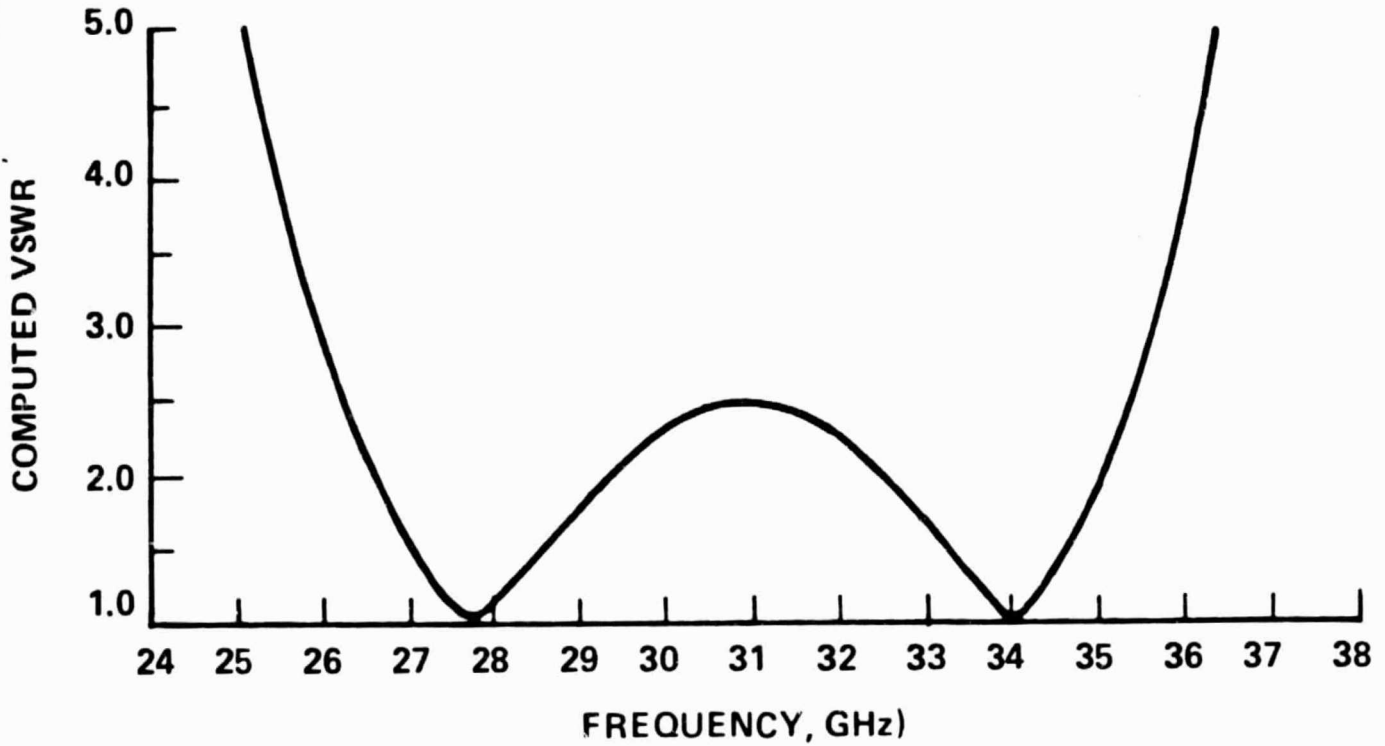


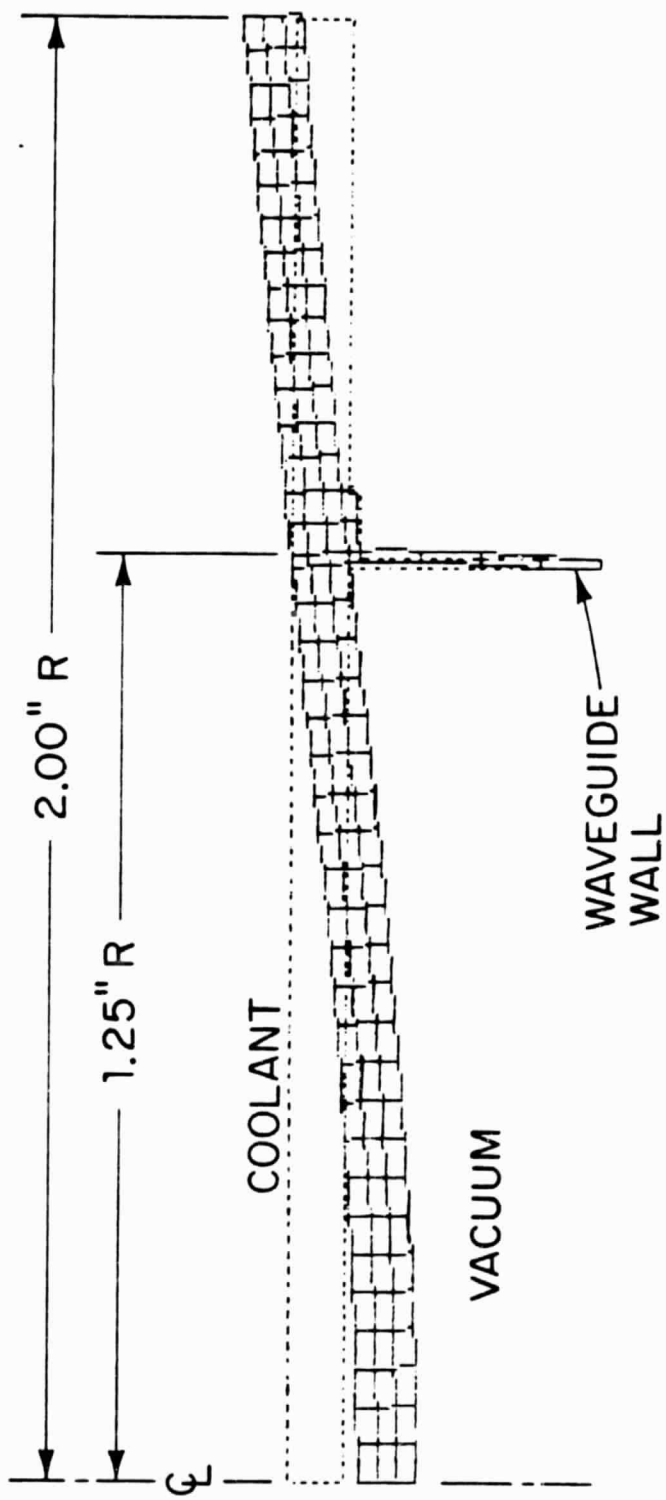
FIGURE 41. OUTPUT WINDOW





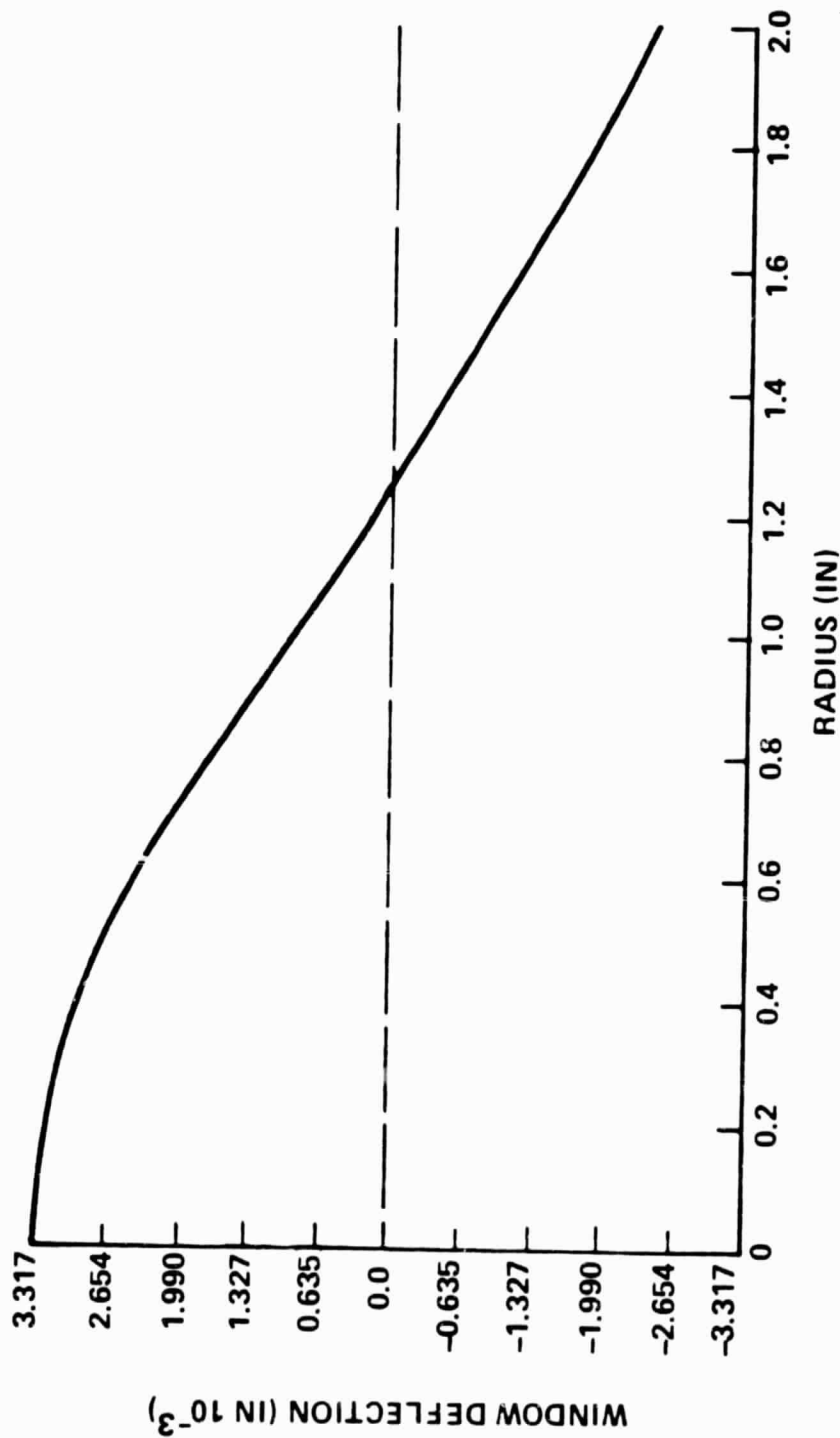
**NOTE: CALCULATION INCLUDES TWO SAPPHIRE DISCS AND FC-75 COOLANT LAYER, TE<sub>11</sub> MODE, 2½" GUIDE**

**FIGURE 42. VSWR FOR 34 GHz DOUBLE-DISC WINDOW**



**NOTE: DEFORMATION DUE TO PRESSURE LOAD IS GREATLY EXAGGERATED**  
**TE<sub>11</sub> MODE, 400 KW CW, SAPPHIRE DISCS**

**FIGURE 43. FINITE ELEMENT MESH FOR ONE DISC OF 34 GHz WINDOW**



TE<sub>11</sub> MODE, 400 KW CW, SAPPHIRE DISCS

FIGURE 44. 34 GHz DOUBLE-DISC WINDOW COOLANT-SIDE DEFLECTION

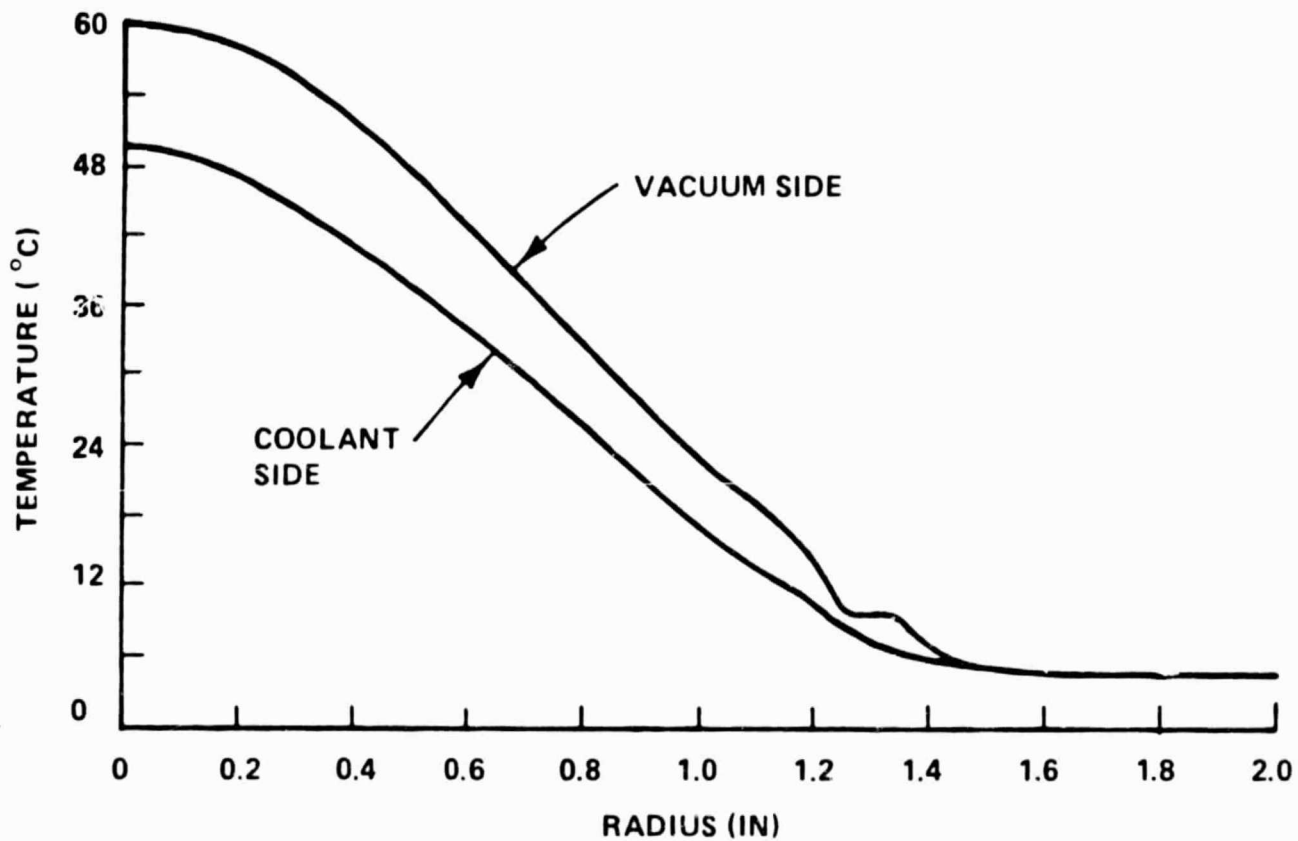
deflections have no significant effect on the microwave properties of the window assembly.

Figure 45 shows the temperature on both the cooled and the vacuum sides of the window. The calculation is done on MARC, using the known power distribution of a rotating  $TE_{11}$  mode in 2.5-inch waveguide and the absorption properties of sapphire at 34 GHz to calculate the power input profile. FC-75 boils at  $107^{\circ}C$  at 1 atm, so this design offers a good safety margin against boiling.

Figures 46 and 47 show the stress profiles on the two sides of the window, including both thermal and pressure-induced stresses. As sapphire is many times stronger in compression than in tension, only the tensile stresses are really of interest here. The ultimate tensile strength of sapphire is typically quoted as 60 kpsi, and 30 kpsi is a good working maximum, so this design offers at least a factor of three safety margin in stress.

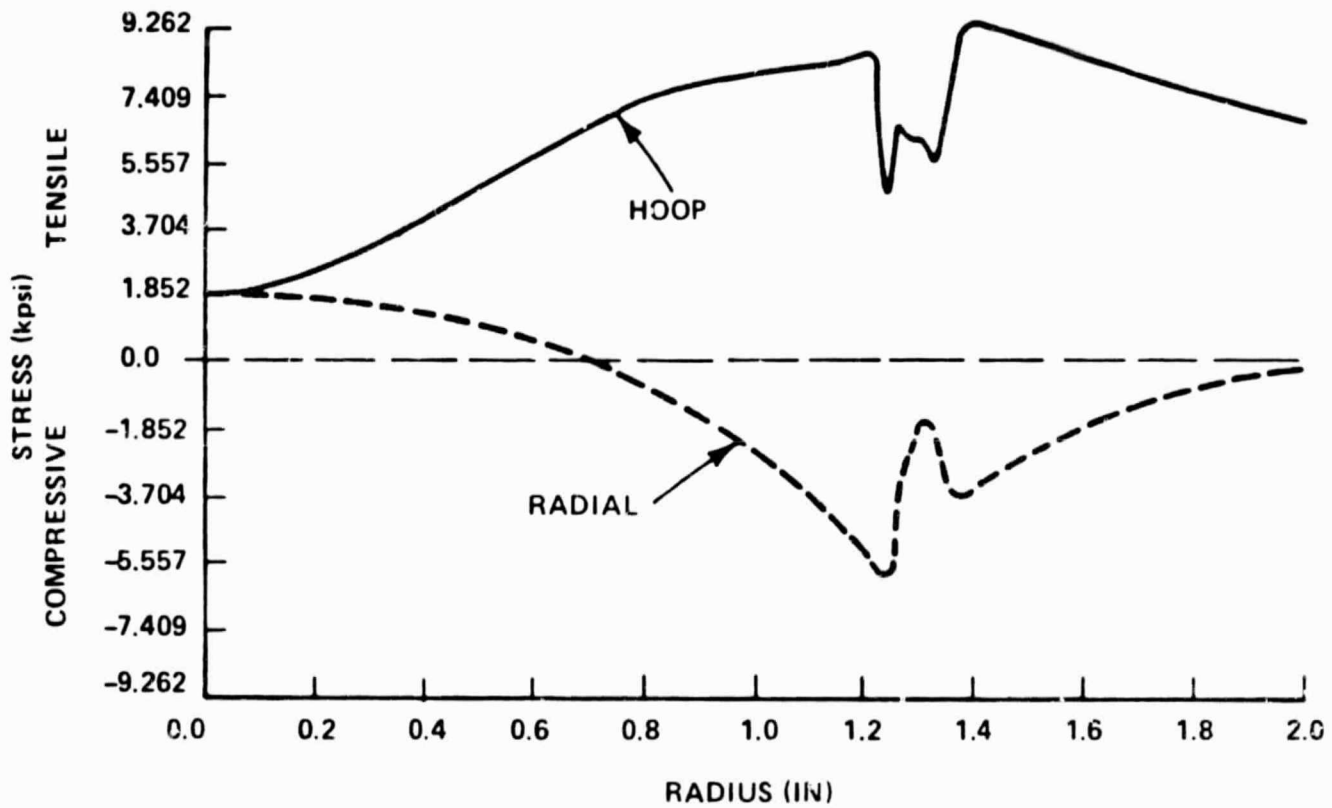
#### B. FEASIBILITY SUMMARY - CW OUTPUT WINDOW

In summary, the double-disc design is a high confidence approach for the JPL gyrokystron, based upon Varian's extensive experience with this geometry, and because of the wide temperature and stress safety margin seen in finite element analysis.



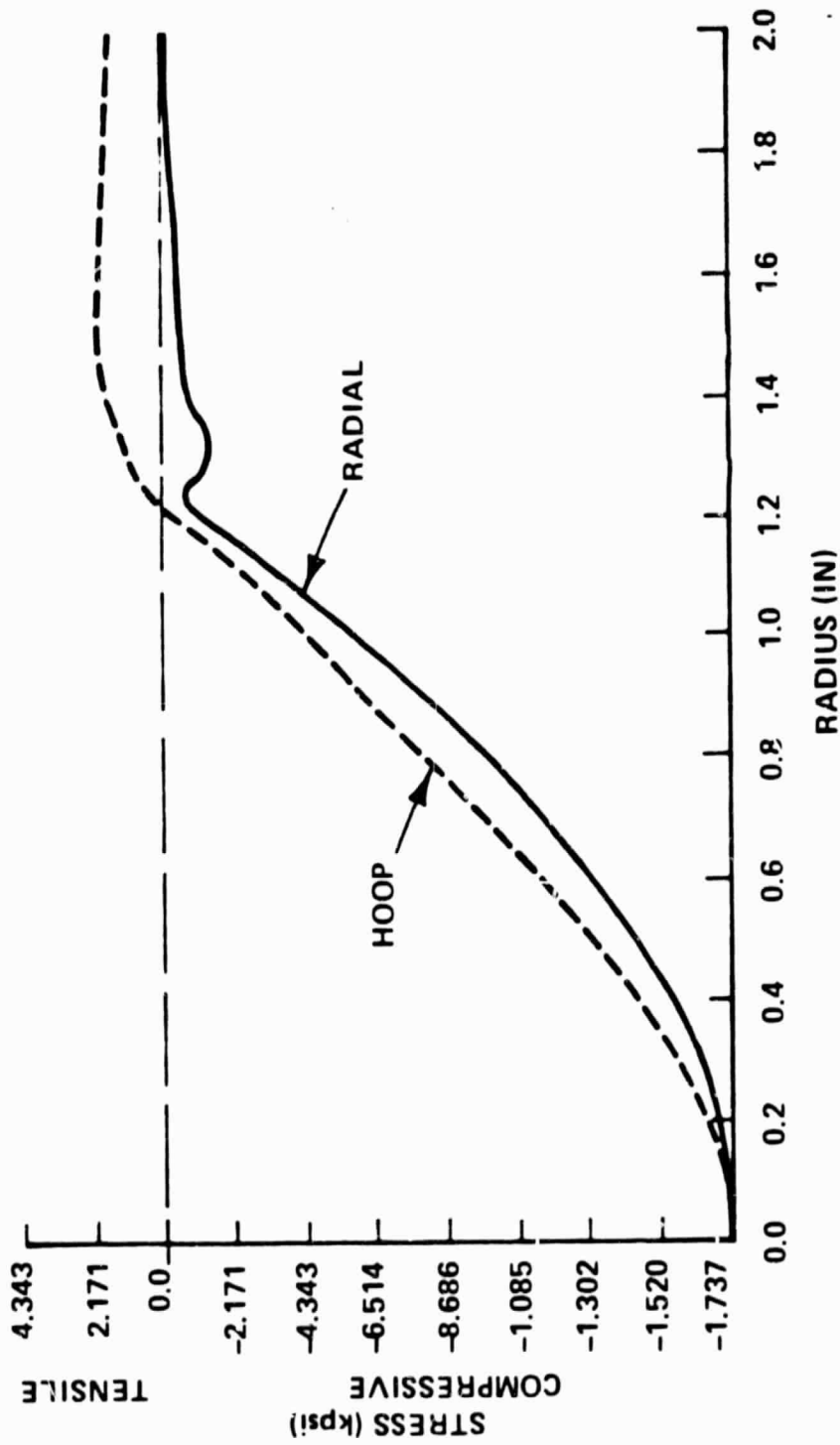
TE<sub>11</sub> MODE, 400 KW CW, SAPPHIRE DISCS

FIGURE 45. 34 GHz DOUBLE-DISC WINDOW TEMPERATURES



TE<sub>11</sub> MODE, 400 KW CW, SAPPHIRE DISCS

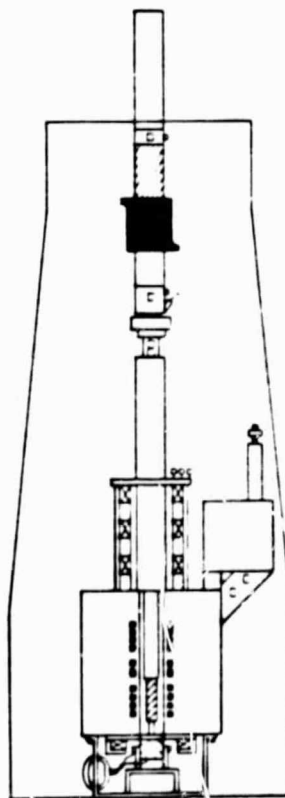
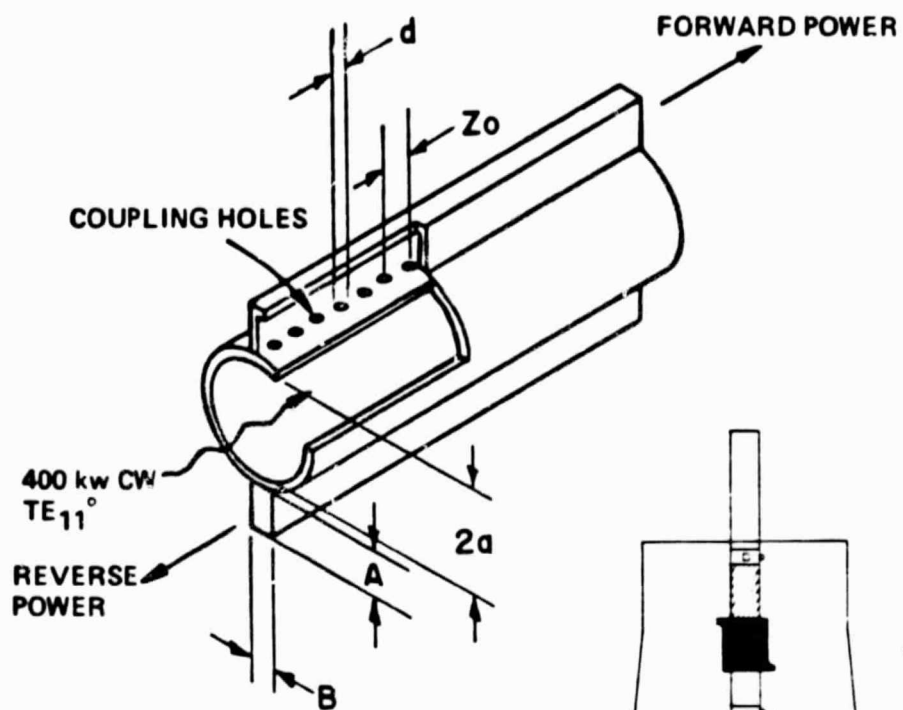
FIGURE 46. 34 GHz DOUBLE-DISC WINDOW VACUUM-SIDE STRESSES



TE<sub>11</sub> MODE, 400 KW CW, SAPPHIRE DISCS

FIGURE 47. 34 GHz DOUBLE-DISC WINDOW COOLANT-SIDE STRESSES

# DIRECTIONAL COUPLER





## VIII. DIRECTIONAL COUPLER

A directional coupler will be needed in the output transmission line to measure the forward or reverse power in a specific mode. For this feasibility study, where forward powers of 200 to 400 kW are assumed, the coupling factor should be in the 60 to 70 dB range to reduce the magnitude of the coupled signal to a reasonable value. With these coupling factors, loose coupling theory can be applied, as presented by Miller<sup>17</sup>.

### A. COUPLER GEOMETRY

A representation of the directional coupler is shown in Figure 48. Power is coupled from the main circular waveguide of radius  $a$  through a series of equally spaced coupling holes into rectangular waveguides. The narrow walls of the rectangular waveguides are adjacent to the circular waveguide.

The coupler is designed to preferentially select a single mode from the main waveguide. The guide wavelength of the  $TE_{10}$  mode in the rectangular waveguide must match the guide wavelength of the mode of interest in the main waveguide. Since the guide wavelength of the  $TE_{10}$  mode in the rectangular guide is a function of the broad dimension,  $A$ , of the rectangular guide, this dimension is specified. The narrow wall,  $B$ , was chosen to be 0.280 inch. Beyond the coupling region, the rectangular waveguide is tapered to the size of the normal fundamental waveguide for the operating frequency. This tapering is done gradually to minimize the possibility of exciting any other  $TE_{m0}$  modes.

The distance between the coupling hole centers,  $z_0$ , is chosen to be  $\lambda_g/4$  for the primary mode of interest. This causes the microwave signal to couple strongly in the forward direction and cancel in the backward direction<sup>18</sup>. The diameter,  $d$ , of the coupling holes can be varied to give the desired coupling coefficient, so long as  $d \ll \lambda_0$ ,  $d \ll a$  and  $d < z_0$ .

C - 2

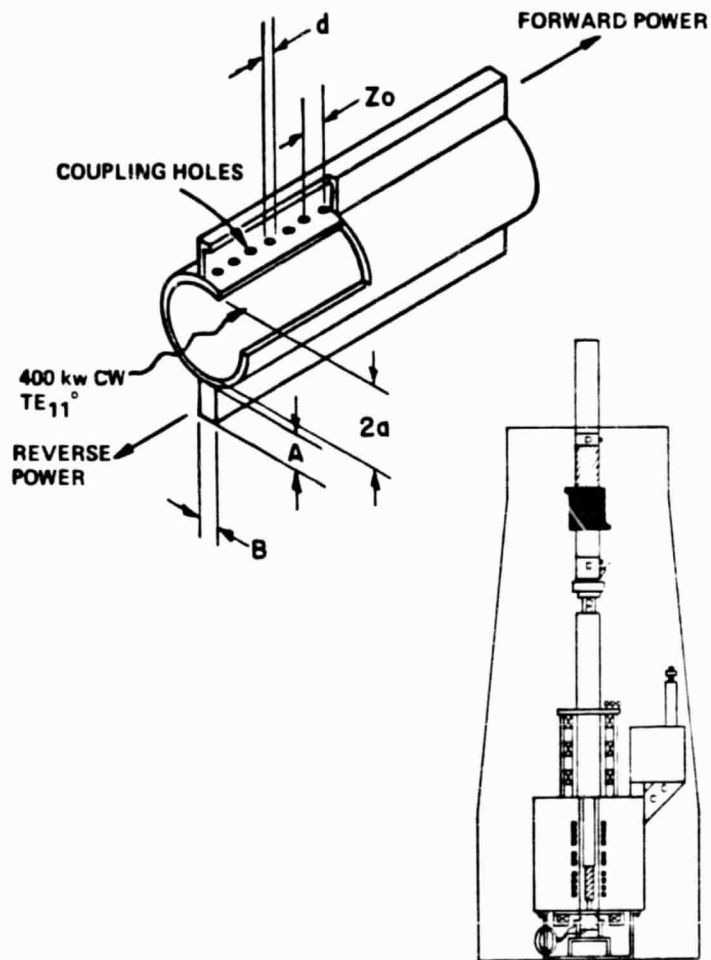


FIGURE 48. DIRECTIONAL COUPLER

## B. COUPLING COEFFICIENT

The formula that was used to calculate the coupling values was derived in Reference 14. There were two assumptions made in the derivation of the equation for the coupling. These are 1) loose coupling and 2) thin waveguide walls.

The coupling coefficient is defined as:

$$\text{Coupling coefficient} \equiv \frac{\text{Coupled power in TE}_{10} \text{ from TE}_{mn}^0}{\text{Total power in TE}_{mn}^0}$$

and is given by the equation

$$C = \frac{1}{12} \sqrt{\frac{\epsilon_n}{2\pi}} \frac{d^3 \lambda_0}{A \sqrt{AB} a^2} \frac{L}{z_0} \frac{1}{((1 - f_c^{o2}/f^2) (1 - f_c^{\square 2}/f^2))^{1/4}} \sqrt{\frac{X_{mn}^2}{m^2 - X_{mn}^2}}$$

where

$f_c^o/f$  = cut off ratio of the mode of interest in the circular waveguide.

$f_c^{\square}/f$  = cut off ratio of the fundamental mode in the rectangular waveguide.

$X_{mn}$  = Bessel root of  $TE_{mn}$  mode of the circular waveguide

$L$  = Total length of the coupling region

$\epsilon_n$  = Neumann's number = 2 if  $n \neq 0$   
= 1 if  $n = 0$

The factor of  $\frac{L}{z_0}$  results from an N hole coupler having N times the coupling strength of a single hole coupler<sup>18</sup>. The  $TM_{mn}$  modes from the circular waveguide will not couple into the rectangular waveguide due to the symmetry along the X axis<sup>14</sup>.

Note that the coupling value in dB is  $20 \log_{10} C$ .

### C. DIRECTIVITY AND SELECTIVITY

Two other parameters of interest in the coupler are the directivity in the mode of interest and the selectivity of the coupler with respect to coupling to other modes. These are defined as

$$\text{Directivity} \equiv \frac{\text{Forward coupled power in TE}_{10} \text{ from TE}_{mn}^{\circ}}{\text{Reverse coupled power in TE}_{10} \text{ from TE}_{mn}^{\circ}}$$

$$\text{Selectivity} \equiv \frac{\text{Forward coupled power in TE}_{10} \text{ from TE}_{mn}^{\circ}}{\text{Forward coupled power in TE}_{10} \text{ from TE}_{m'n'}^{\circ}}$$

where the  $\text{TE}_{m'n'}^{\circ}$  mode is any mode other than the  $\text{TE}_{mn}^{\circ}$  mode.

Expressions for both D and S are derived in Reference 17. The evaluation of D and S depends on the parameter  $\theta$  where

$$\theta \pm = \pi L \left( \frac{1}{\lambda_{g1}} \pm \frac{1}{\lambda_{g2}} \right)$$

Where  $\lambda_{g1}$  is the guide wavelength of the mode of interest in the circular waveguide, and  $\lambda_{g2}$  is the guide wavelength of the fundamental mode in the coupled waveguide. Two types of coupler arrays were compared; uniform coupling and linearly tapered coupling.

### D. UNIFORM COUPLING

In uniform coupling, the holes are equally spaced and of the same diameter.

Then

$$D(\text{dB}) = 20 \log_{10} \left( \frac{\theta_+}{\sin \theta_+} \right)$$

$$S(\text{dB}) = 20 \log_{10} \left[ \frac{\theta_-}{\sin \theta_-} \frac{C_p}{C_s} \right]$$

where

$C_p$  = coupling coefficient for the primary mode of interest

$C_s$  = coupling coefficient for secondary mode

#### E. LINEARLY TAPERED COUPLING

In linearly tapered coupling, the holes are equally spaced but the hole diameters change with length to taper the coupling in a linear fashion.

Since  $C \propto d^3$  (electric dipole coupling),  $d$  varies with the axial distance  $z$  as

$$d(z) = d_o \left( \frac{z}{L/2} \right)^{1/3} \quad 0 < z < \frac{L}{2}$$

$$d(z) = d_o \left( \frac{L-z}{L/2} \right)^{1/3} \quad \frac{L}{2} < z < L$$

where  $d_o$  is the maximum hole diameter. Also, for linearly tapered coupling, the coupling coefficient expression has an additional factor of  $1/2$  in it, a correction factor to account for the non-constant coupling.

The directivity and selectivity for this case are given by

$$D(\text{dB}) = 20 \log_{10} \left[ \left( \frac{\theta+2}{\sin(\theta+2)} \right)^2 \right]$$

$$S(\text{dB}) = 20 \log_{10} \left[ \left( \frac{\theta-2}{\sin(\theta-2)} \right)^2 \frac{C_p}{C_s} \right]$$

Once the coupling distribution is specified, the length is chosen to maximize the discrimination of the coupling against a certain mode. This mode is usually the one with guide wavelength closest to the guide wavelength of the primary mode. The length of the coupler must also be some integer multiple of  $z_0$ . The advantage of uniform coupling is that the required length is shorter than that for linearly tapered coupling. However, selectivity and directivity are increased with tapered coupling. The theory was found to agree with the data presented in Reference 19.

#### F. CONCEPTUAL DESIGN

For this project, the primary mode of interest is the  $TE_{11}^0$  mode. Therefore, the coupler will be designed to couple to this mode and to discriminate against the  $TE_{12}^0$ ,  $TE_{13}^0$  and  $TE_{14}^0$  modes. These latter modes are the most likely spurious modes to be generated by the tube. The discrimination (selectivity) will be maximized against the  $TE_{12}^0$  mode.

Listed in Tables 10 and 11 are the results of calculations on designs in both 1.75-inch and 2.5-inch-diameter waveguides. Software has been developed at Varian during this study program to carry out this first-cut design (see Appendix B).

The most likely waveguide diameter to be chosen is 1.75 inches. Because of the higher directivity and selectivities, the linearly-tapered coupling design would be preferred. The results of the calculations on this design are shown graphically in Figures 49 and 50.

Table 10  
 $TE_{11}^O$  Directional Coupler  
 1.75-Inch-Diameter Waveguide

$F_o = 34$  GHz  
 $z_o = 0.087$  inch  
 $B = 0.28$  inch  
 $d_o = 0.05$  inch  
 $A = 1.493$  inch

Uniform Coupling

$L = 6.73$  inch

Coupling at  $F_o = 66.6$  dB

	<u>Worst</u>	<u>33 GHz</u>	<u>34 GHz</u>	<u>35 GHz</u>
$TE_{11}$ directivity	41 dB	42 dB	42 dB	43 dB
$TE_{12}$ selectivity	22	22	>60	22
$TE_{13}$ selectivity	12	27	19	12
$TE_{14}$ selectivity	10	10	14	23

Linearly Tapered Coupling (Figure 49, 50)

$L = 13.46$  inch

Coupling at  $F_o = 66.7$  dB

	<u>Worst</u>	<u>33 GHz</u>	<u>34 GHz</u>	<u>35 GHz</u>
$TE_{11}$ directivity	83 dB	84 dB	85 dB	87 dB
$TE_{12}$ selectivity	52	52	>100	52
$TE_{13}$ selectivity	38	67	51	38
$TE_{14}$ selectivity	36	36	45	64

Table 11  
 $TE_{11}^0$  Directional Coupler  
 2.5-Inch-Diameter Waveguide

$F_o = 34$  GHz  
 $z_o = 0.087$  inch  
 $B = 0.28$  inch  
 $d_o = 0.05$  inch  
 $A = 2.133$  inch

Uniform Coupling

$L = 14.023$

Coupling at  $F_o = 71.0$  dB

	<u>Worst</u>	<u>33 GHz</u>	<u>34 GHz</u>	<u>35 GHz</u>
$TE_{11}$ directivity	48 dB	54 dB	48 dB	56 dB
$TE_{12}$ selectivity	22	22	41	23
$TE_{13}$ selectivity	10	22	14	10
$TE_{14}$ selectivity	10	20	12	10

Linearly Tapered Coupling

The required coupling length  $L$  is 28 inches. The directivity and selectivities were not calculated.



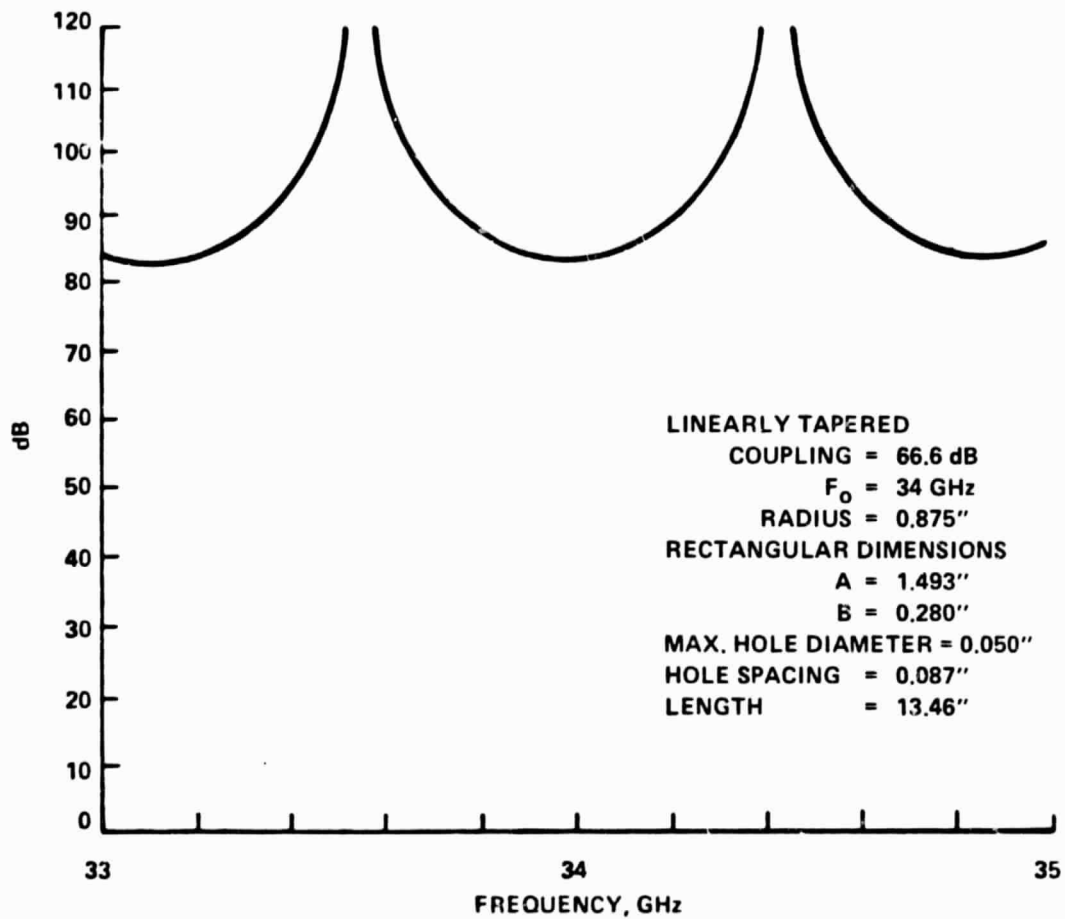


FIGURE 49. DIRECTIVITY vs FREQUENCY

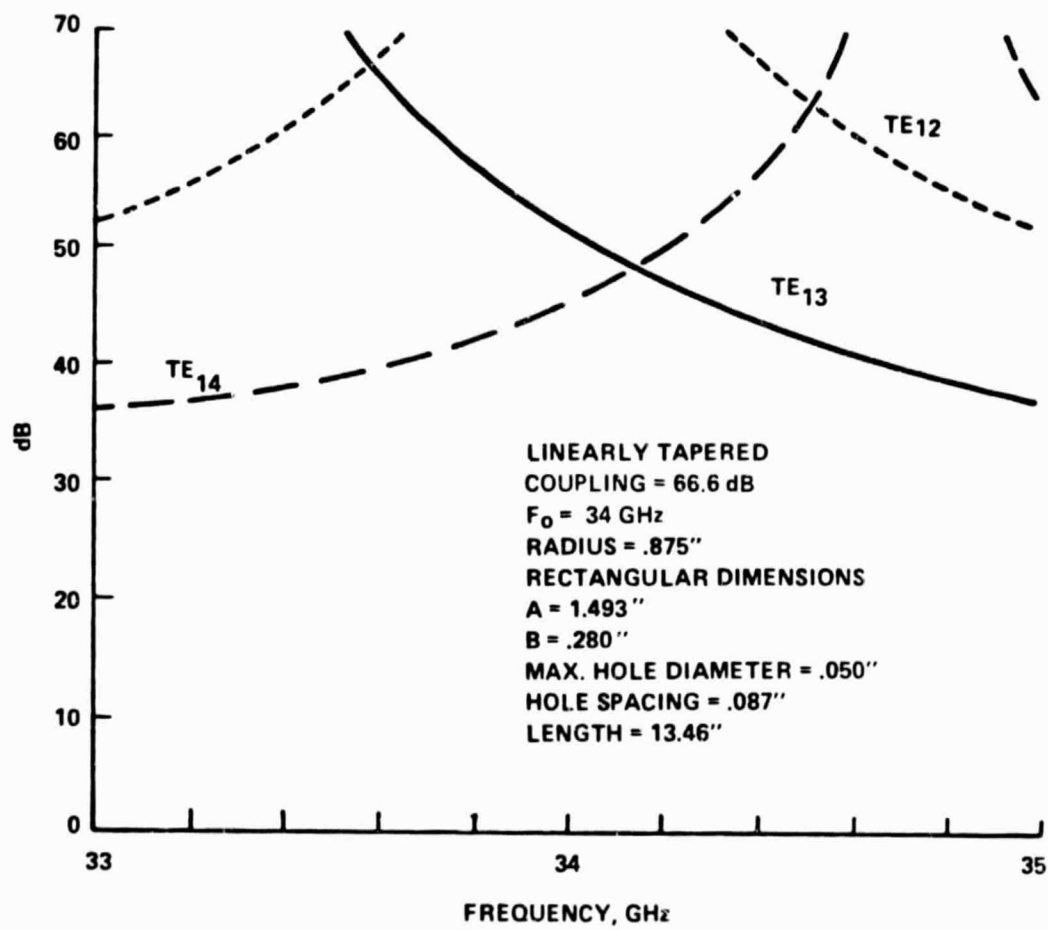
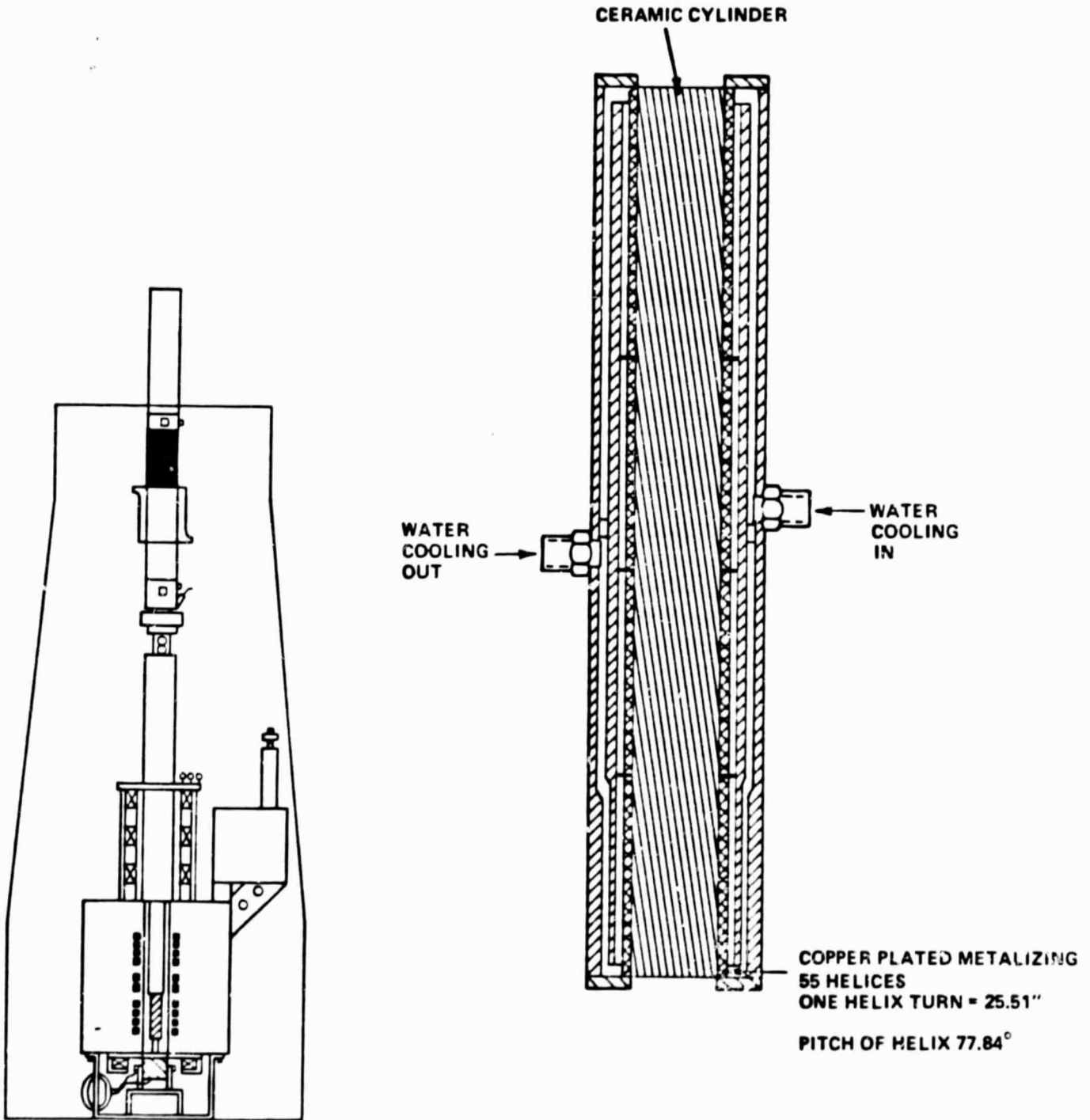


FIGURE 50. SELECTIVITIES vs FREQUENCY

G. FEASIBILITY SUMMARY - DIRECTIONAL COUPLER

The  $TE_{11}^0$  directional coupler can be designed with a coupling length of 13.5 inches and with better than 35 dB selectivity. However, the calculations ignore finite hole depth, hole spacing tolerances, and the effect of the coupling holes on the  $TE_{10}$  mode waveguide cutoff. Extensive cold testing of the coupler will be required to determine the actual values of coupling, directivity, selectivity and the effect of machining tolerances.

# MODE FILTER



## IX. MODE FILTER

The JPL gyrokystron must meet stringent requirements for mode purity. The present requirement is for a -30 dBc or lower power level in each spurious mode. However, the anticipated actual spurious mode level could be as high as -15 dBc. Therefore, a mode filter is required in the transmission line system.

The chosen design approach for the mode filter is a conducting helix metallized and plated on the inside of a ceramic cylinder as shown in Figure 51. The pitch of the helix is chosen to provide minimum loss for the right circularly polarized  $TE_{11}$  circular waveguide mode. The loss for all other modes, including the left circularly polarized  $TE_{11}$  mode, will be much higher. The loss will be provided by a layer (or jacket) of water flowing over the outside of the ceramic cylinder.

### A. THEORY

The theoretical propagation constants of the spurious modes were calculated from the theory presented in Reference 20. The calculations involve solving the following transcendental equation.

$$\begin{aligned} & \zeta_2 \left[ \left( \zeta_1 \tan \psi - \frac{hn}{\zeta_1 a} \right)^2 \frac{J_n(\zeta_1 a)}{J_n'(\zeta_1 a)} - \omega^2 \mu_0 \epsilon_0 \frac{J_n'(\zeta_1 a)}{J_n(\zeta_1 a)} \right] \\ & = \zeta_1 \left[ \left( \zeta_2 \tan \psi - \frac{hn}{\zeta_2 a} \right)^2 \frac{H_n^{(2)}(\zeta_2 a)}{H_n^{(2)'}(\zeta_2 a)} - \omega^2 \mu_0 \epsilon_0 (\epsilon' - i\epsilon'') \frac{H_n^{(2)'}(\zeta_2 a)}{H_n^{(2)}(\zeta_2 a)} \right] \end{aligned} \quad (1)$$

where the parameters in this equation are:

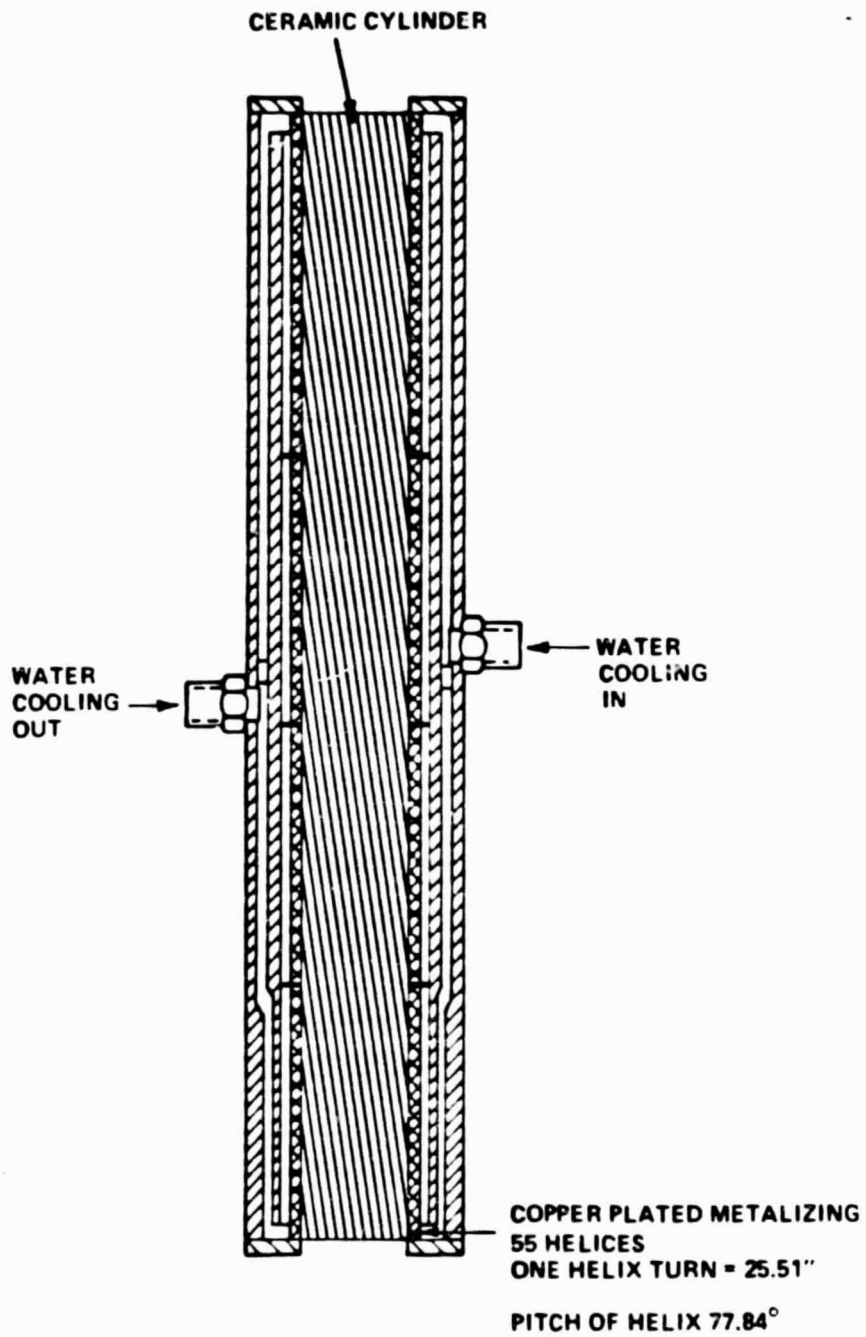


FIGURE 51. MODE FILTER

a	Inner radius of waveguide
$h = \beta - i\alpha$	Complex phase constant
n	Angular mode index (positive for right circular polarization, negative for left)
$\alpha$	Attenuation constant
$\beta$	Phase constant
$\beta_0 = 2\pi/\lambda_0 = \omega(\mu_0 \epsilon_0)^{1/2}$	Free space phase constant
$\mu_0$	Permeability of waveguide interior medium and of lossy jacket
$\epsilon_0$	Permittivity of waveguide interior
$\epsilon'$	$\epsilon/\epsilon_0$
$\epsilon''$	$\sigma/\omega\epsilon_0$
$\epsilon$	Permittivity of lossy jacket
$\sigma$	Conductivity of lossy jacket
$\omega$	Angular frequency
$\psi$	Pitch angle of helix
$\zeta_1$	$[\omega^2 \mu_0 \epsilon_0 - h^2]^{1/2}$
$\zeta_2$	$[\omega^2 \mu_0 \epsilon_0 (\epsilon' - i\epsilon'') - h^2]^{1/2}$
$J_n(x)$	Bessel function of the first kind
$J_n'(x)$	$d J_n(x)/dx$
$H_n^{(2)}(x)$	Hankel function of the second kind
$H_n^{(2)'}(x)$	$d H_n^{(2)}(x)/dx$

This equation assumes that the helix conducts perfectly in the helical direction but does not conduct in any other direction, and that the helix is surrounded by an infinite homogeneous conducting medium. The equation is valid for any values of permittivity and conductivity of the outer lossy jacket. Note also that the assumption of an infinite outer medium is satisfied by a finite lossy jacket which is thick enough that the fields at its outer surface are negligible. This is true of a reasonable thickness of water at 34 GHz.

To facilitate finding solutions of (1), it is useful to note that when the outer jacket conductivity is sufficiently high, approximate solutions to (1) may be found (Reference 20). In this case, the propagation constants may be written in the form

$$ih = \alpha + i (\beta_{nm} + \Delta\beta)$$

where  $\beta_{nm} = (2\pi/\lambda_0) (1 - v^2)^{1/2}$  are the mode propagation constants for the lossless case. Here  $v = \lambda_0/\lambda_c$ , where  $\lambda_c$  is the mode cutoff wavelength.

Then the following approximation formulas hold, to the first order

TM<sub>nm</sub> modes

$$\alpha + i\Delta\beta = \frac{\chi + i\eta}{a(1-v^2)^{1/2}} \frac{1}{1 + \tan^2 \psi} \quad (2)$$

TE<sub>nm</sub> modes

$$\alpha + i\Delta\beta = \frac{\chi + i\eta}{a(1-v^2)^{1/2}} \frac{v^2 p^2}{p^2 - n^2} \frac{[\tan\psi - n(1-v^2)^{1/2}/pv]^2}{1 + \tan^2 \psi} \quad (3)$$

where

$$\chi + i\eta = (\epsilon' - i\epsilon'')^{-1/2}$$

$p = m^{\text{th}}$  zero of  $J_n'(x)$  for the TE<sub>nm</sub> modes

(2) and (3) are valid when

$$\frac{a(1-v^2)^{1/2}}{v} |\alpha + i\Delta\beta| \ll 1$$

## B. CALCULATION OF ATTENUATION CONSTANTS

The complex propagation constants, including the attenuation constants, were calculated from (1) for the following modes of interest: TE<sub>11</sub>, TE<sub>12</sub>, TE<sub>13</sub>, TE<sub>14</sub>, TM<sub>11</sub>, TM<sub>12</sub>, TM<sub>13</sub>, TM<sub>14</sub> of both right and left polarization. The calculations were done for two filter waveguide inner diameters, 1.75 inches and 2.50 inches. The helix pitch angle was calculated for each



one from

$$\psi = \tan^{-1} [n (1-v^2)^{1/2} / pv]$$

for the  $TE_{11}$  right circularly polarized mode ( $n = 1$ ,  $p = 1.841$ ). This is the angle which gives zero theoretical attenuation for that mode.

The theoretical model for which (1) is derived assumes that the outer conducting medium is immediately adjacent to the conducting helix whereas in our chosen design the helix is separated from the conducting jacket of water by a dielectric cylinder. For the purposes of our calculations, the presence of the dielectric cylinder was included by assuming that its thickness was some odd multiple of a quarter wavelength, and that the cylinder would act as an ideal quarter-wave transformer between the interior of the filter waveguide and the impedance of the water. Also, for the calculations, the ceramic cylinder was assumed to be beryllium oxide. Therefore, the effective permittivity of the outer jacket was assumed to be  $\epsilon' - i\epsilon'' = 1 - i 0.0013$  (0.0013 being the loss factor of beryllium oxide).

To solve (1) for each mode, a root search and predictor subroutine was used. In order to use the approximation Equations (2) and (3) to find trial values for the propagation constants,  $\epsilon''$  was started at the value 2000. The value of  $\epsilon''$  was then decremented during the running of the program. For the first values of  $\epsilon''$ , the approximation equations were used to find trial values. The allowed relative error in the root search was  $10^{-5}$ . After four roots were found, the predictor routine produced all subsequent trial values. In all cases, the values of the attenuation constants produced by the program were larger than the values found by the approximation formulas.

The evaluation of the Bessel function was done using the asymptotic expansion in Reference 21 and was then checked against the values in Reference 22. The expansion was halted when the error term became smaller than the allowed error ( $10^{-4}$ ), or when the  $n + 1$ st error term was larger than the  $n$ th error term. The left circularly polarized  $TE_{11}$  calculations

were the least accurate due to the asymptotic expansion error near one, and the Bessel argument for a TE<sub>11</sub> mode being 1.841.

The Hankel functions cannot be evaluated directly due to their exponential growth away from the origin, since the arguments are generally large at high conductivities. Instead, an expansion of the ratio  $H_n^{(2)}/H_n^{(2)}$  was found.

To check the computer code, several examples were run from Reference 20. Special attention was paid to the TE<sub>11</sub> and TM<sub>11</sub> calculations, corresponding to low Bessel function arguments. It was found that the results agreed to within 2 percent. A crude estimate of error was made by:

$$\Delta\alpha = \Delta\epsilon \frac{d\alpha}{d\epsilon''}$$

The results of the calculations for the two filter waveguide sizes are summarized in Tables 12 and 13.

The attenuation constant  $\alpha$  is not shown for the TE<sub>11</sub> right circularly polarized mode in these tables. This is because (1) assumes that the conductivity of the helix is infinite, and therefore (1) returns an  $\alpha$  of 0 for this mode at the values of  $\psi$  used for the calculations. For comparison, the theoretical  $\alpha$  for the TE<sub>11</sub> right mode in a solid copper cylindrical waveguide would be  $5.5 \times 10^{-4}$  dB/inch in the 1.75-inch waveguide, and  $3.8 \times 10^{-4}$  dB/inch in 2.5-inch waveguide.

The reason that the final value of  $\epsilon''$  shown in the tables is not the assumed value of 0.0013 is that when  $\alpha/\beta \lesssim \epsilon''$ , the imaginary part of the Hankel function changes sign. The changed sign implies that the field strengths outside of the helix grow exponentially with increasing radius, and thus the solution becomes non-physical. The values of  $\epsilon''$  shown are the lowest values before the sign change.

The angles  $\psi$  optimum shown in the last column are the angles for which the attenuation would be lowest for each of the modes. They are listed for

TABLE 12

RESULTS FOR 1.75 IN. WAVEGUIDE,  $\psi = 77.84^\circ$ PRIMARY MODE: TE<sub>11</sub> Right Circularly Polarized

MODE/ CIRCULAR POLARIZATION	$\alpha$ (dB/in)	$\epsilon' - i\epsilon''$	$\beta$ (in <sup>-1</sup> ) - $i\alpha$ ( $\frac{\text{nepers}}{\text{in}}$ )	$\alpha/\beta$	$\psi_{\text{optimum}}$
TE 11 Left	1.07 ± 0.08	1 - i 0.02	17.93 - i 0.123	0.0068	- 77.84°
TE 12 Left	1.20 ± 0.04	1 - i 0.02	17.51 - i 0.139	0.0079	- 27.70°
TE 12 Right	1.92 ± 0.05	1 - i 0.03	17.33 - i 0.221	0.0128	27.70°
TE 13 Left	6.93 ± 0.2	1 - i 0.09	15.93 - i 0.798	0.0501	- 10.38°
TE 13 Right	6.19 ± 0.5	1 - i 0.07	15.93 - i 0.712	0.0447	10.38°
TE 14 Left	12.50 ± 0.1	1 - i 0.13	13.36 - i 1.440	0.1078	- 4.46°
TE 14 Right	11.99 ± 0.2	1 - i 0.12	13.36 - i 1.380	0.1033	4.46°
TM 11 Left	1.26 ± 0.2	1 - i 0.02	17.53 - i 0.145	0.0083	90°
TM 11 Right	2.29 ± 0.2	1 - i 0.03	17.62 - i 0.264	0.0150	90°
TM 12 Left	1.04 ± 0.008	1 - i 0.02	16.22 - i 0.120	0.0074	90°
TM 12 Right	1.35 ± 0.001	1 - i 0.02	16.21 - i 0.155	0.0096	90°
TM 13 Left	0.89 ± 10 <sup>-4</sup>	1 - i 0.009	13.87 - i 0.103	0.0074	90°
TM 13 Right	0.99 ± 10 <sup>-4</sup>	1 - i 0.008	13.86 - i 0.114	0.0082	90°
TM 14 Left	0.99 ± 10 <sup>-4</sup>	1 - i 0.007	9.78 - i 0.115	0.0118	90°
TM 14 Right	1.04 ± 10 <sup>-4</sup>	1 - i 0.008	9.78 - i 0.119	0.0122	90°

TABLE 13

RESULTS FOR 2.5 IN. WAVEGUIDE,  $\psi = 81.45^\circ$ PRIMARY MODE: TE<sub>11</sub> Right Circularly Polarized

MODE/ CIRCULAR POLARIZATION	$\alpha$ (dB in.)	$\epsilon' - i\epsilon''$	$\beta$ (in <sup>-1</sup> ) - $i\alpha$ ( $\frac{\text{nepers}}{\text{in}}$ )	$\alpha/\beta$	$\psi_{\text{optimum}}$
TE 11	< .1				- 81.45°
TE 12 Left	0.600 ± 0.018	1 - i 0.0014	17.82 - i 0.069	0.004	- 36.95°
TE 12 Right	0.874 ± 0.08	1 - i 0.02	17.71 - i 0.101	0.006	36.95°
TE 13 Left	2.91 ± 0.18	1 - i 0.04	17.04 - i 0.335	0.02	- 16.05°
TE 13 Right	2.43 ± 0.18	1 - i 0.04	17.03 - i 0.280	0.02	16.05°
TE 14 Left	4.74 ± 0.21	1 - i 0.06	15.91 - i 0.55	0.03	- 8.02°
TE 14 Right	4.43 ± 0.22	1 - i 0.06	15.90 - i 0.510	0.03	8.02°
TM 11 Left	0.510 ± 0.004	1 - i 0.007	18.02 - i 0.059	0.003	90°
TM 11 Right	1.13 ± 0.16	1 - i 0.02	17.86 - i 0.13	0.007	90°
TM 12 Left	0.474 ± 10 <sup>-4</sup>	1 - i 0.006	17.21 - i 0.055	0.003	90°
TM 12 Right	0.622 ± 10 <sup>-5</sup>	1 - i 0.008	17.21 - i 0.072	0.004	90°
TM 13 Left	0.370 ± 10 <sup>-5</sup>	1 - i 0.005	17.17 - i 0.072	0.0025	90°
TM 13 Right	0.416 ± 10 <sup>-5</sup>	1 - i 0.0045	16.17 - i 0.05	0.003	90°
TM 14 Left	0.320 ± 10 <sup>-5</sup>	1 - i 0.004	14.63 - i 0.037	0.002	90°
TM 14 Right	0.341 ± 10 <sup>-5</sup>	1 - i 0.004	14.63 - i 0.09	0.006	90°

reference only. The angles used for all of the calculations were the first numbers at the top of the column in the tables ( $77.84^\circ$  and  $81.45^\circ$ ).

To obtain a minimum attenuation of 15 dB in all of the modes listed, the filter would need to be about 17 inches long, if made in 1.75-inch waveguide or 47 inches long if made in 2.5-inch waveguide. This latter length ignores the  $TE_{11}$  left mode, whose attenuation seems to be so low that meaningful results could not be obtained from the program.

To achieve the 15 dB desired attenuation in a reasonable length, the 1.75-inch-diameter waveguide is preferred.

### C. SENSITIVITY TO PITCH AND FREQUENCY

The theoretical attenuation of the  $TE_{11}$  right circularly polarized mode was calculated from (!) for the 1.75-inch-diameter case for two conditions: a) varying the frequency over a 2 percent bandwidth while holding  $\Psi$  constant at  $77.84^\circ$ , and b) varying the pitch angle over  $\pm 2^\circ$  while holding the frequency constant at 34 GHz.

For the first condition, the theoretical attenuation constant at the band edges was less than  $5.5 \times 10^{-4}$  dB/inches. At the lower band edge 33.966 GHz,  $\alpha = 3.084 \times 10^{-7}$  dB/inch, at the upper band edge,  $\alpha = 9.71 \times 10^{-8}$  dB/inch. Therefore, we conclude that the sensitivity to frequency is negligible.

For the second condition, the results are tabulated below for a 17 inch length.

<u><math>\Delta\Psi</math>, Degrees</u>	<u>dB Attenuation Per Percent Change From Ideal Pitch</u>
+2	0.150
+1	0.076
+0.5	0.053
-1	0.022
-2	0.050

To attenuate the  $TE_{11}$  right circularly polarized mode less than 2 percent the pitch angle would have to be held to  $\pm 1$  degree.

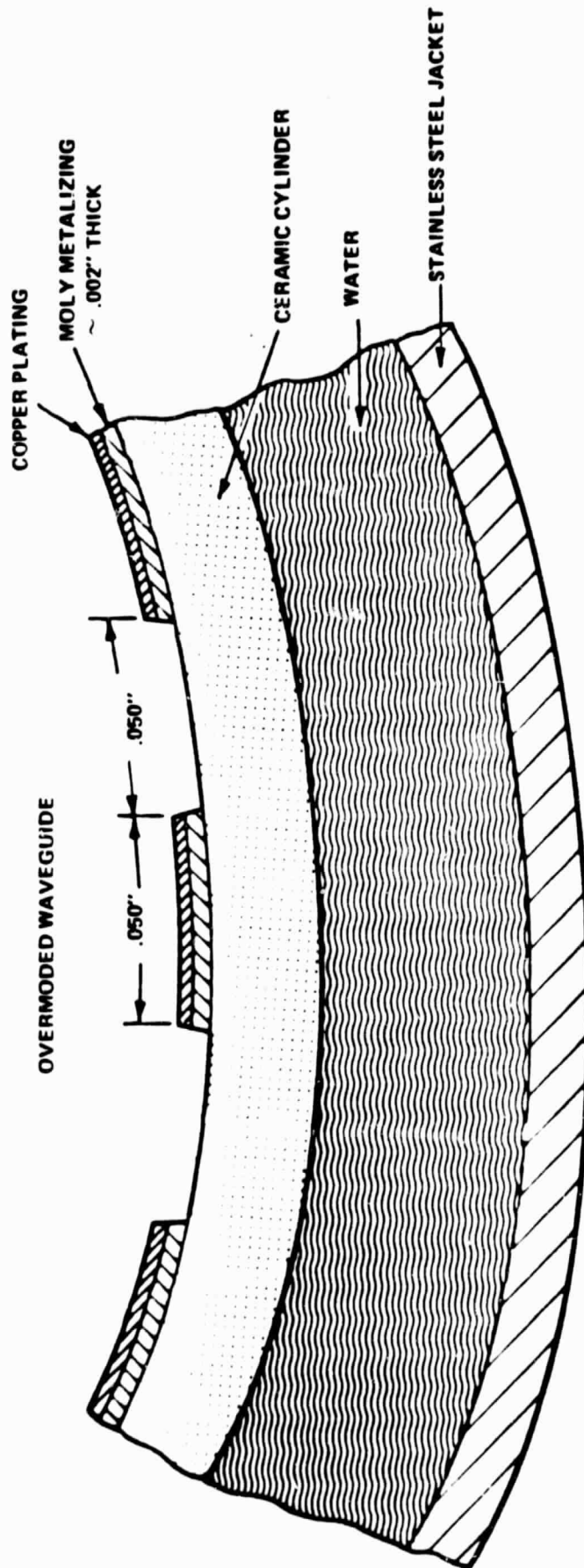
#### D. REALIZATION OF THE HELIX WAVEGUIDE

Considering the results of the calculations, the chosen size of the helix waveguide is a 1.75-inch-inside diameter. The helix will be formed by metallizing and plating helix ribbons on the inside of a ceramic cylinder approximately 17 inches long. Because of the difficulties of making a cylinder this long without significant warpage, the ceramic will probably be made in 2 to 4 sections. Alignment of the sections will be critical to insure continuity of the inside helices.

The spacing between the helix ribbons should be less than a quarter of a wavelength. At the same time, the narrower each helix is, the more difficult the mode filter will be to make. For initial considerations, it is assumed that each helix is 0.050 inch wide with 0.050 inch spacing between the helices. Testing will be needed to determine if this is an acceptable choice or if another choice would be better. For the 1.75 inch waveguide there will be 55 helix ribbons, and one turn of the helix is 25.5 inches long.

Even though beryllia was assumed in the calculations, alumina ceramic will also be considered since the latter is easier and less expensive to process.

The following is a list of possible processes for forming and metallizing the helix ribbons inside the ceramic cylinder as shown in Figure 52.



1. DEVELOP POLYMER MASK FOR HELIX PATTERN
2. PLACE MASK ON ID OF CERAMIC CYLINDER
3. METALLIZE ID OF CYLINDER
4. SINTER METALIZING
5. REMOVE MASK
6. COPPER PLATE HELIX RIBBONS
7. ASSEMBLE IN WATER COOLING JACKET

FIGURE 52. MECHANICAL CONFIGURATION/FABRICATION SCHEME

1) Tape Metallizing

Tape metallizing is metallizing with a polymer or paper backing. The accuracy, when placing the metallizing on the ceramic, is improved over conventional metallizing. After the entire ID is metallized, the tape metallizing can be cut away, leaving only the helix pattern.

2) Screen Pattern

A screen pattern of the helices can be made, and then spray painted or roll painted.

3) Spray Coating

The entire ID can be spray coated and a dental blast pattern made which will blast away the spaces between the helices. This technique can be used only for an alumina cylinder, as beryllia cannot be dental blasted. Another possibility is to sinter the cylinder and then machine out the helix pattern.

4) Machine Painting

A machine can be developed that will accurately paint the helix pattern. The helices can be painted singly or several at one time.

5) Machining the Ceramic

The inside of the ceramic can be machine grooved in the desired helix pattern. The spaces between the helices can be machined away and then the entire ID can be roll coated. The machining is easier to do before hard firing, however, it is an expensive method.



## 6) Polymer Mask

A heat expandable polymer mask can be fabricated. The entire ID can then be spray painted or solution metallized. After sintering, the metallizing over the polymer mask can easily be mechanically blasted away.

The Polymer mask is the preferred approach at this time because it is accurate and relatively easy to put in place.

## E. FEASIBILITY SUMMARY - MODE FILTER

The chosen approach for the mode filter is a multitude of ribbon helices metallized and copper plated on the inside of a 1.75-inch ceramic cylinder which is 17 inches long. The helix pitch will be 77.8 degrees. The ceramic cylinder will be supported inside of a solid metal cylinder, with space between the two to allow water to flow over the ceramic. The anticipated attenuation in all modes, other than the  $TE_{11}$  right circularly polarized mode, is 15 dB minimum.

There are several aspects of the filter which will need further study and cold testing before the design is finalized.

Additional study needs to be done to more thoroughly evaluate the effect of having the dielectric (ceramic) layer between the helix and the water. In the calculations, it was assumed that the ceramic acts as an ideal quarter-wave transformer. For that to be true, the ceramic not only needs to be an odd multiple of quarter-wavelengths thick, but its dielectric constant needs to be the geometric mean of the dielectric constants of the waveguide interior ( $\epsilon = \epsilon_o$ ) and the outer jacket ( $\epsilon = \epsilon_{\text{water}}$ ). However, the relative dielectric constant of beryllia is 6.7 and of alumina is 9.6 whereas at 34 GHz, the dielectric constant of water is about 20 at 20°C. Unger (Reference 23) has treated the case of a dielectric layer between the helix and the outer jacket for the zero pitch helix filter with various

approximations. It may be that his work, or similar, may be applied to our filter design. If not, considerable cold testing may be required to evaluate the effect of the ceramic layer.

An analysis needs to be done to select the optimum length for the ceramic cylinder sections.

Calculations of the dissipated power density in the helix ribbons and cooling through the ceramic needs to be done. In addition, overall power handling capabilities of the mode filter need to be considered, both in terms of heating and of rf arcing.

## X. SENSITIVITY ANALYSIS

One of the major tasks in this feasibility study was to examine the sensitivity of the transmitter performance to small variations in the control parameters. The purpose of the sensitivity analysis is to establish the degree of electronic regulation and the size of mechanical tolerances which will be required to limit spurious variations in transmitter performance.

The methodology for performing the sensitivity analysis is to first establish the critical control parameters (e.g., magnet coil currents, beam voltage, inlet coolant temperatures, etc.). Second, we relate the control variables to physics variables (e.g., magnet coil currents are related to changes in magnetic fields). Third, we calculate variations in signal amplitude, phase, and mode purity as a function of small variations in the physics variables from the nominal operating point. Details of these calculations are given in Appendix C.

As an example, consider the calculation of amplitude modulation sensitivity with respect to variation in circuit magnetic field. Referring to the calculation of power versus circuit magnetic field given in Figure 24, at the operating point we find, the rate of change of rf power with respect to circuit magnetic field,

$$\left( \frac{dP}{dB} \right)_{\text{circuit}} = \frac{0.344 \text{ dB}}{1.269\%} = 0.271 \text{ dB}/\%$$

The conceptual design for the solenoid (see Section III) contains three individually energized coils which generate the circuit magnetic field. A small variation of the current in one of these coils leads to a variation in the value of the magnetic field averaged over the length of the circuit,

$$\frac{dB_{\text{circuit}}}{dI_{\text{main coil}}} = 0.353\%/\%$$

The amplitude modulation sensitivity for main magnet coil current is then computed as follows,

$$\begin{aligned} \frac{dP}{dI_{\text{main coil}}} &= \left( \frac{dP}{dB} \right)_{\text{circuit}} \cdot \left( \frac{dB_{\text{circuit}}}{dI_{\text{main coil}}} \right) \\ &= 0.271 \text{ dB/\%} \cdot 0.353 \text{ \%/} \\ &= 0.0957 \text{ dB/\%} \end{aligned}$$

The amplitude modulation sensitivities for the conceptual design of the JPL gyrokystron are summarized in Table 14. In the right hand column we have also provided the values of parameter regulation which will be required to hold the spurious amplitude modulation to below 0.1 dB. The "remarks" column highlights the impact of the regulation requirement on equipment design. The cathode voltage regulation required is typical of gyrotron oscillators and is straightforward to achieve in practice by providing for active regulation of the high voltage dc beam supply. Regulated constant current power supplies are required to meet the regulation given for the various electromagnet currents. The inlet coolant temperature in the body must be regulated because thermal changes in the cavity sizes will affect the tube output power. However, size changes due to temperature variations in the collector and output transmission lines will have no effect on the signal amplitude because there is no beam-wave interaction in these regions.

Phase modulation sensitivities are given in Table 15 along with the parameter regulation required to hold the spurious phase modulation below one degree of arc. As in the case of the AM sensitivity to beam voltage, the dc beam supply voltage must be regulated to 0.2 percent to hold the spurious phase modulation below 1 degree. However, the PM sensitivities for solenoid coil currents lead to a factor of ten more stringent regulation than is implied by the AM sensitivities. Although this regulation can be achieved with regulated supplies, this requirement favors the use of high inductance magnets, namely, superconducting electromagnets. The regulation required for the wiggler bifilar helix current can also be met by regulated supplies but favors a wiggler configured with permanent magnets.

TABLE 14  
CALCULATED AM SENSITIVITIES

<u>CONTROL PARAMETER</u>	<u>AM SENSITIVITY</u>	<u>REGULATION FOR AM &lt; 0.1 dB</u>	<u>REMARKS</u>
CATHODE VOLTAGE	0.45 dB/%	0.2%	ACTIVE REGULATION ON DC BEAM SUPPLY
MAIN MAGNET COIL CURRENT	0.096 dB/%	1.0%	
WIGGLER SOLENOID COIL CURRENT	0.45 dB/%	0.2%	CONSTANT CURRENT, REGULATED SUPPLIES
WIGGLER BIFILAR HELIX CURRENT	0.69 dB/%	0.1%	
GUN COIL CURRENT	0.013 dB/%	7%	-
FILAMENT VOLTAGE (PIERCE GUN)	0.009 dB/%	11%	-
LOAD VSWR	1.6 dB FOR VSWR = 2:1 OSCILLATION FOR VSWR > 2.4:1	VSWR < 1.2:1	TYPICAL FOR ANY POWER AMPLIFIER
RF DRIVE (INPUT POWER)	0.007 dB/%	-	-
INLET COOLANT TEMPERATURE (BODY)	0.003 dB/°C	33° C	-

TABLE 15  
CALCULATED PM SENSITIVITIES

<u>CONTROL PARAMETER</u>	<u>PM SENSITIVITY</u>	<u>REGULATION FOR PM &lt; 1°</u>	<u>REMARKS</u>
CATHODE VOLTAGE	5.2 deg/%	0.2%	ACTIVE REGULATION ON DC BEAM SUPPLY
MAIN MAGNET COIL CURRENT	37 deg/%	0.03%	
WIGGLER SOLENOID COIL CURRENT	12 deg/%	0.08%	
WIGGLER BIFILAR HELIX CURRENT	23 deg/%	0.04%	FAVORS PERMANENT MAGNET WIGGLER
FILAMENT VOLTAGE (PIERCE GUN)	0.13 deg/%	7%	-
RF DRIVE (INPUT POWER)	0.35 deg/%	2%	-
INLET COOLANT TEMPERATURE (BODY)	0.66 deg/°C	1.5°C	COOLANT TEMP. REGULATION
INLET COOLANT TEMPERATURE (COLLECTOR)	1.5 deg/°C	0.6°C	
INLET COOLANT TEMPERATURE (TRANSMISSION LINE)	1.8 deg/°C	0.5°C	

Finally, the inlet coolant temperature must be regulated to within  $0.5^{\circ}\text{C}$  in the transmission line coolant loop and to within  $0.6^{\circ}\text{C}$  in the collector coolant loop. The latter requirement will be difficult to satisfy when the rf drive is switched on or off because of the volumetric flow rates required to handle up to 1 MW CW of dissipation in the collector. For example, as the rf drive is turned on, the collector dissipation suddenly drops to 600 kW and the average inlet coolant temperature will tend to fall sharply in a closed loop heat exchanger system. The practical solution is to allow for a short settling time when the rf drive is turned off or on to allow the collector coolant temperature, and therefore the phase of the output signal, to stabilize.

Mechanical tolerances in the tube and transmission line are summarized in Table 16. The body assemblies within the tube must be aligned with the magnetic axis of the solenoid within 0.2 mrad to prevent electron beam interception in the drift tunnels. This requirement is typical for present production gyrotron oscillators.

The requirement for mode purity on the other hand leads to some difficult tolerances on perpendicularity for joints in the mode filter and feed horn.<sup>24</sup> These tolerances imply that to hold the spurious mode level to -30 dBc an "optical bench" support frame will be required to quasi-optically align the transmission line components in the system. For small tilt angles, and constant waveguide diameter, the perpendicularity scales in proportion to the square root of the spurious mode level. Thus if the requirement were reduced from -30 dBc to -10 dBc, the perpendicularity tolerances would increase by a factor of ten and the optical bench would clearly not be required. At some intermediate spurious mode level, in the range -13 dBc to -20 dBc, the optical bench becomes a necessity. The tilt angle at a butt joint is zero for perfectly aligned parts. When it departs from zero at a series of N joints mode conversion occurs according to

$$P_{\text{converted}} \text{ (dBc)} = 20 \log_{10} \left[ \frac{20.77}{\pi} \frac{D\theta\sqrt{N}}{\lambda} \right]$$

TABLE 16  
MECHANICAL TOLERANCES

<u>ALIGNED ELEMENTS</u>	<u>TILT</u>	<u>PERPENDICULARITY / DIA</u>	<u>REMARKS</u>
DRIFT TUNNEL TO MAGNETIC AXIS	≤ 0.2 mrad	—	BEAM INTERCEPTION
COLLECTOR SECTION TO COLLECTOR SECTION	≤ 0.6 mrad	≤ 0.0024"/4"	-20 dBc SPURIOUS MODES
TRANS. LINE SECTION TO TRANS. LINE SECTION (BEFORE MODE FILTER)	≤ 0.9 mrad	≤ 0.0016"/1.75"	-20 dBc SPURIOUS MODES
TRANS. LINE SECTION TO TRANS. LINE SECTION (MODE FILTER AND FEED)	≤ 0.4 mrad	≤ 0.0007"/1.75"	-30 dBc SPURIOUS MODES



where  $\theta$  is the tilt angle tolerance for alignment between the axis of the parts in radians,  $D$  is the waveguide inner diameter, and  $\lambda$  is the free space wavelength. The perpendicularity,  $\Delta p$ , diameter, and tilt angle are related by

$$\theta = \frac{\Delta p}{D}$$

For a given spurious mode level, the maximum allowed tilt tolerance is

$$\theta(\text{rad}) = \frac{\Delta p}{D} = \frac{\pi}{20.77} \frac{\lambda}{D\sqrt{N}} 10^{(0.05 P_{\text{converted}} \text{ (dBc)})}$$

For the collector,  $D = 4''$ ,  $N = 5$ ,  $\lambda = 0.347''$ , and a reasonable requirement on spurious mode level is  $-20$  dBc since the mode filter can be used to reduce this level by another 10 dB to  $-30$  dBc. Similarly, in the transmission line before the mode filter,  $D = 1.75''$ ,  $N = 12$ ,  $\lambda = 0.347''$ ,  $P_{\text{converted}} = -20$  dBc. The system requirement for spurious mode level at the feed is  $-30$  dBc and within the mode filter and feed we have  $D = 1.75''$ ,  $N = 5$ ,  $\lambda = 0.347''$ ,  $P_{\text{converted}} = -30$  dBc. These parameters may be substituted into the equation for tilt tolerance, with the results shown in Table 16.

## XI. CRITICAL TECHNICAL ISSUES AND SUMMARY

The critical technical issues which were brought out in the preceding sections are, in decreasing order of technical risk,

- gyrokystron circuit stability,
- electron beam quality,
- mode purity at the antenna feed,
- window power handling.

We have outlined technical approaches for handling the problems anticipated in these areas. The problem of circuit stability will be addressed by designing for  $TE_{11}^0$  (non-overmoded) buncher resonators and an intrinsically stable output cavity, and conducting extensive hot tests to validate the design.

Poor electron beam quality can also degrade tube performance, particularly efficiency. Our approach on this facet of the tube development will be to optimize the circuit design for insensitivity to beam quality (velocity spread), optimize the gun design using a beam analyzer apparatus, and develop a back-up magnetron injection gun in the event that the Pierce gun/wiggler approach fails to provide adequate performance in hot test.

The technical risk in the area of mode purity is derived from the high degree of mode purity (-30 dBc spurious mode level) which has been specified. Meeting this specification will require optimization of collector-tapers and the mode converter, extensive hot tests of the mode filter with the tube, and the development of an "optical bench" support frame for the transmission line components. Much of the risk in this area will be eliminated if the spurious mode requirement is relaxed to a level (~-12 dBc) which would obviate development of the mode filter and optical bench.

At the present time, we have a high degree of confidence that the present gyrotron double-disc window configuration will prove satisfactory for handling 400 kW CW at 34 GHz. This configuration has been successfully

demonstrated for 340 kW CW at 28 GHz and 200 kW CW at 60 GHz and only a conservative extrapolation of the proven designs is required to achieve the goal of 400 kW CW at 34 GHz.

In conclusion, we have studied the requirements for the gyrokystron and related waveguide components for the 400 kW CW 34 GHz transmitter, and have found that both the tube and the components are technically feasible. An extensive hardware development effort will be necessary to demonstrate the required performance. The probability that this hardware will be developed on schedule and meet all the performance requirements is high if the hardware development phase is properly staffed and supported.

## XII. REFERENCES

1. R. S. Symons and H. R. Jory, "Cyclotron Resonance Devices", in Advances in Electronics and Electron Physics, Vol. 55, pp. 1-75 (1981).
2. G. Huffman, D. Boilard and D. Stone, "Power Limits for Accelerator Tubes from UHF to Ka-Band", In Proceedings of the 1984 Linear Accelerator Conference, Seeheim/Darmstadt, Federal Republic of Germany, May 7-11, 1984.
3. H. Jory, "Status of Gyrotron Developments at Varian Associates", in Proceedings of Symposium on Heating in Toroidal Plasmas, Rome, March 1984.
4. S. Hegji, H. Jory and J. Shively, "Development Program for a 200 kW CW 28 GHz Gyroklystron", Quarterly Report No. 6, Union Carbide Contract No. 53X01617C, Varian Associates, July - September 1977.
5. M. Caplan, "Gain Characteristic of Staggered-Tuned Multi-Cavity Gyroklystron Amplifiers", 8th International Conference on Infrared and Millimeter Waves (1983) W4.2.
6. K. Spangenberg, Vacuum Tubes, McGraw-Hill Book Company, Page 300-310 (1948).
7. K. Spang et. al., "High Power Linear Beam Tubes Proceedings of the I.E.E.E., Vol. 61, March 1973.
8. G. S. Nusinovich, "Mode Interaction in Gyrotrons", Int. J. Elec. 51 (4) 457, Oct. 1981.
9. Dr. Bruce Danly MIT, Private Communication.
10. Dr. Hulbert Hsuan PPPL - Private Communication.
11. M. Caplan, A. T. Lin, K. R. Chu, "A Study of the Saturated Output of a  $TE_{01}$  Gyrotron using an Electromagnetic Finite Size Particle Code", International Journal of Electronics Vol. 53, No. 6, Dec. 1982.
12. C. Moeller, "Mode Converters Used in the Doublet ECH Microwave System" International Journal of Electronics Vol. 53, No. 6, Dec. 1982.
13. L. Solyman, "Spurious Mode Generation in Non-Uniform Waveguide", IRE Transactions on Microwave Theory and Techniques (1959).
14. F. Sporleder and H. G. Unger, Waveguide Tapers, Transitions, and Couplers, Institution of Electrical Engineers, London, 1979, Chapter 2.
15. H. G. Unger, "Circular Waveguide Taper of Improved Design", Bell System Technical Journal, July 1958.

16. H. Jory, et. a., "60 GHz Gyrotron Development Program" Quarterly Report No. 20, April through June 1984, report prepared by Varian Associates, Inc., under Subcontract Purchase Order No. 53Y-21453C for Oak Ridge National Laboratory.
17. S. E. Miller, "Coupled Wave Theory and Waveguide Applications", The Bell System Technical Journal, May 1954.
18. R. E., Collin, Foundations for Microwave Engineering, McGraw Hill, Inc., New York, 1966, pp. 270-282.
19. G. Janzen, H. Stickel, "Mode Selective Directional Couplers in Overmoded Circular Waveguides", IEEE Int. Conf. on Infrared and Millimeter Waves, Miami Beach, FL, 1983 TH 4.6.
20. S. P. Morgan, and J. A. Young, "Helix Waveguide," The Bell System Technical Journal, Nov. 1956.
21. M. Abramowitz and I. A. Stegun, Handbook of Mathematical Function with Formulas, Graphs, and Mathematical Tables, Dover Publications, New York, 1968. pp. 358-365.
22. R. W. B. Ardill, and K. J. M. Moriarty, "Accurate Bessel Functions in  $J_n(Z)$ ,  $Y_n(Z)$ ,  $H_n^{(1)}(Z)$ , and  $H_n^{(2)}(Z)$  of Integer Order and Complex Argument," Computer Physics Communications, North Holland Publishing Co. 17 (1979), pp. 321-336.
23. H. G. Unger, "Helix Waveguide Theory and Application", The Bell System Technical Journal, Nov. 1958.
24. J. P. Quine, "Oversize Tubular Metallic Waveguide", Microwave Power Engineering, ed. E. C. Okress Academic Press, New York, 1968.

APPENDIX A  
INJECTION LOCKED GYROTRON OSCILLATOR

During the study, we were asked to consider the possibility of using an injection locked gyrotron oscillator rather than a gyrokystron amplifier in the JPL application. After some investigation, we concluded that a locked oscillator would have insurmountable performance problems related to inadequate frequency and phase control, and some of the ancillary hardware needed for running a locked oscillator also requires high risk technology development. A summary of our investigation of the locked oscillator scheme is given here.

The phenomenon of injection locking a free-running oscillator by an external signal of nearly the same frequency has been applied to a variety of oscillators, including vacuum tube oscillators and solid state oscillators. The concept can be understood from the basic forced simple harmonic oscillator. If the injected frequency is sufficiently close to the natural frequency and if the coupling between the two sources is strong enough, frequency and phase locking takes place. The possibility of applying the concept to an injection lock gyrotron oscillator will be examined. An estimated performance will be compared to the gyrokystron amplifier requirements.

Some theoretical work on injection locked gyrotrons has been done in the Soviet Union. However, no familiarity with their theory or experimental results are available.

A. BASIC THEORY OF INJECTION LOCKED OSCILLATORS

The fundamentals of injection locked oscillators are based on the forced harmonic oscillator problem. Assuming that the oscillator is locked or in synchronism with an external driver, the phase difference between the output and the external driver in steady-state is

$$\sin \psi \sim \frac{\omega_1 - \omega'}{P_{inj}}$$

where

$\omega_1$  is the free-running oscillator frequency

$\omega'$  is the injection frequency

and  $P_{inj}$  is the injected power level.

Thus, as the injected power level is increased, the phase difference is reduced. Note that modulating the injected power would modulate the output phase. To reach the steady-state, a synchronization time is required:

$$\tau = \frac{1}{\left[ (K_1 P_{inj})^2 - (\omega_1 - \omega')^2 \right]^{1/2}}$$

where  $K_1$  is a constant. If synchronization does not take place, a modulation of the amplitude can be seen with period

$$\tau_m = \frac{1}{\left[ (\omega_1 - \omega')^2 - (K_1 - P_{inj})^2 \right]^{1/2}}$$

The synchronizing band  $\Delta\omega$  is proportional to the injected power, assuming that the power is over the threshold for synchronization. Typical minimum injected power levels for magnetron oscillators are -20 to -30 dB below the free-running magnetron output power level. The threshold power level for an injection locked gyrotron oscillator would be about the same as an injection locked magnetron oscillator.

#### B. EXAMPLE OF AN INJECTION LOCKED MAGNETRON

Figure 1-A depicts the setup for a magnetron injection lock experiment. The magnetron tube has a rated maximum output power of 1 MW at a frequency of 3.2 GHz for a pulse duration of 10  $\mu$ s. The external driver consists of a voltage controlled oscillator and a TWT amplifier with a maximum output of 100 watts. The circulator had a 0.5 dB insertion loss. The final output of the injection locked signal was limited to 100 kW. Increased power showed no evidence of locking. Also, in order to resolve the narrow bandwidth, a

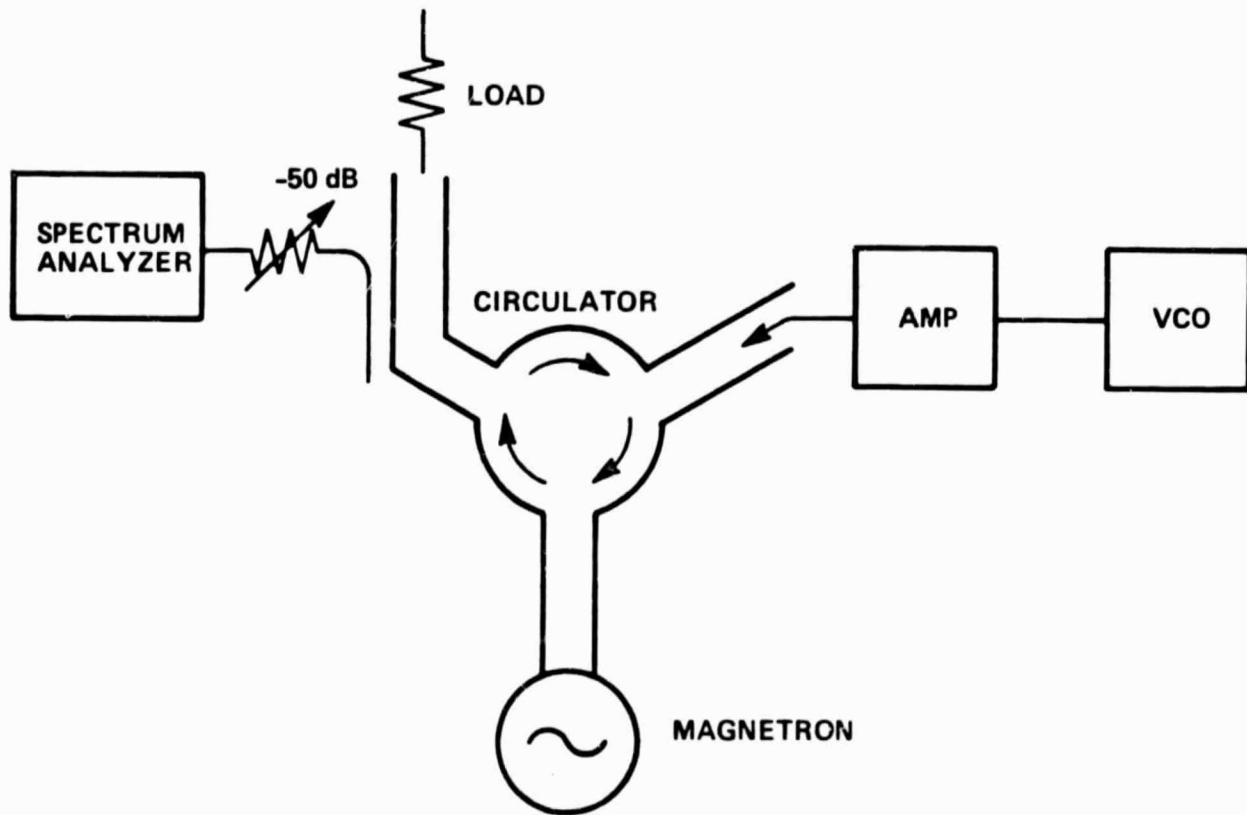


FIGURE 1-A. MAGNETRON INJECTION LOCK EXPERIMENT



longer pulse width of 35  $\mu$ s was required. The modulator pulse width was a limiting factor. The bandwidth was  $\Delta\omega/\omega_0 = 2.5 \times 10^{-5}$  with a maximum gain of 30 dB. This confirms a typical minimum injected power of about -30 dB for the magnetron oscillator. The widest bandwidth of an injection locked magnetron is typically equal to the frequency pushing range due to electron beam loading. Assuming that the same is true for gyrotron oscillators, the yield would be a maximum bandwidth of 0.1% for the 60 GHz gyrotron.

The operation of a long pulse or CW gyrotron oscillator usually takes place in the high efficiency (>40%) regime where a mode-locking effect of the free-running oscillator already takes place. To force the gyrotron out of its natural mode-lock in this regime might require an additional amount of injected power. This might result in a very narrow ( $\ll$  0.1%) bandwidth. Operation of the gyrotron in the low efficiency (<20%) regime may yield the desired 0.1% bandwidth.

### C. INJECTION LOCKED GYROTRON OSCILLATOR CONFIGURATIONS

#### Configuration A

A schematic of an injection locked 34 GHz, 400 kW CW gyrotron oscillator is shown in Figure 2-A. In this configuration, the driver is injected through the output window. Assuming that the window has the bandwidth and can withstand the additional power, additional technical problems arise. An overmoded waveguide directional coupler with about -10 dB coupling is required. The directional coupler sidearm must couple and propagate 40 kW. A 40 kW termination on the sidearm is required. Assuming that an injected power of about -26 dB (optimistic) is required for locking (and bandwidth), it necessitates having a 10 kW injection oscillator at 34 GHz. Finally, a 40 kW circulator would be required. Increasing the directional coupler coupling would require a larger circulator. Decreasing the directional coupler coupling would increase the injection oscillator power requirement. Each component, aside from the 34 GHz, 400 kW CW gyrotron is either at the state of the art or would require an extensive development effort. Clearly, Configuration A is not a viable option.

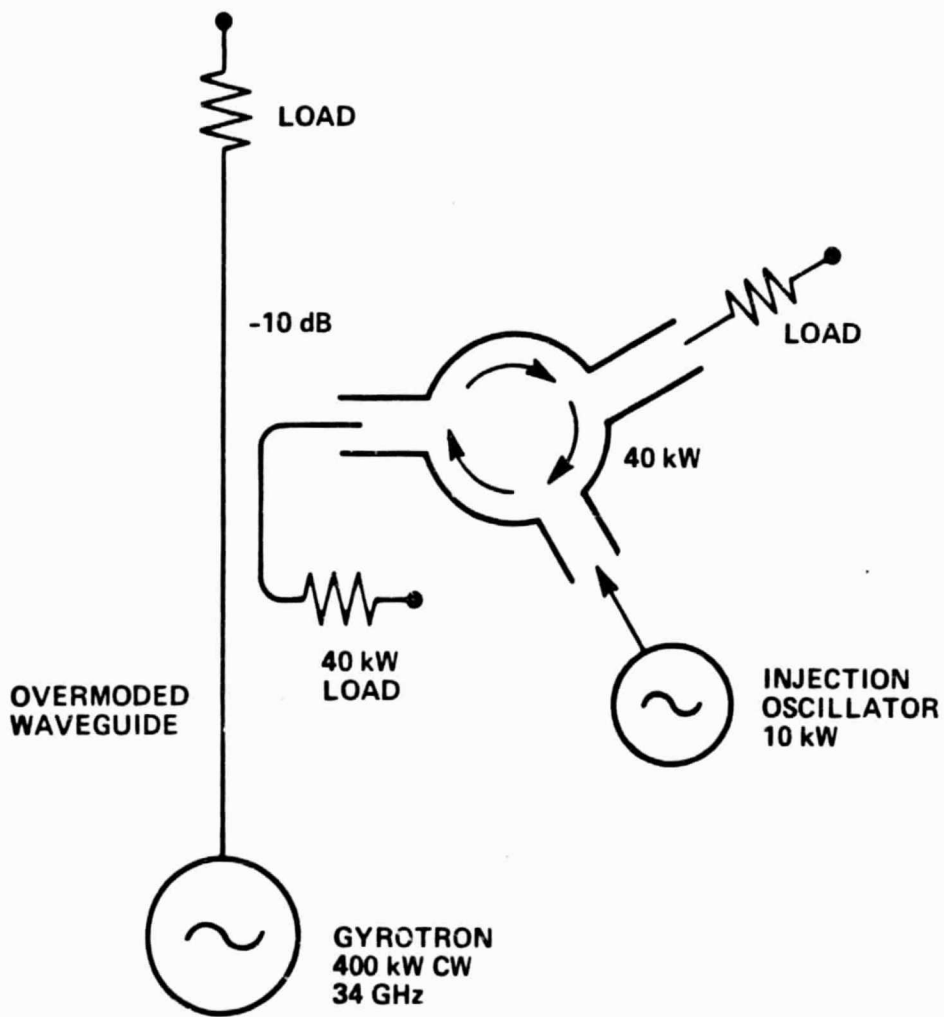


FIGURE 2-A. INJECTION LOCKED GYROTRON OSCILLATOR, CONFIGURATION A

### Configuration B

An improved configuration for an injection locked gyrotron might be a quasi-gyroklystron configuration. Figure 3-A depicts a single cavity excited oscillator. By accessing the gyrotron cavity in the proper mode, a highly overmoded waveguide directional coupler is avoided. The injection power requirement would still be fairly high, about 10 kw. However, coupling along the back end of the cavity would reduce the power leakage out, which reduces the circulator power requirement. There is also a reduction of the main output window requirements. This type of configuration would require development of an aperture hole coupling technique that would not seriously perturb the oscillator. Cavity cooling and cavity interaction problems must be studied. Bandwidth might still be too narrow in this configuration. A change in the cavity mode from a  $TE_{0n1}$  circular mode to a  $TE_{121}$  circular mode would simplify the cavity coupling problem. However, this would not allow one to use existing electron guns.

### Configuration C

A further improvement of the injection locked scheme is a two-cavity gyroklystron "oscillator" as shown in Figure 4-A. By using a precavity, the total injected power requirement would be reduced significantly by improving the input match. Also, the bandwidth could be improved by stagger tuning the precavity and output cavity resonances. This configuration, however, is tantamount to developing a gyroklystron amplifier.

### C. FINAL CONFIGURATION

The gyroklystron amplifier as shown in Figure 5-A has several advantages. The use of multiple cavities would increase the bandwidth significantly. A gyroklystron amplifier does not have the "synchronizing" threshold requirement, and can support multiple modulating frequencies. Components, such as the overmoded waveguide coupler and a high power circulator, are eliminated. Power requirements for the driver are drastically reduced.

In conclusion, the well designed locked gyrotron oscillator configuration is actually a gyroklystron.

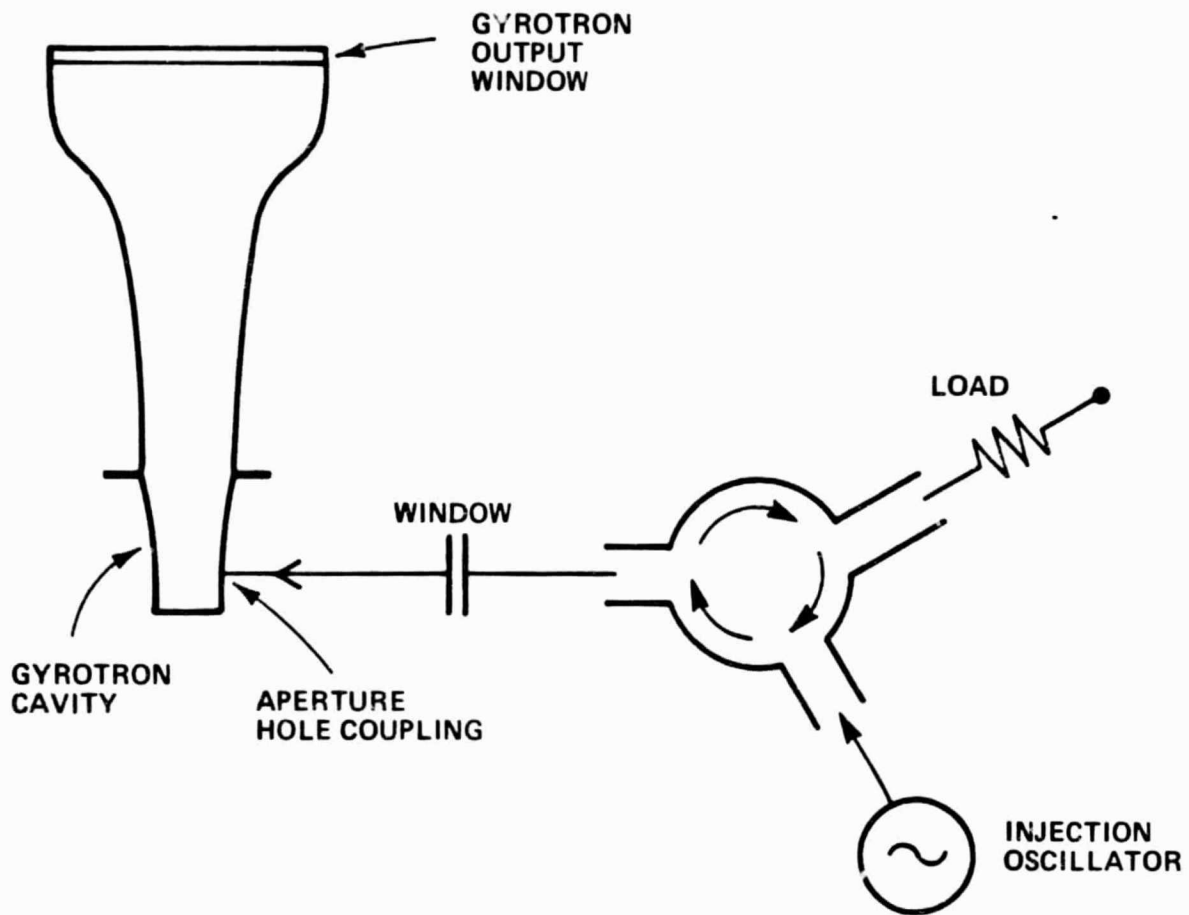


FIGURE 3-A. QUASI GYROKLYSTRON, CONFIGURATION B

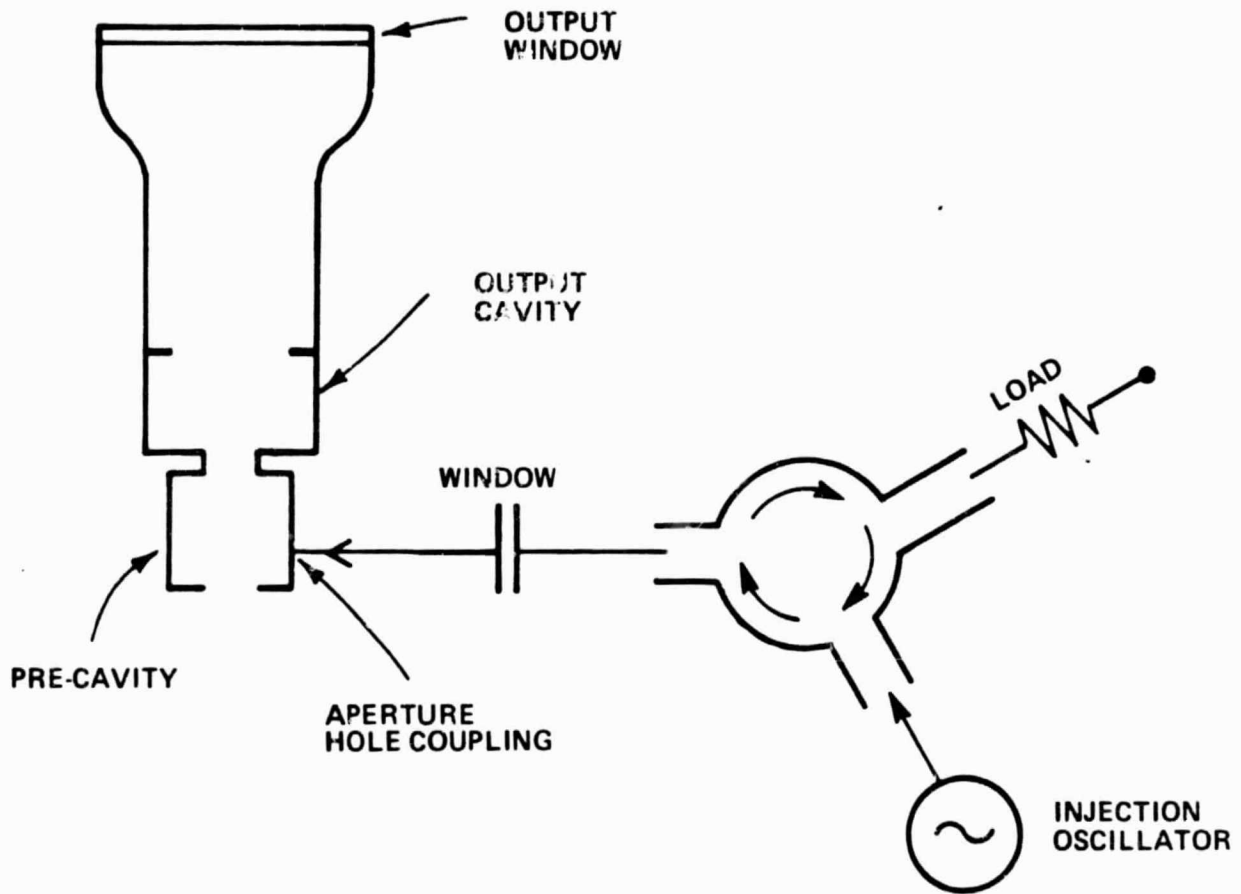


FIGURE 4-A. GYROTON "OSCILLATOR", CONFIGURATION C

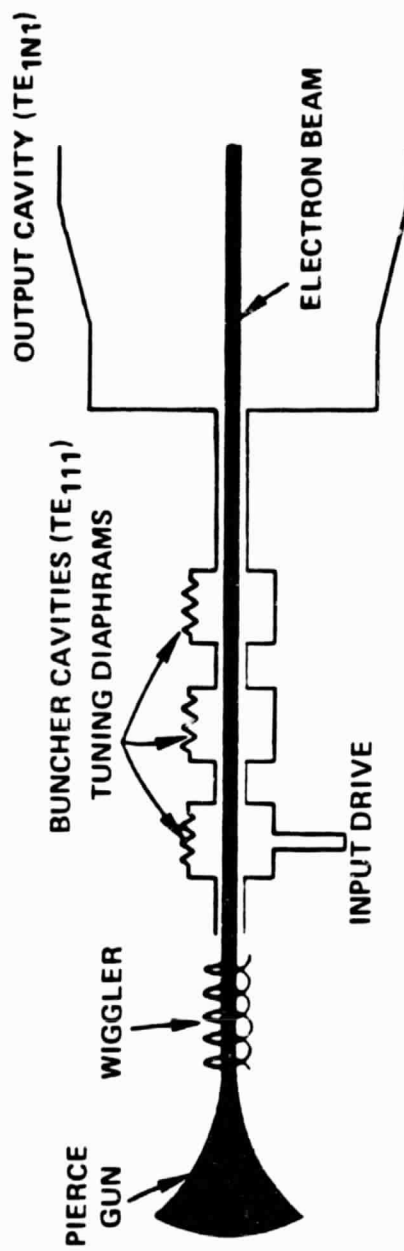


FIGURE 5-A. SCHEMATIC OF PROPOSED GYROKLYSTRON CONFIGURATION

## APPENDIX B

The following computer program was developed for a first-cut design of the directional coupler. It was written for a Tektronix 4050 desk top computer.

```
100 PAGE
110 PRINT "This Program is for use in the design of linearly tapered"
120 PRINT "directional couplers. The design is as follows: there is"
130 PRINT "a rectangular waveguide attached to a circular waveguide"
140 PRINT "along the narrow edge of the rectangular waveguide."
150 PRINT "All of the lengths are in inches and frequency in GHz"
160 PRINT
170 PRINT "What is the center frequency of the device?"
180 INPUT FO
190 FO=FO*1.0E+9
200 C1=1.18E+10
210 W=C1/FO
220 PRINT "What is the radius of the circular waveguide?"
230 INPUT R
240 PRINT "What is the primary mode?"
250 INPUT M$
260 PRINT "What bessel root does this correspond to?"
270 INPUT P1
280 P2=P1
290 P=P1
300 A=PI*R/P1
310 PRINT "What m value does this correspond to?"
320 INPUT M1
330 M2=M1
331 IF M1=0 THEN 335
332 E1=SQR(2)
333 E2=E1
334 GO TO 340
335 E1=1
336 E2=E1
```

```

340   U$="TE 10"
370   O=1
380   PRINT "The appropriate value for the long edge of the rectangular"
390   PRINT "is ";A
400   PRINT "What would you like the short edge of the waveguide to be?"
410   INPUT B
440   PRINT "What is the diameter of the coupling holes?"
450   INPUT D
460   PRINT "What do you want the hole spacing to be?"
470   INPUT Z0
480   W=W/(1-(W*PI/2/PI/R)+2)+0.5
490   U=INT((Z0-W/4)*2/W)
500   Z1=U*W/2+W/4
510   Z2=(U+1)*W/2+W/4
520   PRINT "Do you want Z0 to be ";Z1;" or ";Z2
530   INPUT U
540   IF U=1 THEN 570
550   Z0=Z2
560   GO TO 580
570   Z0=Z1
580   W=C1/F0
590   PRINT "Do you want to change the 1) frequency or the 2) length?"
600   INPUT K
610   IF K=1 THEN 700
620   PRINT "What is the starting length?"
630   INPUT L1
640   X1=L1
650   PRINT "What is the ending length?"
660   INPUT L2
670   X2=L2
680   Q=1
690   GO TO 870
700   PRINT "What is the starting frequency?"
710   INPUT L1
720   X1=L1
730   L1=L1*1.0E+9

```



```

740 PRINT "What is the ending frequency?"
750 INPUT L2
760 X2=L2
770 L2=L2*1.0E+9
780 Q=1.0E+9
790 PRINT "What length do you want?"
800 INPUT L
810 P=P1
820 M=M1
825 E0=E1
830 GOSUB 1860
840 C3=C
850 PRINT "The Coupling for this is ";C
860 GO TO 870
870 PRINT "Do you want to graph 1)discrimination or 2)directivity?"
880 INPUT G
890 IF G=2 THEN 970
900 PRINT "What is the mode that you are investigating?"
910 INPUT N$
920 PRINT "What is the corresponding bessel root?"
930 INPUT P2
940 P=P2
950 PRINT "What is the corresponding m value?"
960 INPUT M2
961 IF M2=0 THEN 965
963 E2=SQR(2)
964 GO TO 966
965 E2=1
966 E0=E2
967 M=M2
970 PRINT "What is the maximum dB that you want to graph?"
980 INPUT J
990 PRINT "What is the minimum dB that you want to graph?"
- 1000 INPUT V
1010 PRINT "What is the spacing on the x axis?"
1020 INPUT X8

```

```
1030 PRINT "What is the spacing on the y axis?"
1040 INPUT X9
1050 X8=X8*Q
1060 PAGE
1070 VIEWPORT 10,125,10,95
1080 WINDOW L1,L2,V,J
1090 AXIS X8,X9,L1,V
1100 MOVE 0,0
1110 FOR I=0 TO 99
1120 P=P2
1121 M=M2
1122 EO=E2
1130 GOSUB 1480
1140 DRAW X,Y
1150 NEXT I
1160 VIEWPORT 0,130,0,100
1170 WINDOW 0,130,0,100
1180 MOVE 3,50
1190 PRINT "dB"
1200 MOVE 8,7
1210 PRINT X1
1220 MOVE 123,7
1230 PRINT X2
1240 MOVE 6,10
1250 PRINT 0
1260 MOVE 3,93
1270 PRINT J
1280 IF K=1 THEN 1320
1290 MOVE 50,7
1300 PRINT "Length in inches"
1304 MOVE 5,96
1305 PRINT "The rectangular mode is ";U$
1310 GO TO 1390
1320 MOVE 50,7
1330 PRINT "Frequency in GHz"
1340 MOVE 5,96
```

```

1350 PRINT "Coupling for ";M$;"=";C3;" at f0, rectangular mode is ";V$
1360 MOVE 105,99
1370 PRINT "length=";L
1380 MOVE 40,96
1390 IF G=1 THEN 1430
1400 MOVE 5,99
1410 PRINT "Directivity ";M$
1420 GO TO 1450
1430 MOVE 5,99
1440 PRINT "Selectivity: main mode ";M$;", spurious mode ";N$
1450 MOVE 10,1
1460 PRINT "R=";R;" A=";A;" B=";B;" D=";D;" Z0=";Z0;" F0=";F0
1470 END
1480 IF K=1 THEN 1530
1490 L=(L2-L1)/100*I+L1
1500 X=L
1510 F=F0
1520 GO TO 1550
1530 F=(L2-L1)/100*I+L1
1540 X=F
1550 W=C1/F
1560 GOSUB 1800
1570 IF G=1 THEN 1600
1580 GOSUB 1830
1590 GO TO 1780
1600 P=P1
1610 M=M1
1615 EC=E1
1620 GOSUB 1860
1630 S=PI*L*(1/W1-1/W2)
1640 S=(S/2/SIN(S/2))2
1650 S=C2*S
1660 GOSUB 1830
1670 S=S*(1+1/Y)
1680 P=P2
1690 M=M2

```

```

1695  E0=E2
1700  GOSUB 1860
1710  S=S/C2
1720  P=P1
1730  GOSUB 1800
1740  GOSUB 1830
1750  S=S/(1+1/Y)
1760  Y=S
1770  M=M2
1780  Y=20*LGT(Y)
1790  RETURN
1800  W1=W/(1-(P*W/2/PI/R) ^2) ^0.5
1810  W2=W/(1-(W/2/A) ^2) ^0.5
1820  RETURN
1830  Y=PI*L*(1/W1+1/W2)
1840  Y=(Y/2/SIN(Y/2)) ^2
1850  RETURN
1860  C=1/(24*SQR(2*PI)*Z0*A*SQR(A*B)*R*R)
1870  C=C*D*D*D*W*L
1880  C=C*O
1885  C=C*O*EO
1890  C=C/((1-(P*W/2/PI/R) ^2)*(1-(W*O/2/A) ^2)) ^0.25
1900  C=C*P/SQR(1-M*M/(P*P))
1910  C2=C
1920  C=20*LGT(C)
1930  RETURN

```

APPENDIX C  
DETAILS OF SENSITIVITY CALCULATIONS

1. BEAM VOLTAGE SENSITIVITIES

From Figure 25, with  $V_{ko} = 77.7$  kV,

$$\frac{\Delta \text{power}}{\Delta V_k} = \frac{10 \log_{10}(350/440) \text{ dB}}{\left(\frac{77.7 - 76}{77.7}\right) 100\%} = \frac{0.994 \text{ dB}}{2.188\%} = 0.45 \text{ dB/\%}$$

From Figure 25, with  $V_{ko} = 77.5$  kV,

$$\frac{\Delta \text{phase}}{\Delta V_k} = \frac{312^\circ - 302^\circ}{\left(\frac{79 - 77.5}{77.5}\right) 100\%} = \frac{10^\circ}{1.94\%} = 5.15^\circ/\%$$

2. MAIN COIL CURRENT SENSITIVITIES

From Figure 27, with  $B_{\text{circuit}}^0 = 12.61$  kG,

$$\frac{\Delta \text{power}}{\Delta B_{\text{circuit}}} = \frac{10 \log_{10}(412/446) \text{ dB}}{\left(\frac{12.77 - 12.61}{12.61}\right) 100\%} = \frac{0.344 \text{ dB}}{1.269\%} = 0.271 \text{ dB/\%}$$

$$\frac{\Delta \text{phase}}{\Delta B_{\text{circuit}}} = \frac{0^\circ - (-100^\circ)}{\left(\frac{12.73 - 12.61}{12.61}\right) 100\%} = \frac{100^\circ}{0.952\%} = 105^\circ$$

From simulation of coil geometry given in Figure 17, for a 1% decrease in current in the middle main coil, the calculated average decrease in magnetic field in the circuit region is 0.353%,

$$\frac{B_{\text{circuit}}}{\Delta I_{\text{main coil}}} = 0.353 \text{ \%/}$$

Thus

$$\frac{\Delta \text{power}}{\Delta I_{\text{main coil}}} = (0.271 \text{ dB}/\%) (0.353 \text{ } \%/ \%) = 0.0957 \text{ dB}/\%$$

$$\frac{\Delta \text{phase}}{\Delta I_{\text{main coil}}} = (105^\circ/\%) (0.353 \text{ } \%/ \%) = 37.1^\circ/\%$$

### 3. WIGGLER SOLENOID COIL CURRENT SENSITIVITIES

From Figure 28, with  $B_{\text{z wig}}^0 = 1738.8 \text{ g}$ ,

$$\frac{\Delta \text{power}}{\Delta B_{\text{z wig}}} = \frac{10 \log_{10}(265/430) \text{ dB}}{\left(\frac{1738.8 - 1722.7}{1738.8}\right) 100\%} = \frac{2.10 \text{ dB}}{0.93\%} = 2.26 \text{ dB}/\%$$

$$\frac{\Delta \text{phase}}{\Delta B_{\text{z wig}}} = \frac{-80^\circ - (-135^\circ)}{\left(\frac{1738.8 - 1722.7}{1738.8}\right) 100\%} = \frac{55^\circ}{0.93\%} = 59.1^\circ/\%$$

From simulation of coil geometry given in Figure 17, for a 1% decrease in current in the second wiggler solenoid coil (the third coil above the gun coil), the calculated average decrease in magnetic field in the wiggler region is 0.20%.

$$\frac{\Delta B_{\text{z wig}}}{\Delta I_{\text{z wig}}} = 0.20\%/ \%$$

Thus,

$$\frac{\Delta \text{power}}{\Delta I_{\text{z wig}}} = (2.26 \text{ dB}/\%) (0.20\%/ \%) = 0.452 \text{ dB}/\%$$

$$\frac{\Delta \text{phase}}{\Delta I_{\text{z wig}}} = (59.1^\circ/\%) (0.20 \text{ } \%/ \%) = 11.8^\circ/\%$$

#### 4. WIGGLER BIFILAR HELIX CURRENT SENSITIVITIES

From Figure 28, with  $B_{\text{Twig}}^0 = 19.1 \text{ g}$ ,

$$\frac{\Delta \text{power}}{\Delta B_{\text{Twig}}} = \frac{10 \log_{10} (350/430) \text{ dB}}{\left( \frac{18.85 - 19.1}{19.1} \right) 100\%} = \frac{0.894 \text{ dB}}{1.3\%} = 0.688 \text{ dB/\%}$$

$$\frac{\Delta \text{phase}}{\Delta B_{\text{Twig}}} = \frac{-80^\circ - (-110^\circ)}{\left( \frac{18.85 - 19.1}{19.1} \right) 100\%} = \frac{30^\circ}{1.3\%} = 23^\circ/\%$$

Since the bifilar helix is formed as a single electromagnet coil we have,

$$\frac{\Delta B_{\text{Twig}}}{\Delta I_{\text{helix}}} = 1.0 \text{ \%/}$$

Thus,

$$\frac{\Delta \text{power}}{\Delta I_{\text{helix}}} = (0.688 \text{ dB/\%}) (1.0 \text{ \%/}) = 0.688 \text{ dB/\%},$$

$$\frac{\Delta \text{phase}}{\Delta I_{\text{helix}}} = (23^\circ/\%) (1.0 \text{ \%/}) = 23^\circ/\%$$

#### 5. GUN COIL CURRENT SENSITIVITIES

From Figure 32, if we assume that a realistic tube design operates with  $\Delta v_{\parallel}^0/v_{\parallel} = 5\%$ , interpolating between the curves for  $\Delta v_{\parallel}/v_{\parallel} = 5\%$  and  $\Delta v_{\parallel}/v_{\parallel} = 10\%$ , we find the AM sensitivity to velocity spread,

$$\frac{\Delta \text{power}}{\Delta (\Delta v_{\parallel}/v_{\parallel})} = \frac{10 \log_{10} (300/325) \text{ dB}}{\left( \frac{6 - 5}{5} \right) 100\%} = \frac{0.348 \text{ dB}}{20\%} = 0.0174 \text{ dB/\%}$$

From Figure 9, for 2% beam ripple, the velocity spread rises from 5% to 7% when the M number drops from 4 to 3,

$$\frac{\Delta(\Delta v_{||}/v_{||})}{\Delta M} = \frac{\left(\frac{7-5}{5}\right) 100\%}{\left(\frac{4-3}{4}\right) 100\%} = \frac{40\%}{25\%} = 1.6 \%/%$$

Flux conservation in the beam formation region requires that

$$\pi r_k^2 B_k = \pi r_{wig}^2 B_{zwig} \sqrt{1 - 1/M^2}$$

where  $r_k$  is the cathode radius,  $B_k$  is the magnetic field at the cathode,  $r_{wig}$  is the beam radius in the wiggler drift tube, and  $B_{zwig}$  is the axial wiggler field. Thus, with other parameters fixed

$$B_k \sim \sqrt{1 - 1/M^2}$$

and at the operating point, with  $B_k = 250.3$  g and  $M = 4$ ,

$$\frac{\Delta M}{\Delta B_k} = \frac{\left(\frac{4-3}{4}\right) 100\%}{\left(\frac{250.3 - 243.7}{250.3}\right) 100\%} = \frac{25\%}{2.64\%} = 9.47 \%/%$$

In a typical solenoid configuration for a Ka Band gyro TWT with a Pierce gun/wiggler, the gun coil alone provides a magnetic field on axis at the cathode of 40g - 80g. The computed variation of the total magnetic field at the cathode due to this gun coil variation is 190g - 200g. Thus,

$$\frac{\Delta B_k}{\Delta B_{gc}} = \frac{\left(\frac{200 - 190}{200}\right) 100\%}{\left(\frac{80 - 40}{40}\right) 100\%} = \frac{5\%}{100\%} = 0.05 \%/%$$

Since the iron in the solenoid polepieces is not saturated in these designs, the gun coil field is linear with gun coil current,

$$\frac{\Delta B_{gc}}{\Delta I_{gc}} = 1.0 \%/%$$

Finally, we find the gun coil current AM sensitivity,



$$\frac{\Delta \text{power}}{\Delta I_{gc}} = (0.0174 \text{ dB/\%}) (1.6 \text{ \%/}) (9.47 \text{ \%/}) (0.05 \text{ \%/}) (1.0 \text{ \%/})$$

$$= 0.0132 \text{ dB/\%}$$

The PM sensitivity is calculated in a similar manner and requires a computer calculation of the PM sensitivity with respect to velocity spread. Although this particular calculation was not done during the study because of the limitations of time, the low value of AM sensitivity implies that the phase will also be relatively insensitive to gun coil current variations.

#### 6. FILAMENT VOLTAGE (PIERCE GUN) SENSITIVITIES

From Figure 26, with  $I_k^0 = 12.5 \text{ A}$ ,

$$\frac{\Delta \text{power}}{\Delta I_k} = \frac{10 \log_{10}(390/430) \text{ dB}}{\left(\frac{12.5 - 12}{12.5}\right) 100\%} = \frac{0.424 \text{ dB}}{4\%} = 0.106 \text{ dB/\%}$$

$$\frac{\Delta \text{phase}}{\Delta I_k} = \frac{-79.5^\circ - (-73^\circ)}{\left(\frac{12.5 - 12}{12.5}\right) 100\%} = \frac{6.5^\circ}{4\%} = 1.625 \text{ }^\circ/\%$$

In a typical "roll off" curve for a Pierce gun used on a 95 GHz gyro TWT (Varian model number VGT-8195A), the beam current varies with filament voltage as,

$$\frac{\Delta I_k}{\Delta V_f} = \frac{\left(\frac{4.10 - 3.93}{4.10}\right) 100\%}{\left(\frac{10 - 5}{10}\right) 100\%} = \frac{4.15\%}{50\%} = 0.083 \text{ \%/}$$

Thus,

$$\frac{\Delta \text{power}}{\Delta V_f} = (0.106 \text{ dB/\%}) (0.083 \text{ \%/}) = 0.0088 \text{ dB/\%}$$

$$\frac{\Delta \text{phase}}{\Delta V_f} = (1.625 \text{ }^\circ/\%) (0.083 \text{ \%/}) = 0.13 \text{ }^\circ/\%$$

## 7. LOAD VSWR SENSITIVITIES

The calculation of AM sensitivity to load VSWR is presented in Figure 29. Since load mismatch affects the rf field amplitude in the output cavity, a calculation of phase with respect to rf field amplitude is required to determine the PM sensitivity to load mismatch. This calculation was not done during the study for reasons of time limitations but the approximate size of the phase variation is suggested by the calculation of phase modulation with respect to rf drive (see Figure 1-C).

## 8. RF DRIVE (INPUT POWER) SENSITIVITIES

From Figure 24, with  $f = 34.020$ ,

$$\frac{\Delta_{\text{power}}}{\Delta_{\text{drive}}} = \frac{10 \log_{10} (400/435) \text{ dB}}{\left( \frac{5 - 2.5}{5} \right) 100\%} = \frac{0.364 \text{ dB}}{50\%} = 0.0073 \text{ dB/\%}$$

A special calculation of phase vs drive power at saturation was carried out using a different code than was used to calculate saturated amplitude and linear phase effects in Section IV. The results already presented in Section IV, of course, include large signal effects with the proper cavity Q's but with the rf field profiles of idealized right circular cylindrical cavities. For the nonlinear phase calculation a more detailed analysis is required, including the effects of the tapered output cavity walls and residual beam-wave interaction in the throat of the output taper.

For the same circuit parameters used in Section IV, we ran the nonlinear phase code with the results shown in Figure 1-C. While the saturated power output is 100 kW instead of the 400 kW previously calculated, this discrepancy is due to the fact that in a thorough design effort, once the subtle details of the output cavity geometry are included, the circuit design must be iterated to recover the intrinsic power output (400 kW) and efficiency for JPL gyrokystron configuration. Nevertheless, the nonlinear phase sensitivity results given in Figure 1-C are qualitatively correct for the 400 kW performance. The nonlinear phase

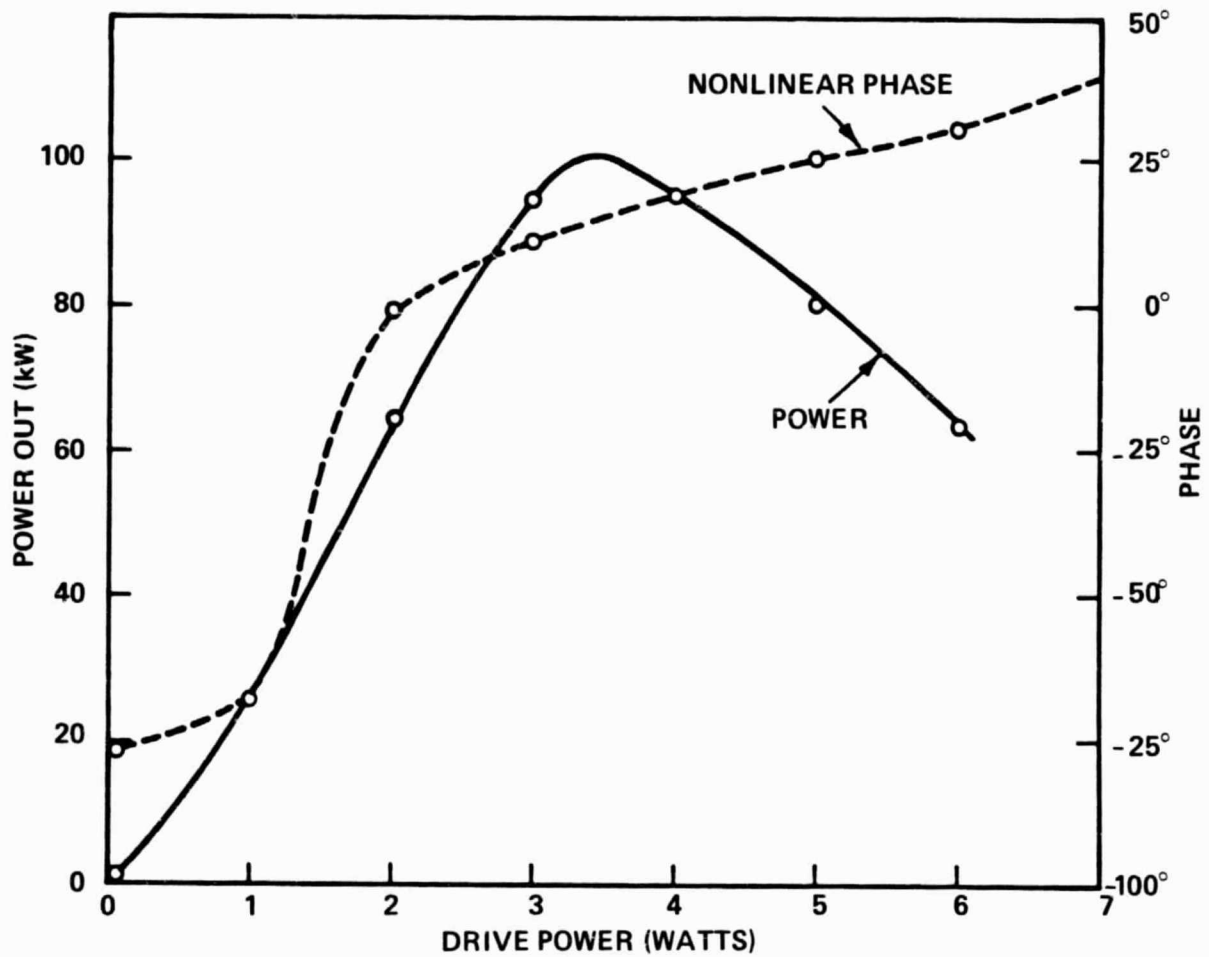


FIGURE 1-C. NONLINEAR PHASE VS DRIVE LEVEL

modulation sensitivity is taken from Figure 1-C at the peak of the power saturation curve,

$$\frac{\Delta \text{phase}}{\Delta \text{drive}} = \frac{(20^\circ - 15^\circ)}{\left(\frac{4 - 3.5}{3.5}\right) 100\%} = \frac{5^\circ}{14.29\%} = 0.350^\circ/\%.$$

#### 9. INLET COOLANT TEMPERATURE (BODY) SENSITIVITIES

Saturated power output and linear phase were calculated as a function of systematic variation in all cold cavity resonant frequencies. The results of the calculation are qualitatively similar to the results given in Figure 27 for circuit magnetic field. This is expected because the rf interaction depends critically on the difference between the circuit magnetic field and the rf frequency. For a 25 percent variation in all cold cavity frequencies we have calculated,

$$\frac{\Delta \text{power}}{\Delta f_{\text{cold}}} = \frac{4.29 \text{ dB}}{0.25 \%} = 1.72 \text{ dB}/\%$$

$$\frac{\Delta \text{phase}}{\Delta f_{\text{cold}}} = \frac{85^\circ}{0.25 \%} = 340^\circ/\%$$

The cold cavity frequencies are inversely proportional to cavity radius,  $R_{\text{cav}}$ , and relatively insensitive to cavity length,

$$\frac{\Delta f_{\text{cold}}}{\Delta R_{\text{cav}}} = 1.0 \%/ \%$$

The coefficient of thermal expansion of the cavity material, OFHC copper, is

$$\frac{\Delta R_{\text{cav}}}{\Delta T} = 1.95 \times 10^{-3} \%/^\circ\text{C}$$

Thus

$$\begin{aligned}\frac{\Delta \text{power}}{\Delta T} &= (1.72 \text{ dB/\%}) (1.0 \text{ \%/\%}) (1.95 \times 10^{-3} \text{ \%}/^{\circ}\text{C}) \\ &= (0.0034 \text{ dB}/^{\circ}\text{C})\end{aligned}$$

$$\begin{aligned}\frac{\Delta \text{phase}}{\Delta T} &= (340 \text{ }^{\circ}/\%) (1.0 \text{ \%/\%}) (1.95 \times 10^{-3} \text{ \%}/^{\circ}\text{C}) \\ &= 0.663 \text{ }^{\circ}/^{\circ}\text{C}\end{aligned}$$

#### 11. INLET COOLANT TEMPERATURE (COLLECTOR AND TRANSMISSION LINE) SENSITIVITIES

No beam-wave interaction occurs in the collector or transmission line. Therefore, only the phase of the signal can be affected in these regions. Phase variation will occur if the lengths of these sections change due to thermal expansion or contraction according to,

$$\Delta \text{phase (}^{\circ}\text{)} = 360 \frac{L}{\lambda_g} \cdot \frac{\Delta L}{L}$$

For OFHC copper we have

$$\frac{\Delta L/L}{\Delta T} = 1.95 \times 10^{-5} /^{\circ}\text{C}$$

Thus

$$\frac{\Delta \text{phase}}{\Delta T} = 360^{\circ} (1.95 \times 10^{-5} /^{\circ}\text{C}) \left( \frac{L}{\lambda_g} \right), \text{ }^{\circ}/^{\circ}\text{C}$$

For the collector, using  $L = 72''$  and  $\lambda_g (34 \text{ GHz}) = 0.347''$ ,

$$\frac{\Delta \text{phase}}{\Delta T} = 360 (1.95 \times 10^{-5}) (72/0.347) = 1.45 \text{ }^{\circ}/^{\circ}\text{C}$$

For the transmission line, using  $L = 89''$  and  $\lambda_g (34 \text{ GHz}) = 0.349''$ ,

$$\frac{\Delta \text{phase}}{\Delta T} = 360 (1.95 \times 10^{-5}) (89/0.349) = 1.79 \text{ } ^\circ/\text{ } ^\circ\text{C}$$